DISCLAIMER NOTICE

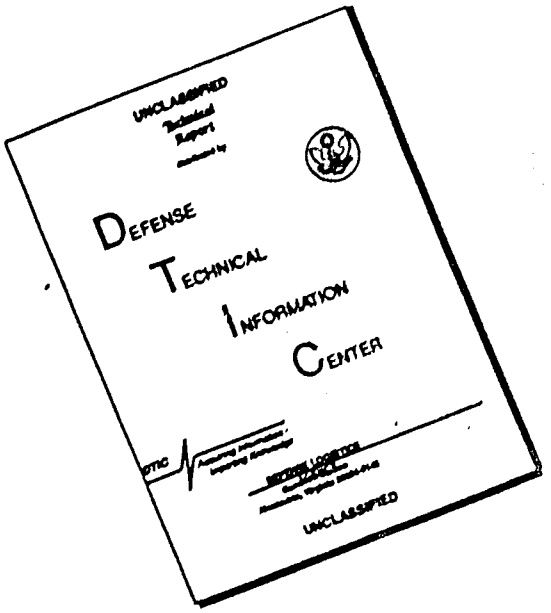

THIS DOCUMENT IS BEST QUALITY AVAILABLE. THE COPY FURNISHED TO DTIC CONTAINED A SIGNIFICANT NUMBER OF PAGES WHICH DO NOT REPRODUCE LEGIBLY.

WADD TR 60-132
Part II

REFRACTORY METAL CONSTITUTION DIAGRAMS

TECHNICAL DOCUMENTARY REPORT NO. WADD TR 60-132 PART II

September 1962

Directorate of Materials and Processes
Aeronautical Systems Division
Air Force Systems Command
Wright-Patterson Air Force Base, Ohio

Project Nr 7351, Task Nr 735101

Prepared under Contract Nr AF 33(616)-7157 by Nuclear Metals, Inc., Concord, Massachusetts, in conjunction with Massachusetts Institute of Technology and Westinghouse Research Laboratories: E. J. Rapperport and M. F. Smith of N. M. I.; J. Wulff, J. Brophy, N. J. Grant and B. C. Giessen of M. I. T.; and A. Taylor and N. Doyle of Westinghouse Research Laboratories, authors.)

NOTICES

When Government drawings, specifications, or other data are used for any purpose other than in connection with a definitely related Government procurement operation, the United States Government thereby incurs no responsibility nor any obligation whatsoever; and the fact that the Government may have formulated, furnished, or in any way supplied the said drawings, specifications, or other data, is not to be regarded by implication or otherwise as in any manner licensing the holder or any other person or corporation, or conveying any rights or permission to manufacture, use, or sell any patented invention that may in any way be related thereto.

Qualified requesters may obtain copies of this report from the Armed Services Technical Information Agency, (ASTIA), Arlington Hall Station, Arlington 12, Virginia.

This report has been released to the Office of Technical Services, U.S. Department of Commerce, Washington 25, D.C., in stock quantities for sale to the general public.

Copies of this report should not be returned to the Aeronautical Systems Division unless return is required by security considerations, contractual obligations, or notice on a specific document.

Aeronautical Systems Division, Dir/Materials and Processes, Metals and Ceramics Lab, Wright-Patterson AFB, Ohio.
Rpt Nr WADD-TR-60-132, Part II. REFRACTORY METAL CONSTITUTION DIAGRAMS. Final report, 185p. incl illus., tables, 43 refs. Sept.62.
Unclassified Report

Data on six binary constitution diagrams and two ternary constitution diagrams of some of the refractory metals are presented. The binary diagrams include Mo-Os, Ta-Ir, Ta-Rh, Ta-Zr, W-Ir, and W-Rh; the ternaries are Mo-Hf-Re and Ta-W-Zr.

Care was taken to obtain reliable diagrams. In particular the purity of the constituents

(over)

(99.9 percent plus) was protected at all times, and the temperatures were measured to an accuracy of ± 20°C.

1. Refractory metals
2. Metallurgy
I. AFSC Project 7351, Task 735101
II. Contract AF 33 (616)-7157
III. Nuclear Metals, Inc., Concord, Mass.
IV. E. J. Rapperport, et al.
V. Secondary Report No. 9237
VI. Aval fr OTS
VII. In ASTIA collection

Aeronautical Systems Division, Dir/Materials and Processes, Metals and Ceramics Lab, Wright-Patterson AFB, Ohio.
Rpt Nr WADD-TR-60-132, Part II. REFRACTORY METAL CONSTITUTION DIAGRAMS. Final report, 185p. incl illus., tables, 43 refs. Sept.62.
Unclassified Report

Data on six binary constitution diagrams and two ternary constitution diagrams of some of the refractory metals are presented. The binary diagrams include Mo-Os, Ta-Ir, Ta-Rh, Ta-Zr, W-Ir, and W-Rh; the ternaries are Mo-Hf-Re and Ta-W-Zr.

Care was taken to obtain reliable diagrams. In particular the purity of the constituents

(over)

(99.9 percent plus) was protected at all times, and the temperatures were measured to an accuracy of ± 20°C.

1. Refractory metals
2. Metallurgy
I. AFSC Project 7351, Task 735101
II. Contract AF 33 (616)-7157
III. Nuclear Metals, Inc. Concord, Mass.
IV. E. J. Rapperport, et al.
V. Secondary Report No. 9237
VI. Aval fr OTS
VII. In ASTIA collection

Aeronautical Systems Division, Dir/Materials and Processes, Metals and Ceramics Lab, Wright-Patterson AFB, Ohio.
Rpt Nr WADD-TR-60-132, Part II. REFRACTORY METAL CONSTITUTION DIAGRAMS. Final report, 185p. incl illus., tables, 43 refs. Sept.62.
Unclassified Report

Data on six binary constitution diagrams and two ternary constitution diagrams of some of the refractory metals are presented. The binary diagrams include Mo-Cs, Ta-Ir, Ta-Rh, Ta-Zr, W-Ir, and W-Rh; the ternaries are Mo-Hf-Re and Ta-W-Zr.

Care was taken to obtain reliable diagrams. In particular the purity of the constituents

(over)

(99.9 percent plus) was protected at all times, and the temperatures were measured to an accuracy of ± 20°C.

1. Refractory metals
2. Metallurgy
I. AFSC Project 7351, Task 735101
II. Contract AF 33 (616)-7157
III. Nuclear Metals, Inc. Concord, Mass.
IV. E. J. Rapperport, et al.
V. Secondary Report No. 9237
VI. Aval fr OTS
VII. In ASTIA collection

Aeronautical Systems Division, Dir/Materials and Processes, Metals and Ceramics Lab, Wright-Patterson AFB, Ohio.
Rpt Nr WADD-TR-60-132, Part II. REFRACTORY METAL CONSTITUTION DIAGRAMS. Final report, 185p. incl illus., tables, 43 refs. Sept.62.
Unclassified Report

Data on six binary constitution diagrams and two ternary constitution diagrams of some of the refractory metals are presented. The binary diagrams include Mo-Cs, Ta-Ir, Ta-Rh, Ta-Zr, W-Ir, and W-Rh; the ternaries are Mo-Hf-Re and Ta-W-Zr.

Care was taken to obtain reliable diagrams. In particular the purity of the constituents

(over)

(99.9 percent plus) was protected at all times, and the temperatures were measured to an accuracy of ± 20°C.

1. Refractory metals
2. Metallurgy
I. AFSC Project 7351, Task 735101
II. Contract AF 33 (616)-7157
III. Nuclear Metals, Inc. Concord, Mass.
IV. E. J. Rapperport, et al.
V. Secondary Report No. 9237
VI. Aval fr OTS
VII. In ASTIA collection

FOREWORD

This report was prepared by Nuclear Metals, Inc., Concord, Mass., under USAF Contract No. AF 33(616)-7157. This contract was initiated under Project No. 7351, "Metallic Materials," Task No. 735101, "Refractory Metals." The work was administered under the direction of the Directorate of Materials and Processes, Deputy Commander/Technology, Aeronautical Systems Division, Wright-Patterson Air Force Base, Ohio. Mr. T. Cooper was the project engineer.

This report covers work done from April 1960 to December 1961.

Dr. S. Moll of Advanced Metals Research Corporation, Somerville, Mass., performed a number of electron microbeams probe analyses for investigators at Nuclear Metals, Inc., and at M.I.T. The microbeam probe work helped the phase diagram determinations to a great degree, and the investigators wish to acknowledge this help.

ABSTRACT

Data on six binary constitution diagrams and two ternary constitution diagrams of some of the refractory metals are presented. The binary diagrams include Mo-Os, Ta-Ir, Ta-Rh, Ta-Zr, W-Ir, and W-Rh; the ternaries are Mo-Hf-Re and Ta-W-Zr.

Care was taken to obtain reliable diagrams. In particular the purity of the constituents (99.9 percent plus) was protected at all times, and the temperatures were measured to an accuracy of $\pm$ 20°C.

This report has been reviewed and is approved.

I. Perlmutter
Chief, Physical Metallurgy Branch
Metals and Ceramics Division
Directorate of Materials and Processes

TABLE OF CONTENTS

TABLE OF CONTENTS (Continued)

TABLE OF CONTENTS (Continued)

TABLE OF CONTENTS (Continued)

LIST OF ILLUSTRATIONS

LIST OF ILLUSTRATION (Continued)

LIST OF ILLUSTRATIONS (Continued)

LIST OF ILLUSTRATIONS (Continued)

LIST OF ILLUSTRATIONS (Continued)

LIST OF ILLUSTRATIONS (Continued)

LIST OF TABLES

LIST OF TABLES (Continued)

I. SUMMARY

A. Constitution Diagrams

The constitution diagrams which have been determined in the phase of the work detailed in this report are presented below in Figures I:1, I:2, and I:3.

The four laboratories which cooperated in this research were Nuclear Metals, Inc., Westinghouse Research Laboratories, and two separate groups at Massachusetts Institute of Technology, with Nuclear Metals, Inc. as the prime contractor.

B. Experimental Techniques

1. Materials

The purity of all the elements used was at least 99.9 percent. This purity was enchanced by arc melting, and was considered adequate for this program in view of the extremely high cost of purer starting stock.

2. Alloy Preparation

The most widely used technique of alloy preparation was non-consumable arc melting on water-cooled copper hearths, using inert atmospheres.

3. Composition Determination

The primary method of establishing the composition of alloys was the use of weight balances at various stages of alloy preparation. In addition, direct chemical analysis, X-ray fluorescence analysis, and lattice parameter measurements were used when applicable.

4. Temperature Measurement

Optical pyrometry was the principal temperature measurement technique. The pyrometers used at Nuclear Metals, Inc. and at Westinghouse Research Laboratories were calibrated at the National Bureau of Standards, and the two M.I.T. instruments were checked against the NMI instrument using a black-body cavity. The accuracy of temperature measurement is within $\pm$ 25^{0}C in nearly all cases.

5. Phase Boundary Determinations

a. Solidus

Several techniques were utilized to allow direct observation of a melting specimen and to obtain its temperature reliably. These were considered less satisfactory than the incipient fusion technique, which was also used. This technique locates the solidus by metallographic observation of microstructural changes characteristic of melting.

Manuscript released by authors March 1962 for publication as a WADD Technical Report.

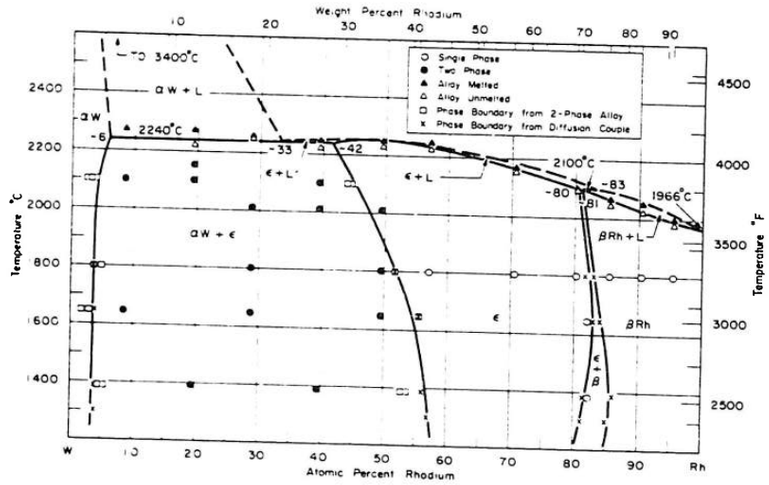

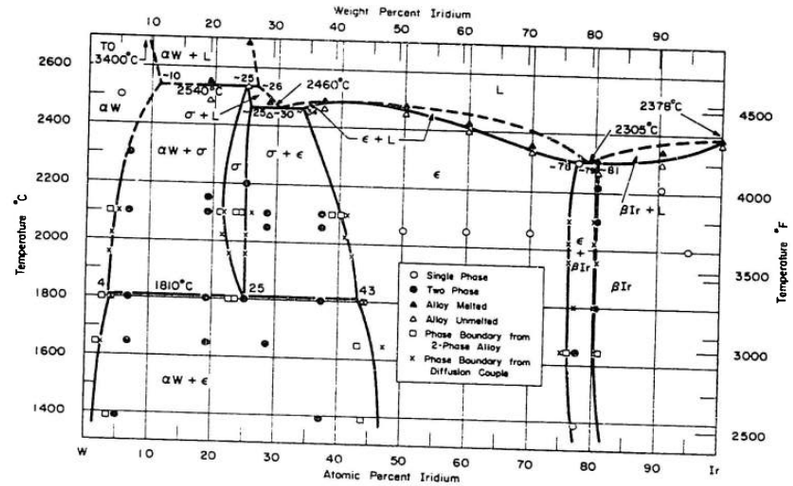

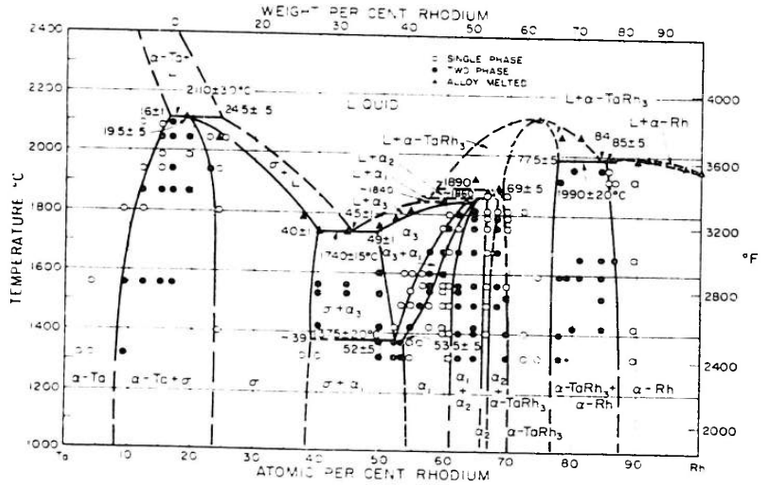

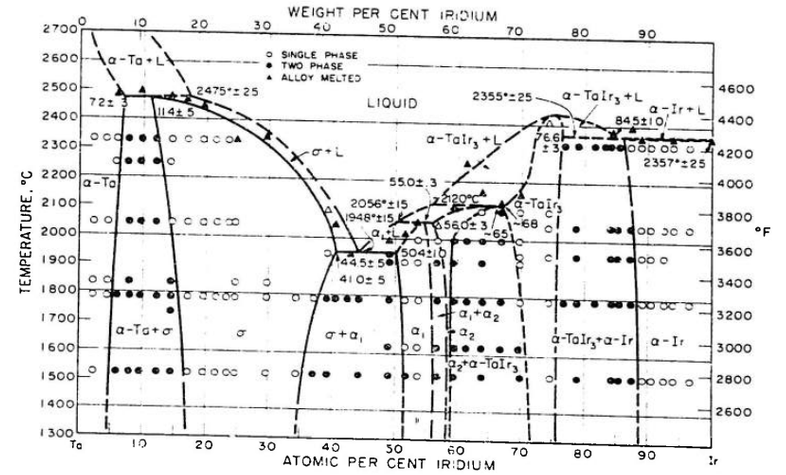

Figure I:1 - Constitution diagrams of tungsten-rhodium; tungsten-iridium; tantalum-rhodium; and tantalum-iridium.

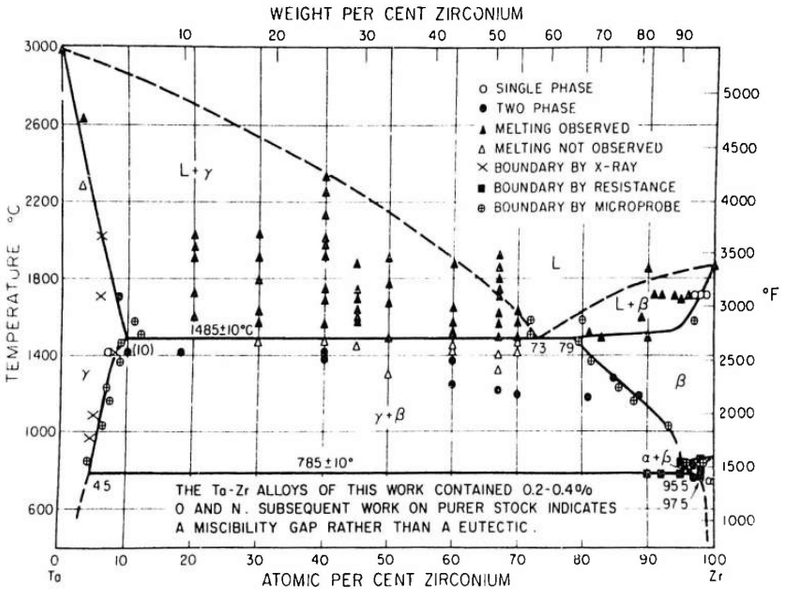

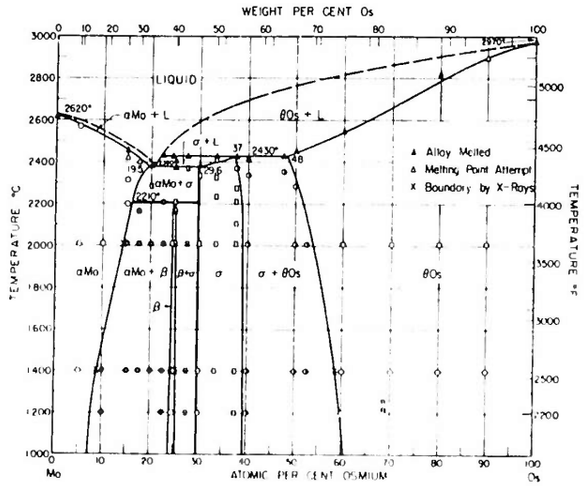

Figure I:2 - Constitution diagrams of tantalum-zirconium and molybdenum-osmium.

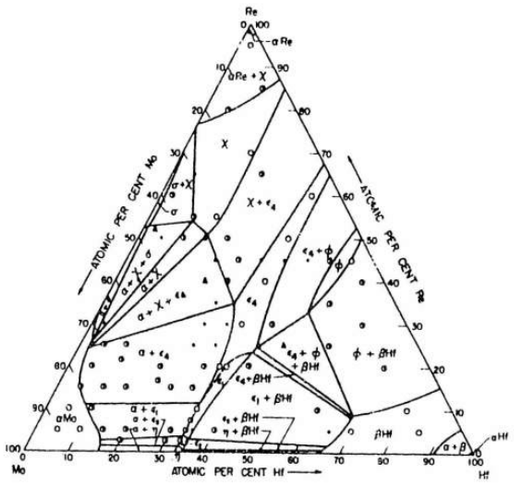

1600°C

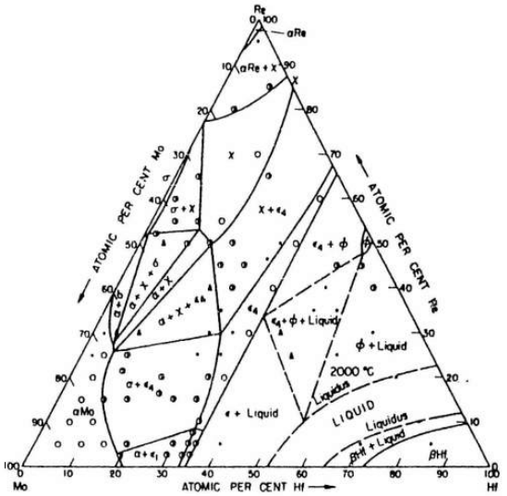

2000°C

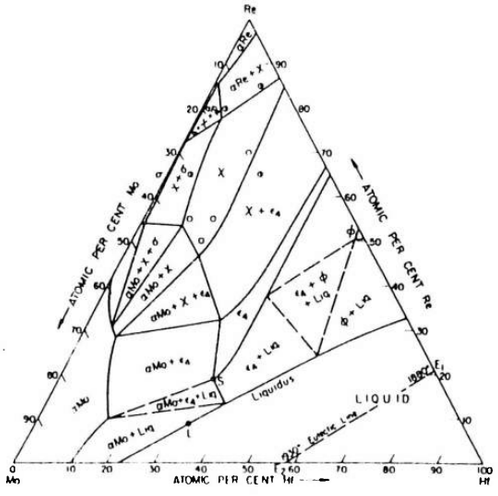

2400°C

Figure I:3 - Constitution diagrams of molybdenum-rhenium-hafnium.

b. Phase Boundaries

The techniques employed in this work include metallography, X-ray powder patterns, thermal analysis, and electron microbeam probe analysis. The basis of all of these techniques is the detection of physical differences, e.g., in microstructure, crystal structure, or chemical composition, between the phases present in the various alloy systems. Except for thermal analysis, all the methods utilized quenched specimens.

II. INTRODUCTION

A. Background

This report terminates the investigation of some eight binary and ternary phase diagrams. The program was a continuation of a previous investigation of phase relationships among various binary and ternary combinations of refractory metals (i.e., metals melting above $\sim 2000^{\circ}C$). This work was initiated because of the lack of knowledge of the phase relationships among the refractory metals. Although a number of refractory metal phase diagrams do appear in the literature, most of these are not reliable because of impure melting stock, inaccurate temperature measurement, inadequate heat treating equipment, and the relatively short times allowed to attain thermal equilibrium.

It is only in recent years that the refractory metals have become available in purities high enough to make the studies of phase diagrams meaningful. Until recently there was no particular technological need for alloys of these rather exotic elements; however, current interest in materials for high temperature service under adverse stress and environmental conditions has motivated the investigation of alloys of the refractory metals.

Constitution diagrams of various combinations of the refractory metals have many applications. One of the most direct uses of these diagrams is the prediction of the physical structures of specific alloys equilibrated at various temperatures. Since the microstructure of an alloy often dictates, to a large extent, its physical properties, it is extremely important to know how the microstructures vary with temperature and composition.

Carefully determined equilibrium diagrams may be useful in the determination of various thermodynamic functions, as well as in studies of phase transformation kinetics. In these cases it is frequently the slopes of the various phase boundary curves that are of major interest.

Reliable constitution diagrams also are valuable in extending alloy theory. Among the particular concerns of alloy theory specialists are the theoretical prediction of terminal solubilities and the presence and crystal structures of intermediate phases in various alloy systems. In order to develop and test such theories, reliable phase diagrams are necessary for comparison with the theoretical predictions. The current lack of reliable diagrams for the refractory metals should be alleviated somewhat by this program.

B. Approach to the Problem

As in the initial contract period, the four groups participating in these studies worked, to a large extent, independently of one another. Nevertheless, frequent consultations among the member groups were held in order to develop satisfactory techniques for specific aspects of the program. Such topics as temperature measurement, techniques of composition determination, and the details of X-ray analysis were thoroughly discussed among the investigators.

During the contract period, several meetings were held at which representatives from the participating laboratories presented tentative diagrams, along with their most recent and significant supporting data. The others present criticized the work and made suggestions. Individual problems in experimental technique were often clarified by investigators with specific experience in one or another phase of this type of research.

C. Organization of Work

Nuclear Metals, Inc., Concord, Massachusetts was the prime contractor and manager for this work, with the other participating laboratories acting as subcontractors. Table II:1 gives the diagrams investigated together with the sites and principal investigators.

Table II:1*

Systems Investigated, Laboratories and Principle Investigators

Nuclear Metals, Inc. Dr. E. J. Rapperport M. F. Smith	MIT Prof. J. Wulff Prof. J. Brophy	MIT Prof. N. J. Grant Dr. B.Giessen	Westinghouse Research Labs. Dr. A. Taylor
W-Rh	Ta-Zr	Ta-Ir	Mo-Os
W-Ir	Ta-W-Zr	Ta-Rh	Mo-Hf-Re

* Tables and Figures are numbered individually with respect to the sections in which they appear.

D. Organization of Report

Each of the four participating laboratories has contributed a separate section in this report. These independent sections give full details on the experimental techniques and procedures employed by each group of investigators.

III. CONSTITUTION DIAGRAMS W-Rh, W-Ir (Work done at Nuclear Metals, Inc. by E. J. Rapperport and M. F. Smith)

A. General

Nuclear Metals, Inc. was responsible for the determination of the tungsten-rhodium and tungsten-iridium binary phase diagrams. Both of these diagrams had relatively large terminal solubility at the low-tungsten side with relatively little solubility at the high tungsten side. The techniques and processes employed in the determination of these diagrams are presented in detail below.

B. Materials

Although the materials used in these phase diagrams are available in extremely pure forms from Johnson and Matthey Company, the cost of these ultra-pure materials in the quantities needed was considered prohibitive. Instead, material of lower purity (and lower cost) was used and the arc-melting procedure was utilized for some purification. The tungsten employed in this investigation was specified as 99.9+% pure and was supplied by General Electric. The rhodium and iridium, both specified as 99.9% pure, were obtained from Bishop and Co. All the elements were bought as fine powders (-100 mesh) to facilitate uniform blending and compacting.

The purifying effect of arc-melting on refractory metals has been well established. This effect is particularly prominent in metals and alloys melted repeatedly under vacuum or inert atmospheres. While no spectroscopic analyses were made in this program, a high level of confidence in the final purity of the alloys seems justifiable in the light of previous experience.(1)

C. Alloy Preparation

The following techniques were employed in preparing alloys for both systems. An initial series of alloys, at 10 atom percent intervals, was made for each system by weighing out appropriate amounts of pure metal powders, and mixing, compacting, vacuum sintering and arc-melting these powders to produce one 25-gram ingot of each composition. An additional series of composition standards was made for each system by combining arc-melted pellets of the pure materials. This technique is described in detail below.

1. Compacting

Powders were placed in a massive tool-steel die and compacted with a steel plunger to pressures of 30,000 psi. The resulting compacts were easily handled although somewhat fragile. Care was exercised during this procedure to avoid contamination of the compacts by extraneous elements.

- - - - - - - - - - - -

(1) References for each section are listed at the end of the section.

2. Sintering

The compacts were placed in tungsten-lined tantalum buckets, and vacuum-sintered at approximately 1500°C in order to purge them of adsorbed gases and accomplish partial densification. The final vacuum attained at 1500°C was usually about 10^{-4} mm Hg, and the sintering process for each batch required less than one hour. The average weight loss during sintering was of the order of 0.1 gm for the 25-gm compacts.

3. Melting

Arc-melting was carried out on a water-cooled copper hearth, using a non-consumable unthoriated tungsten electrode and an inert atmosphere. This equipment is discussed in detail in Appendix I.

Before melting, the chamber was evacuated and flushed several times with argon, the final evacuation resulting in pressures of 5×10^{-5} mm Hg or less. Following this final evacuation, an atmosphere of purified helium with a small amount of purified argon was admitted to a pressure of approximately 500 mm Hg to form the arc-melting atmosphere.

Standard procedure was to melt each sample, turn it over, remelt it, and so on for a total of 4 to 6 melts. X-ray fluorescent analyses at various locations in the arc-melted buttons showed that this procedure resulted in good homogeneity.

4. Composition Determination

Quantitative analysis techniques for the combinations tungsten-rhodium and tungsten-iridium have not yet been developed. Therefore, since the scope of this program did not include the development of analytical methods, reliance was placed on weight-balance calculations, both for alloys to be used in the study of phase relations and for those to be used as composition standards for the microbeam probe. By weighing the pure materials, the compacts before and after sintering, and the final arc-melted ingots, and attributing the entire loss first to one component, then to the other, the maximum deviation in chemical composition was obtained for each alloy. These data are presented for the two binary systems in Tables III:1 and III:2.

Composition standards were prepared by a slightly different technique from that used for the initial series of alloys. In particular, the pure elements were compacted separately and arc-melted in the form of small 1-gram pellets. This had the effect of purifying the starting materials individually and permitted the final weighing of the stock to be carried out with virtually no handling losses. The alloys were then made by arc melting together suitable amounts of pellets of the pure materials, rather than by arc-melting mixed, compacted and sintered powders. The primary advantage of this technique for alloy preparation is that it keeps the weight losses during the final arc melting to a minimum. Thus the overall composition uncertainty of the standard alloys is less than $\pm$ 0.25 atom percent in all cases, and less than $\pm$ 0.10 atom percent in all but three cases. Compositions of the standard alloys for the two systems are given in Tables III:3 and III:4.

Table III:1

Compositions and Tolerances of W-Rh Alloys

Intended Composition, a/o Rh	Minimum a/o Rh	Maximum a/o Rh	Nominal a/o Rh	Tolerance a/o Rh
10	6.76	10.20	8.48	± 1.72
20	18.75	20.18	19.47	± 0.72
30	26.71	30.77	28.74	± 2.03
40	38.37	40.60	39.49	± 1.12
50	48.05	51.07	49.56	± 1.51
60	~56*	59.37	57	
70	68.97	72.07	70.52	± 1.55
80	79.41	81.30	80.36	± 0.95
82.2	81.96	82.50	82.23	± 0.27
85	84.53	86.48	85.51	± 0.98
90	89.76	91.18	90.47	± 0.71
95	94.89	96.14	95.52	± 0.63

* Tungsten electrode melted and dripped into alloy.

Table III:2

Compositions and Tolerances of W-Ir Alloys

Intended Composition, a/o Ir	Minimum a/o Ir	Maximum a/o Ir	Nominal a/o Ir	Tolerance a/o Ir
10	2.05	10.79	6.42	± 4.37
20	18.11	20.26	19.19	± 1.08
30	24.22	32.61	28.44	± 4.20
40	~35*	39.11	37	
50	49.31	50.72	50.02	± 0.71
60	59.55	60.72	60.14	± 0.59
70	69.62	70.94	70.28	± 0.66
77.5	77.42	77.49	77.46	± 0.04
80	79.61	81.18	80.40	± 0.79
90	89.86	91.33	90.60	± 0.74

* Tungsten electrode melted and dripped into alloy.

Table III:3

Compositions and Tolerances of W-Rh Composition Standards

Minimum ^{a}/o Rh	Maximum ^{a}/o Rh	Nominal ^{a}/o Rh	Tolerance ^{a}/o Rh
3.89	4.15	4.02	± 0.13
24.17	24.56	24.37	± 0.20
55.30	55.43	55.37	± 0.07
69.76	69.87	69.82	± 0.06
79.77	79.83	79.80	± 0.03
94.76	94.81	94.78	± 0.03

Table III:4

Compositions and Tolerances of W-Ir Composition Standards

Minimum ^{a}/o Ir	Maximum ^{a}/o Ir	Nominal ^{a}/o Ir	Tolerance ^{a}/o Ir
5.04	5.23	5.14	± 0.10
25.29	25.30	25.29	± 0.01
40.56	40.64	40.60	± 0.04
54.61	54.78	54.70	± 0.09
69.12	69.49	69.30	± 0.19
93.95	94.01	93.98	± 0.03

The inherent disadvantage in this technique is the difficulty of producing an alloy with exactly the desired composition. On the other hand, although it is easier to weigh out an exact predetermined amount of powder, the rather large losses which attend the melting of powder compacts probably make it somewhat inferior to the technique of combining pre-melted pellets.

These standard alloys were used by the Advanced Metals Research Corporation of Somerville, Massachusetts for electron microbeam probe determination of compositions of other alloys and of individual phases in alloys. This work is described in detail in Section E, Alloy Analysis Techniques.

D. Thermal Treatments of Alloys

1. Preliminary Solidus

Before a reasonable program of homogenization and equilibration treatments could be planned, it was necessary to make a preliminary determination ($\pm$ 50°C) of the solidus temperatures for the various alloys. Two techniques, the "tantalum-block" technique and the "tungsten-ribbon" technique, were employed in the preliminary solidus determinations. These are described below.

The more reliable of the two techniques was the "tantalum-block" technique, illustrated in Figure III:1. The sample to be melted is wired to the tantalum block, and protected by thoria as shown. The actual measurements of the blocks used for this purpose were about 2 inches by 1/4 inch by 3/8 inch, and the drilled sight-holes were about 1/8 inch in diameter and 1 to 1-1/2 inches deep. This approximated a blackbody cavity whose temperature could be accurately read with an optical pyrometer, as described in Appendix II. The fixture with the attached sample was placed in a vertical tube furnace, described in detail in Appendix III, and observed from above. The projecting portion of the sample was examined as the temperature was raised in 20°C increments. When the sample melted or changed shape, the temperature of the tantalum block, as read in the long cavity by an optical pyrometer, was taken as the melting point, or preliminary solidus, of the alloy.

The "tungsten-ribbon" technique was used on many of the alloys instead of the "tantalum-block" technique, because it is much less cumbersome; and although the temperature measurement is less accurate in this technique, it was considered adequate for preliminary work. The sample to be melted was placed in a folded ribbon-type heating element made from 0.002-inch thick tungsten sheet having a cover with a 1/8-inch hole placed on in such a way that the sample could be seen through the hole. Although this deviated from blackbody conditions the apparent melting temperature, indicated by optical pyrometer readings on the surface of the sample, was usually found to be within 100°C of the true solidus.

More careful determinations of solidus temperatures were eventually made, using the incipient fusion technique, which is described in detail in Section 4.

2. Homogenization

Many of the alloys used in this program required high temperature homogenization prior to equilibration treatments at various temperatures. Samples to be homogenized were loaded in tungsten-lined tantalum buckets and placed in the furnace. Liners made of tungsten sheet were used in order to prevent tantalum pick-up from the heating elements by the alloys.

The containers used were approximately 3-inches long by 1/2-inch in diameter and the maximum temperature difference along their length was found to be less than 30°C. In most cases the homogenizing temperatures were measured and maintained with sufficient accuracy to permit the as-homogenized samples to be regarded as equilibrated at the homogenization temperatures. Homogenization was conducted for

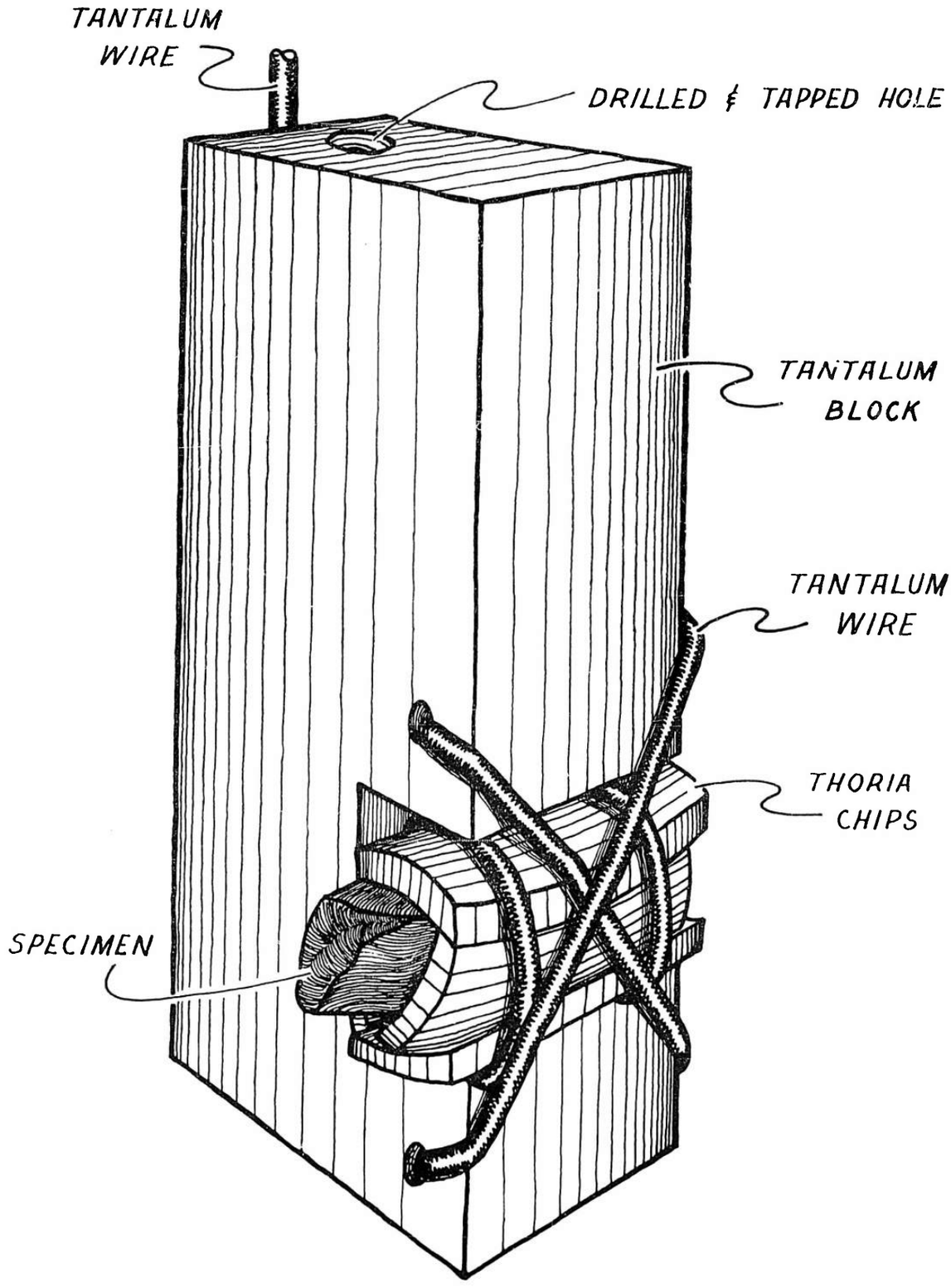

Figure III:1 - Tantalum fixture used in preliminary solidus determination by the tantalum block technique.

10 to 15 hours at temperatures about 200°C below the solidus for most alloys; this was generally found to be satisfactory on the basis of metallographic appearance and the sharpness of Debye-Scherrer X-ray patterns.

3. Equilibration

Nearly all equilibration runs were performed at temperatures above 1500°C in the tantalum tube furnace described in Appendix III. The two lowest-temperature equilibrations, those at 1300°C and 1385°C, were made in molybdenum-wound furnaces. For these runs, temperature measurements were made with (Pt)-(Pt - 10% Rh) and W-Re thermocouples. Measurements of the gradients along the furnace tubes, and of the fluctuations of temperature with time at a given point within a tube, yielded an overall accuracy of ± 25°C for equilibration temperatures.

Many of the equilibration runs extended overnight and through weekend periods. During the workday the temperatures were read at approximately one hour intervals. Such readings sometimes extended well into the night and some readings were obtained on weekends. At other times the furnaces were monitored by the thermocouples, or Leeds and Northrup Rayovac Radiation Pyrometers, connected to recorders. These devices provided excellent checks as to the constancy of temperature within the furnaces. Except for those runs which were so high as to cause vapor deposition on the sight glasses, the radiation pyrometers proved quite successful as monitors.

4. Final Solidus

The tantalum-block technique outlined above for preliminary solidus determinations was considered satisfactory for pure elements and for alloys melting isothermally. However, for alloys which melt over a wide temperature range, this technique may yield erroneous results, since such an alloy may not change shape even though much of it has been melted.

Since most of the alloys do not melt isothermally the technique of "incipient fusion" was relied upon to give more accurate solidus temperatures. In this technique, a small sample of homogenized alloy was placed in a thoria crucible and heated to a previously selected temperature for about 10 minutes. The furnace was then turned off (radiation quench) and the sample removed and examined metallographically. If the solidus temperature had been exceeded, the portion of the sample which melted showed the typical as-cast structure for the composition involved. Since the samples for these experiments were initially in the homogenized condition, it was usually possible to tell by metallographic inspection whether or not melting had occurred. The precision to which the solidus of a given alloy can be determined by this technique is limited mainly by the number of samples which are prepared, heated, sectioned, polished and inspected metallographically for evidence of melting. Since the preliminary solidi were known, four additional samples were generally sufficient to establish the true solidi within about 20°C. Figure III:2 shows several microstrucutres of the same alloy, including one heated just below the solidus and another just above it.

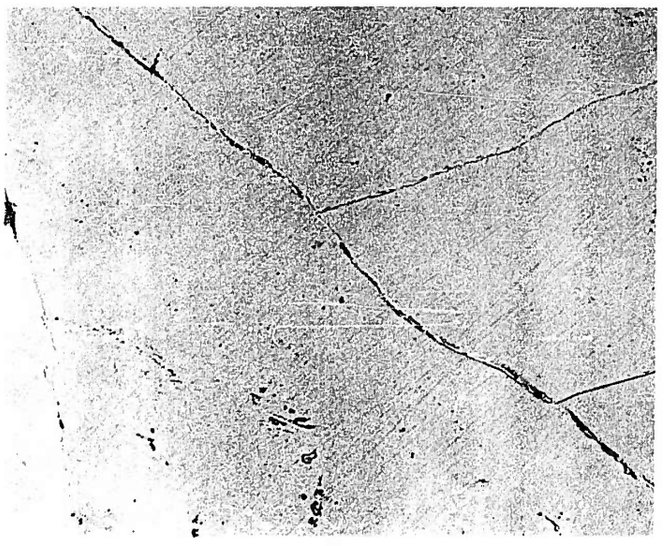

(a) A-4086-8

Previously homogenized alloy heated to 2150°C. No melting has occurred.

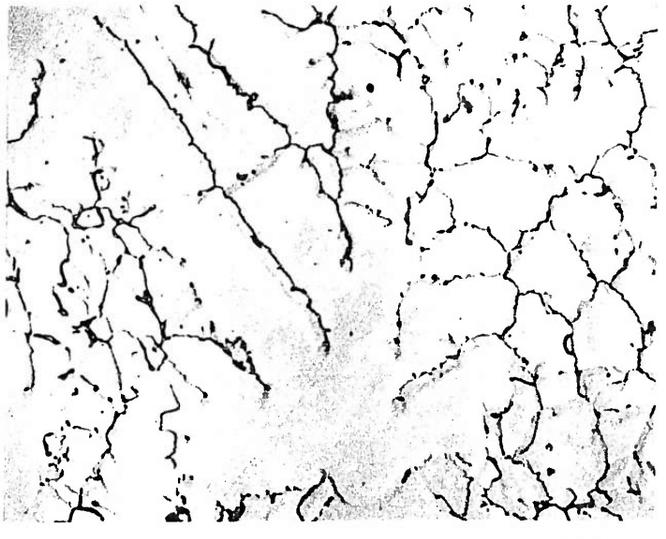

(b) A-4086-9

Previously homogenized alloy heated to 2170°C. Alloy has begun to melt. Solidus is between 2150°C and 2170°C.

Figure III:2 - 70 a/o Rh, 30 a/o W alloys, illustrating the incipient fusion technique for solidus determination.

E. Alloy Analysis Techniques

1. Metallography

Metallographic examination was used throughout the program for studying phase relationships in alloys. Examination of as-cast alloys frequently helped establish the general forms of the phase diagrams; for example, peritectic or eutectic type reactions could often be identified by examination of as-cast alloys.

Metallographic examination of homogenized and equilibrated alloys provided information concerning phase boundaries, homogeneity of alloys, solid-state reactions, precipitation, etc. The use of metallography in the incipient-fusion technique of solidus determination has already been discussed.

Most of the alloys were successfully prepared by polishing through one micron diamond paste on cloth wheels and etching by the A.C. electrolytic technique described in Appendix IV. A few were prepared using a Syntron vibratory polisher and etched with potassium ferricyanide as described in Appendix V.

2. Debye-Scherrer X-Ray Photographs

Debye-Scherrer X-ray patterns were made using a 57.3 millimeter camera. Patterns were made for all alloys, both in the as-cast condition and after homogenization and equilibration. These patterns gave valuable information on the phases present in the binary systems; in particular, their number, identity, and solubility limits.

The relative sharpness of the lines on the Debye-Scherrer photographs gave an indication of the degree of homogenization and the efficacy of the annealing treatments. In addition, they allowed approximate phase boundary determination by observation of the relative intensities of the lines from each phase in a two-phase field. It was frequently possible to bracket a particular phase boundary between two known compositions, one showing a particular phase in a two-phase pattern, and the other not showing it.

3. Electron Microbeam Probe

The electron microbeam probe is an instrument capable of focusing a beam of electrons on a spot approximately one micron in diameter. These electrons excite X-rays, both "white radiation" and wavelengths characteristic of the elements irradiated. The wave lengths emitted by the elements in the spot are separated by diffraction from an analyzing crystal, and their intensities are recorded by radiation counters. By comparing the normalized intensity of characteristic radiation from the sample with that from carefully made composition standards, a quantitative analysis can be obtained for the irradiated spot.

Electron microbeam probe data can be only as accurate as the composition standards from which the probe is calibrated. The standards for this work were made very carefully (as previously discussed) and their compositions were very

well known. An indication of their consistency and quality is shown by the composition-intensity plots, Figures III:3 and III:4. These curves show very little scatter, and were quite reproducible. They are considered accurate to within 0.5 atom percent.

Data was obtained in two ways from the microbeam probe:

a. Two-Phase Alloys

Phase boundaries can be found by determining the compositions of the phases in two-phase alloys, by techniques discussed above. The chemical compositions of the two phases are determined by focussing the electron beam on each phase and analyzing the excited characteristic radiation in the usual way. Since the phases are presumed to be in equilibrium with one another, the phase boundary compositions are equal to the compositions of each of the two phases.

b. Diffusion Couples

In this technique, slabs of two elements (or two alloys) are placed in intimate contact and allowed to diffuse together. The microbeam probe is then used to determine the compositions at approximately 10^{-4}-inch intervals across the diffusion zone and a plot of composition vs. diffusion distance is derived. Discontinuities in this curve indicate phase boundary compositions. A typical diffusion plot is given in Figure III:5.

4. Thermal Analysis

Thermal analysis was used to determine the eutectoid decomposition temperature in the tungsten-iridium system. The temperature of the sample was measured and recorded by a tungsten-rhenium thermocouple and a Leeds-Northrup Speedomax recorder. The temperature of the furnace was raised or lowered at a uniform rate by driving the Powerstat shaft at a uniform speed by means of an electric motor-variable speed reduction combination. Thermal arrests were determined from the recorder charts by graphical methods.

F. Tungsten-Rhodium Constitution Diagram

1. General

The proposed constitution diagram for the tungsten-rhodium system is given in Figure III:6. The data for this diagram was obtained by techniques already outlined; the diagram is discussed in detail below. In general, good agreement prevailed among the metallographic, X-ray, and electron microbeam probe techniques.

2. Presentation of Data

a. Solidus

The solidus temperatures were determined in this system by finding first the preliminary melting points of alloys at 10 $^{a}/_{o}$ increments across

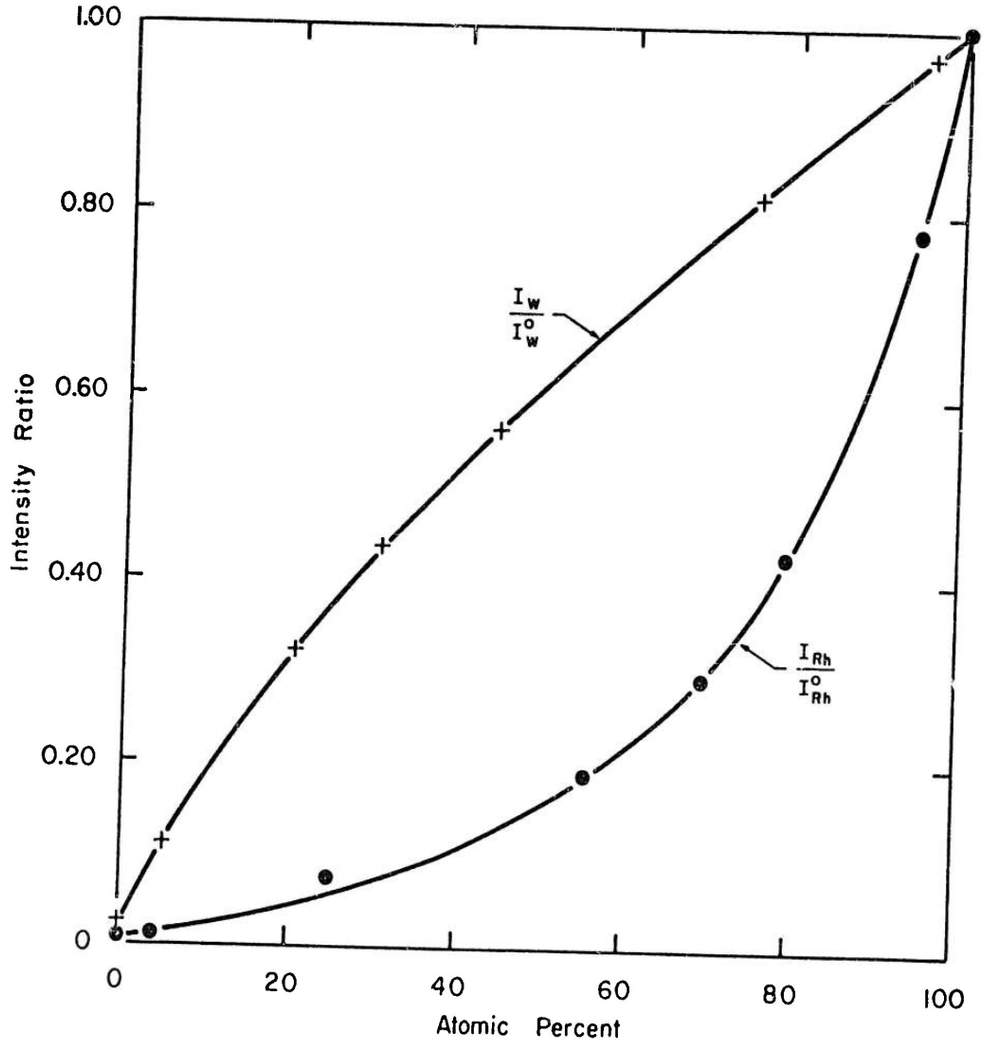

Figure III:3 - Plot of normalized intensity of characteristic radiation of Rh + W vs composition.

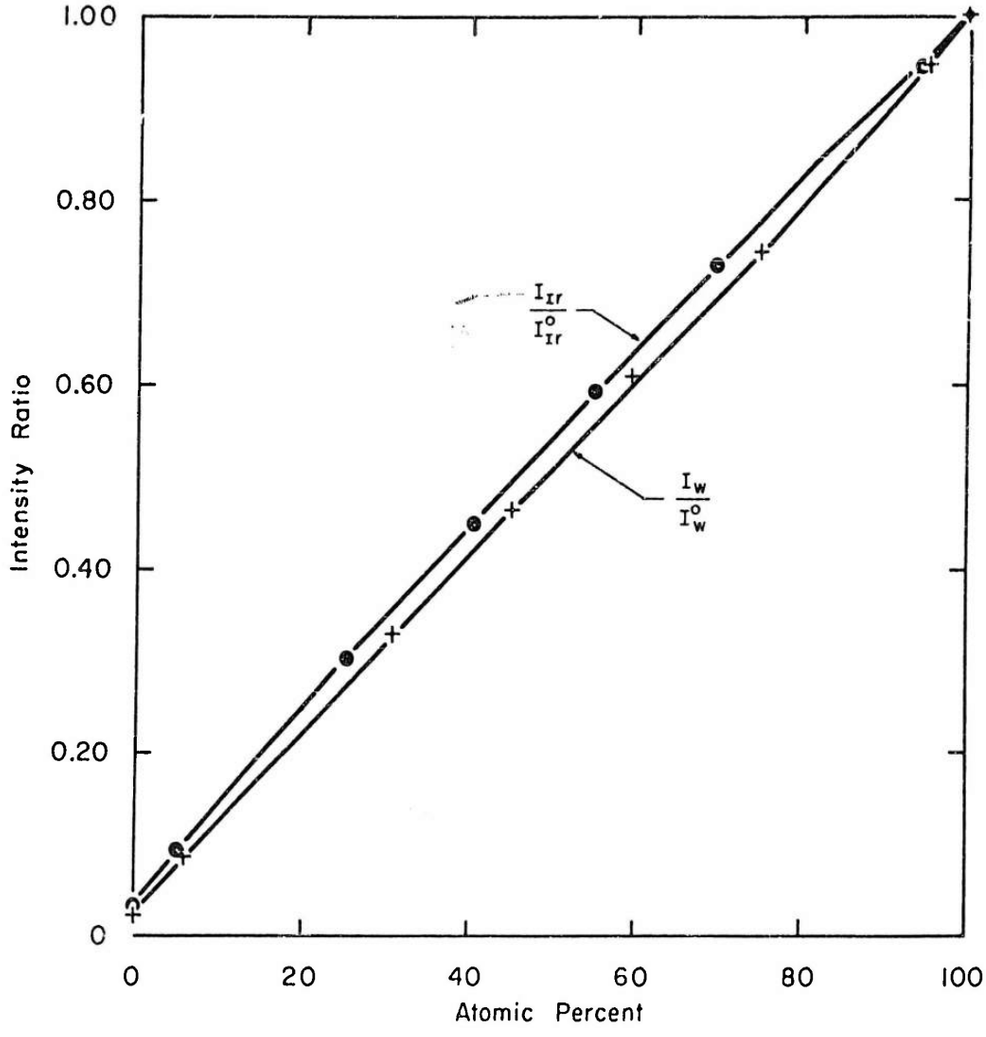

Figure III:4 - Plot of normalized intensity of characteristic radiation of Ir + W vs composition.

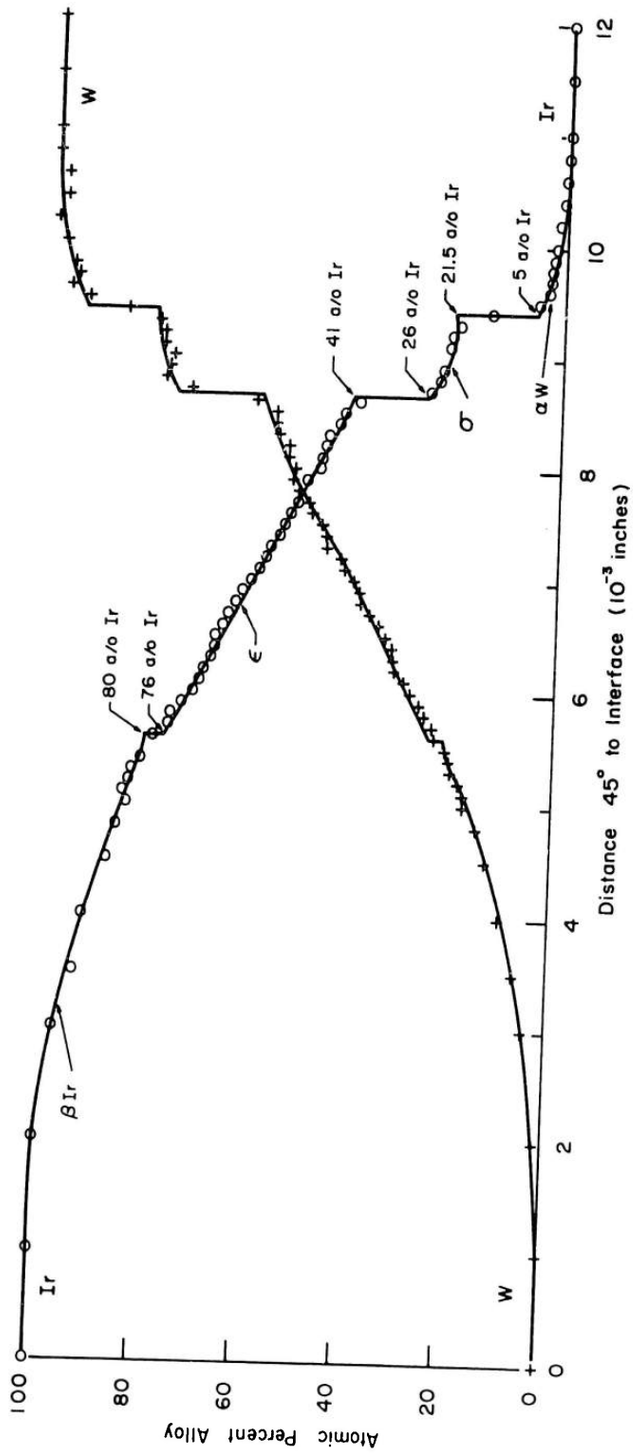

Figure III:5 - Plot of composition vs distance for tungsten-iridium diffusion couple, annealed 52 hours at 2100°C.

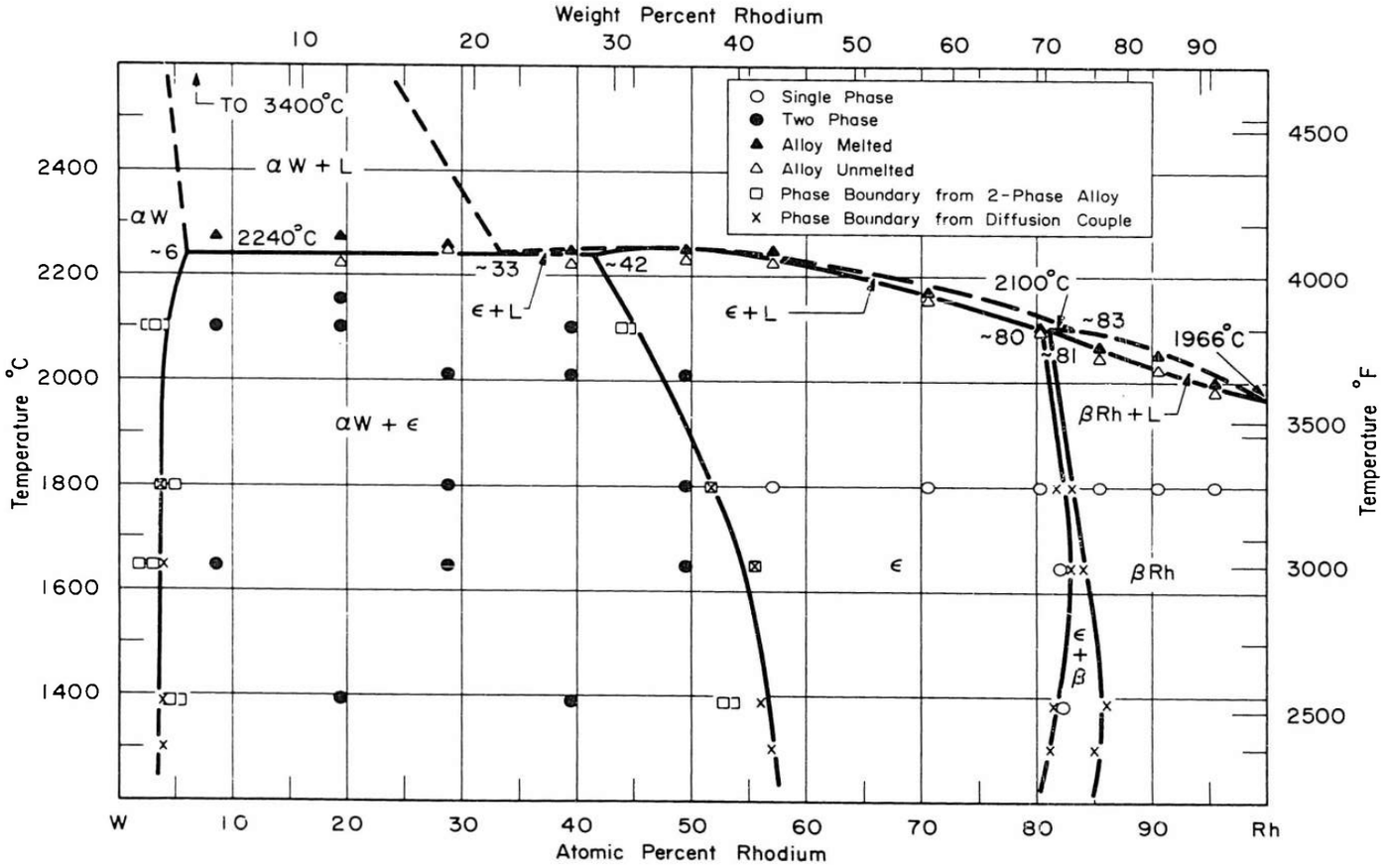

Figure III:6 - Tungsten-rhodium constituion diagram.

the diagram. These preliminary solidus observations guided the choice of homogenization and equilibration temperatures for the alloys. They were ultimately followed by more accurate determinations, utilizing the incipient fusion technique. Additional alloys were also prepared, and their solidi carefully determined.

A summary of the solidus data for the tungsten-rhodium system is given below in Table III:5. The solidus in the diagram in Figure III:6 is seen to lie between the temperatures indicated in Table III:5 for each alloy.

Table III:5

Solidus Data, Tungsten-Rhodium System

Composition ^{a}/o Rh	Maximum Temperature Without Melting ^{o}C	Minimum Temperature Melting Observed ^{o}C
10	----	2275
20	2220	2275
30	2250	2260
40	2220	2250
50	2230	2250
60	2220	2250
70	2150	2170
80	2095	2100
85	2040	2060
90	2020	2050
95	1980	2000

b. Equilibration

Table III:6 summarizes the thermal equilibration treatments given the alloys in the tungsten-rhodium system, and the number and kind of phases present for the various conditions of temperature and composition. No distinction is made between homogenization of as-cast alloys and other equilibration, since equilibrium is assumed to be achieved during homogenization. In general, the homogenization treatment was that having the highest temperature shown; all other treatments having been preceded by this treatment.

c. Composition Limits of Phases

The data which was used to construct the phase boundaries in Figure III:6 is tabulated below in Table III:7. All quantitative observations as to the locations of phase boundaries are included, and the techniques by which they were determined are indicated.

Table III:6

Equilibration Treatments and Phases Present, Tungsten-Rhodium Alloys

Nominal Composition a/o Rh	Phases Present As-Cast	Temp. °C	Time hrs.	Phases Present	Temp. °C	Time hrs.	Phases Present	Temp. °C	Time hrs.	Phases Present	Temp. °C	Time hrs.	Phases Present
4	αW												
10	α + E	2275	7	α + L	2095	28	α + E	1645	300	α + E			
20	α + E	2275	7	α + L	2150	16	α + E	2095	28	α + E	1385	417	α + E
30	α + E	2010	7	α + E	1800	200	α + E	1645	300	α + E			
40	α + E	2095	28	α + E	2010	7	α + E				1385	417	α + E
50	E	2010	7	α + E	1800	200	α + E	1645	300	α + E			
60	E	1805	9	E									
70	E	1805	9	E									
80	E	1805	9	E									
82.2	E	1770	17	E				1645	300	E	1385	417	E
85	βRh	1800	8	β + E	1800	200	E(+β?)						
90	βRh	1805	9	βRh									
95	βRh	1800	8	βRh									

Table III:7

Phase Boundary Data in the W-Rh System

Temperature °C	Solubility Range (a/o Rh)						Technique*
	αW		E		βRh		
	Min.	Max.	Min.	Max.	Min.	Max.	
2095		3.5					1
2095		2.9	44.5				1
2095		2.5	44.1				1
1800	0	3.8	51.7	81.7	83	100	2
1800		3.8	51.5				1
1800		5	51.8				1
1645		1.8	55				1
1645		3.0	54.7				1
1645			55.9				1
1645	0	3.8	55.5	83	84	100	2
1385	0	4	56	81.6	86.0	100	2
1385		4.5	53.6				1
1385		5.0	52.8				1
1300	0	4	57	81	85	100	2

* 1: Microprobe analysis of two-phase alloys.

2: Microprobe analysis of diffusion couples.

d. Metallographic Data

The photomicrographs of Figures III:7 and III:8 are representative of the types of structures present in binary alloys of the W-Rh system. The as-cast microstructures give the initial evidence as to the type of solidification reactions involved (later verified by solidus measurements); the homogenized microstructures show the typical condition of samples analyzed for equilibrium phase relationships by Debye-Scherrer analysis and by the microbeam probe.

3. Discussion

The foregoing presentation of data is felt to justify the diagram as shown in Figure III:6. The overall temperature accuracy, except where otherwise indicated, is plus or minus 25°C; and compositions are accurate to within 1 atom percent for solid lines and within 5 atom percent for dotted lines.

150X (a) A-4086-2

30 a/o Rh, 70 a/o W, as-arc-melted. Alpha tungsten precipitate in epsilon matrix.

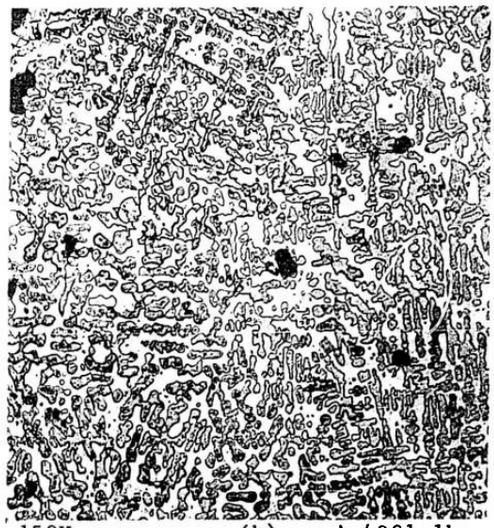

150X (b) A-4001-1b

30 a/o Rh, 70 a/o W, equilibrated 200 hours at 1800°C.

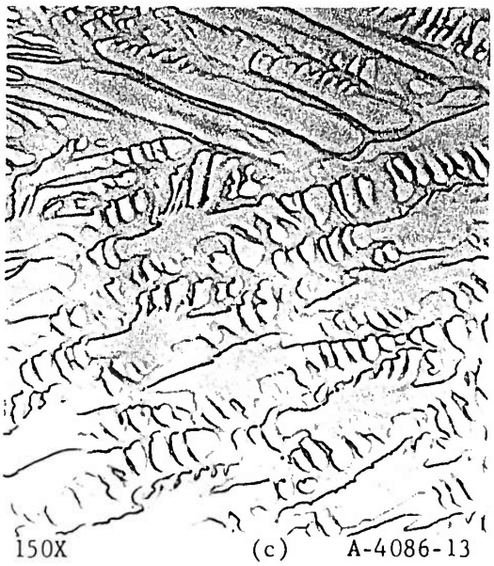

150X (c) A-4086-13

90 a/o Rh, 10 a/o W, as-arc-melted. Cored beta rhodium structure.

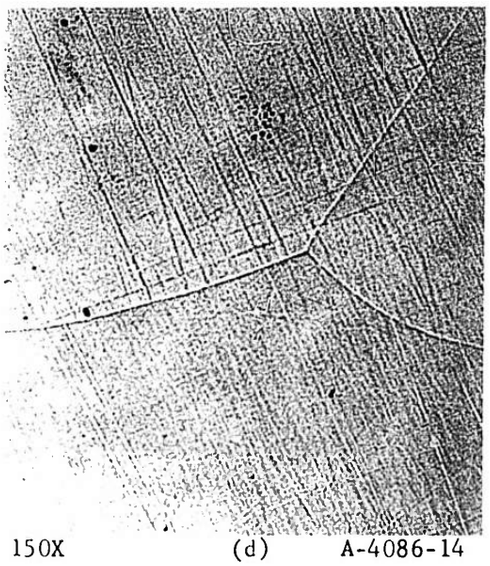

150X (d) A-4086-14

90 a/o Rh, 10 a/o W, equilibrated 9 hours at 1800°C.

Figure III:7 - Microstructures of tungsten-rhodium alloys.

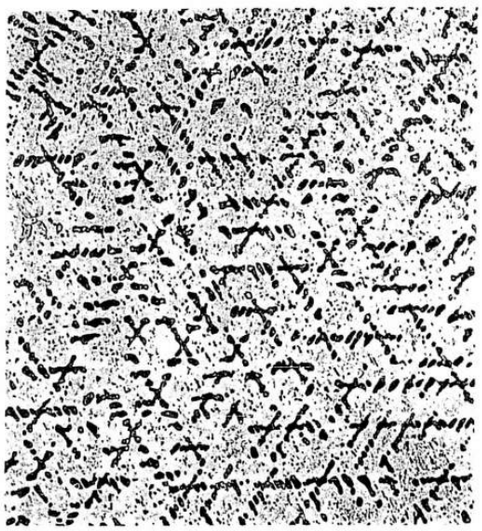

150X (a) A-4086-4

40 a/o Rh, 60 a/o W, as-arc-melted. Dark phase is alpha tungsten, which surrounds particles of primary epsilon.

500X (b) A-4086-4a

Same alloy as (a). Higher magnification clearly shows divorced eutectic. Some normal eutectic is also evident.

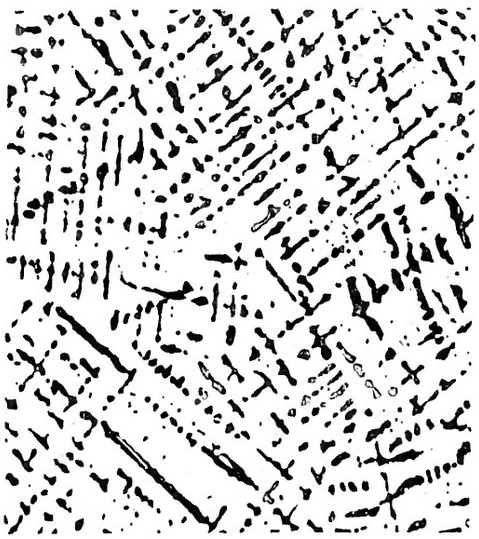

150X (c) A-4086-5

40 a/o Rh, 60 a/o W, equilibrated 28 hours at 2095°C.

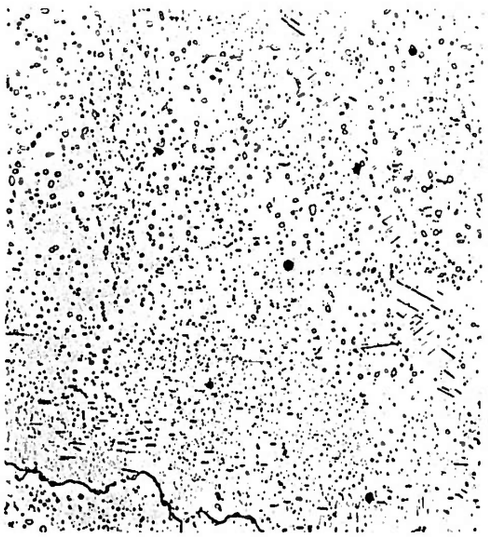

150X (d) A-4001-2a

50 a/o Rh, 50 a/o W, equilibrated 200 hours at 1800°C.

Figure III:8 - Microstructures of tungsten-rhodium alloys.

Several unsuccessful attempts were made to determine the boundaries of the two-phase epsilon plus beta-rhodium region. It will be noted that Debye-Scherrer analysis of the 85 ^{a}/o Rh alloy indicates the presence of only beta-rhodium in the as-cast condition, and of only epsilon after 200 hours at 1800^{o}C. The microbeam probe also could detect only one phase in this equilibrated alloy. However, the Debye Film of a specimen homogenized for 8 hours at 1800^{o}C (initially in the as-cast condition) shows both the epsilon and the beta patterns. The 8-hour treatment was considered insufficient for equilibration since the Debye pattern was not as sharp as is normal for equilibrated alloys.

Several effects may be responsible for these inconsistencies. In particular, the microbeam probe indicated that an alloy initially containing 82.2 $\pm$ 0.3 ^{a}/o Rh (in the as-cast condition, as calculated by weight balances) contained only 78 ^{a}/o Rh after 300 hours at 1645^{o}C, and then consisted of a single phase only. It may be that rhodium was lost by vaporization during vacuum heat treatment; this could explain the change in structure of the 85 ^{a}/o Rh alloy from beta to epsilon. Also, since the composition difference between the two phases appears to be very small, the sensitivity of the microbeam probe may be insufficient to resolve the compositions of the individual phases. Additional work in this area seems desirable, although diffusion-couple data can be used to define the solubility limits adequately for present purposes.

Generally speaking, good agreement exists between the present results and those of prior investigations. Raub[2] makes the general statement that rhodium and iridium, when alloyed with the body-centered cubic metals of group VI A, form a c.p.h. intermediate phase having the characteristic structure of the close-packed hexagonal metals of groups VII and VIII. The present work bears this out, both in regard to the W-Rh system, and in the W-Ir system which is discussed in the next section. The results of Greenfield and Beck[3] are also verified by those presented above.

G. Tungsten-Iridium Constitution Diagram

1. General

The proposed constitution diagram for the tungsten-iridium system is given in Figure III:9. The data for this diagram, obtained by techniques previously discussed, is presented below.

2. Presentation of Data

a. Solidus

Preliminary solidi were determined from as-cast alloys, and more careful determinations were made following suitable homogenization. The solidus data from which the diagram was constructed is given in Table III:8.

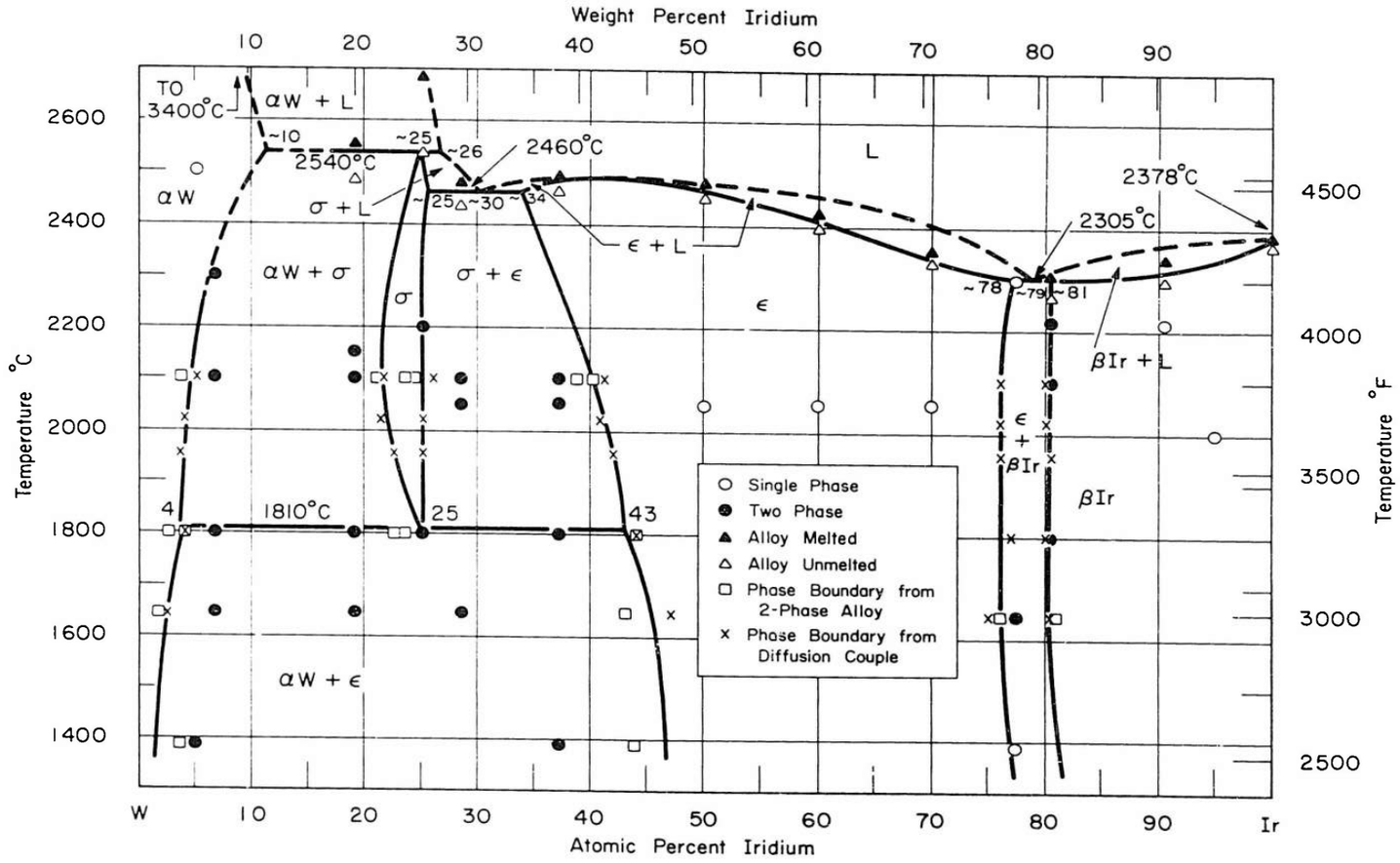

Figure III:9 - Tungsten-iridium constitution diagram.

b. Equilibration

The equilibration treatments given to tungsten-iridium alloys are summarized in Table III:9, along with the phases present in the equilibrated alloys. The homogenization treatment for each alloy is that of the highest temperature shown. This treatment preceded all subsequent equilibrations and was the first treatment given to the as-cast alloys.

Table III:8

Solidus Data - Tungsten-Iridium System

Composition a/o Ir	Maximum Temperature Without Melting °C	Minimum Temperature Melting Observed °C
10	----	2850
20	2485	2550
25	2535	2685
30	2440	2480
40	2460	2490
50	2450	2480
60	2400	2430
70	2330	2355
80	2270	2310
90	2295	2340
100	2370	2385

c. Composition Limits of Phases

The data from which the phase boundaries in Figure III:9 were constructed is tabulated below in Table III:10. The composition ranges of the phases at various temperatures are listed, as are the techniques by which the data was obtained.

d. Metallographic Data

The photomicrographs below in Figures III:10 and III:11 show representative structures of W-Ir alloys. The individual captions of the photomicrographs discuss the structures shown in relation to the phase diagram.

Table III:9

Equilibration Treatments and Phases Present, Tungsten-Iridium Alloys

Nominal Composition a/o Rh	Phases Present As-Cast	Temp. °C	Time hrs.	Phases Present	Temp. °C	Time hrs.	Phases Present	Temp. °C	Time hrs.	Phases Present	Temp. °C	Time hrs.	Phases Present
5	αW	2500	4	αW							1385	417	α + Ε
10	α + σ	2300	24	α + σ	2095	28	α + σ	1800	200	α + Ε	1645	300	α + Ε
20	α + σ	2150	44	α + σ	2095	28	α + σ	1800	200	α+σ + Ε	1645	300	α + Ε
25	σ + Ε	2200	23	σ + Ε				1800	200	σ + Ε			
30	σ + Ε	2050	18	σ + Ε	2095	28	σ + Ε				1645	300	α + Ε
40	Ε	2050	18	σ + Ε	2095	28	σ + Ε	1800	200	α + Ε	1385	417	α + Ε
50	Ε	2050	18	Ε									
60	Ε	2050	18	Ε									
70	Ε	2050	18	Ε									
77.5	Ε + β	2300	4	Ε				1645	300	Ε + β	1385	417	Ε
80	Ε + β	2215	6	Ε + β	2095	28	Ε + β	1800	200	Ε + β			
90	βIr	2215	6	βIr									
95	βIr	2000	4	βIr									

Table III:10

Phase Boundary Data in the Tungsten-Iridium System

Temperature °C	Solubility Range, a/o Iridium								Technique*
	αW		σ		E		βIr		
	Min.	Max.	Min.	Max.	Min.	Max.	Min.	Max.	
2110	0	5	21.5	26.0	41.0	76.0	80	100	2
2095		3.5	21.0	23.5	38.7				1
2095		3.8	21.0	24.1	40.1				1
1800		4.1	22.5		43.8				1
1800		2.6	23.4						1
1800	0	4.0	-	-	44.0	77.0	80	100	2
1645		1.8	-	-	43.0	76.1	81.0		1
1645	0	2.5	-	-	47.0	75.0	80.5	100	2
1385		3.5	-	-	44.0				1

* 1: Microprobe analysis of two-phased alloys.

2: Microprobe analysis of diffusion couples.

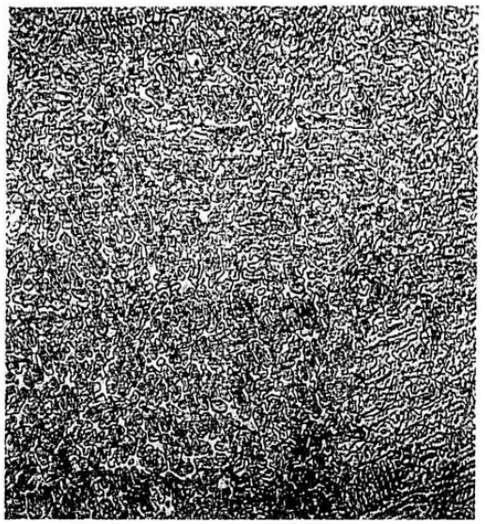

150X Bt. Lt. (a) A-4086-15

10 a/o Ir, 90 a/o W, as-arc-melted. Cored alpha-tungsten plus sigma.

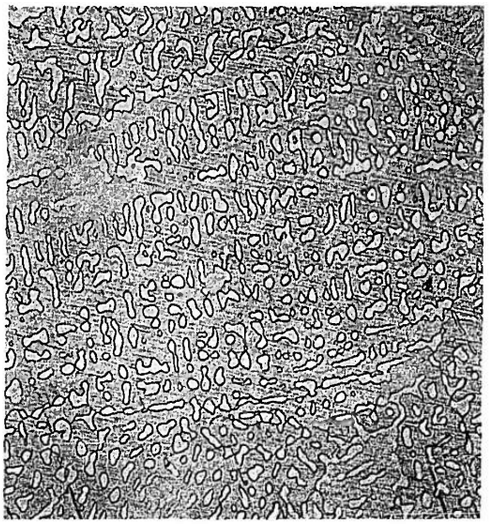

150X Bt. Lt. (b) A-4086-16

10 a/o Ir, 90 a/o W, equilibrated 24 hours at 2300°C. Alpha-tungsten in sigma matrix.

150X Bt. Lt. (c) A-4001-4b

10 a/o Ir, 90 a/o W, equilibrated 200 hours at 1800°C. The sigma matrix has transformed eutectoidally to alpha plus epsilon, and some additional epsilon has precipitated in the primary alpha.

150X Pd. Lt. (d) A-4001-6a

25 a/o Ir, 75 a/o W, equilibrated 200 hours at 1800°C. Untransformed sigma plus fine epsilon precipitate.

Figure III:10 - Microstructures of tungsten-iridium alloys.

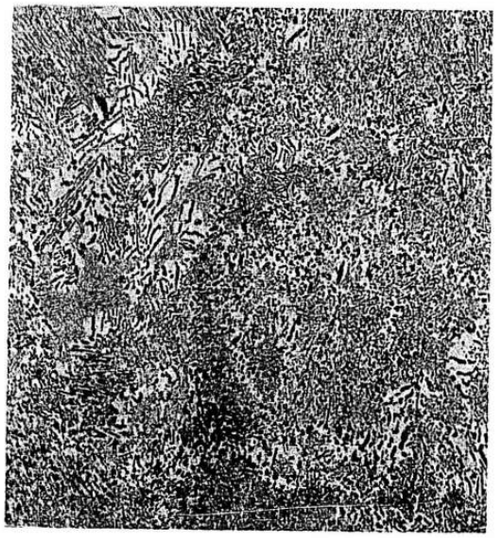

150X Bt. Lt. (a) A-4001-7b

37 ^{a}/o Ir, 63 ^{a}/o W, equilibrated 200 hours at 1800^{o}C. The sigma phase in the eutectic has decomposed eutectoidally. Also, some alpha has precipitated in the primary epsilon.

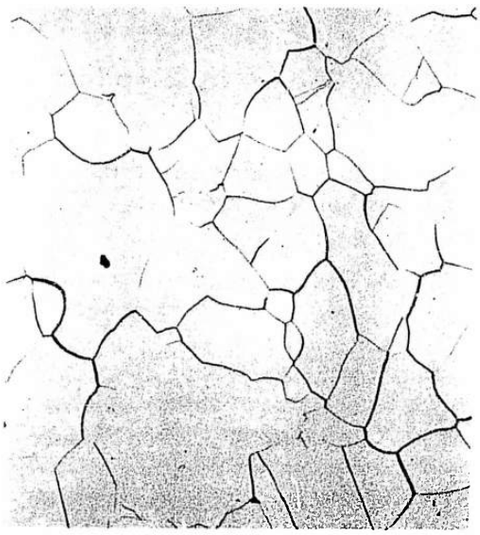

150X Bt. Lt. (b) A-3033-7a

54.7 ^{a}/o Ir, 45.3 ^{a}/o W, as-arc-melted. Single-phase (epsilon) alloy prepared as composition standard.

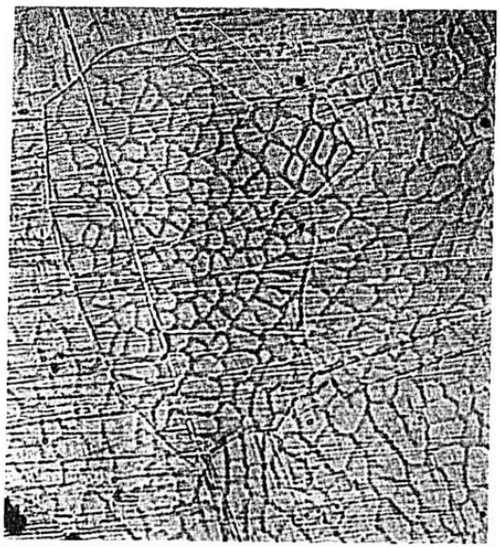

150X Bt.Lt. (c) A-4086-19

80 ^{a}/o Ir, 20 ^{a}/o W, as-arc-melted. Cored beta-Ir.

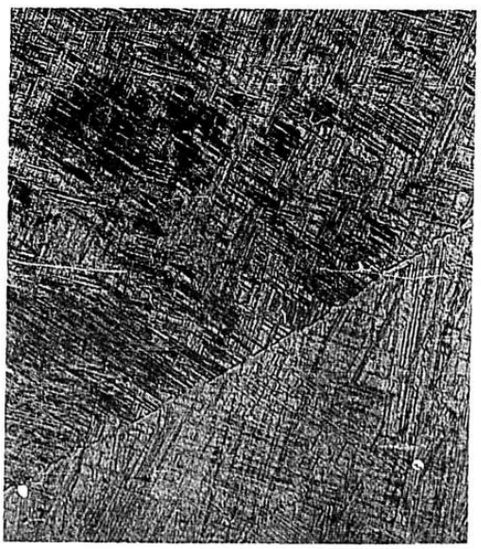

150X Bt.Lt. (d) A-4086-20b

80 ^{a}/o Ir, 20 ^{a}/o W equilibrated 200 hours at 1800^{o}C. Twinned and/or ordered epsilon.

Figure 1:1:11 - Microstructures of tungsten-iridium alloys.

e. Thermal Analysis Data

The eutectoid temperature was determined finally by thermal analysis, having been confined to the vicinity of 1800°C by equilibration runs and by Debye-Scherrer analysis. A tungsten-rhenium thermocouple was used, as previously discussed, to measure the temperature, its output being used to drive a Leeds-Northrup Speedomax Recorder. Three runs were made, using a specially prepared alloy containing 25.29 ± 0.01 a/o Ir. Temperatures were recorded both on heating and on cooling, and the thermal arrest temperatures determined graphically from the chart. All of the arrests fell between 1790 and 1830°C. The invariant temperature is therefore taken as 1810 ± 20°C.

3. Discussion

The constitution diagram of Figure III:9 is felt to be complete and accurate within the limits of the present data. Overall accuracies are as indicated in the discussion of the W-Rh system, i.e., plus or minus 25°C except where otherwise indicated; plus or minus 1 atom percent for solid lines, and plus or minus 5 atom percent for dotted lines.

During the course of the solidus determinations, the melting point of pure iridium was checked and found to be some 75°C lower than the previously accepted value of 2454°C. This disparity was first noted by B. C. Giessen of M.I.T., and verified independently at Nuclear Metals on material from the same source. Giessen's results are presented in the section on the tantalum-iridium system. For the purposes of the W-Ir system, iridium was found to remain unmelted at 2371°C, and to melt completely at 2385°C. Its melting point is therefore taken as 2378 ± 10°C. It should be pointed out that the uncertainty in the sigma decomposition temperature overlaps the temperature variation of the 1800°C equilibration treatment; that is, the phases present in the alloys and diffusion couples could be characteristic of temperatures as high as 1825°C or as low as 1775°C, and the eutectoid temperature is probably between 1790°C and 1830°C. This explains the absence of the sigma phase from the 1800°C diffusion couple and the 10 and 40 a/o Ir alloys, its presence in the 25 a/o Ir alloy, and the presence of three phases in the 20 a/o Ir alloy. (See Table III.9)

Areas which merit further attention in this system include the solvus at the high-tungsten end of the diagram, the solidus between 20 and 40 a/o Ir, and the breadth of the sigma phase at several additional temperatures.

The extent of solubility of iridium in tungsten seems to be a particularly difficult quantity to measure for a number of reasons. First of all, the microbeam probe is quite insensitive in this composition range, giving rise to a rather large scatter in that data. In addition, iridium has very little effect on the lattice parameter of tungsten. The alpha-tungsten Debye lines of a 20 a/o Ir alloy (which also contains sigma) fall at the identical positions as those for pure tungsten. This minimizes the possibilities both of lattice parameter extrapolation and microbeam probe analysis as techniques for determining the solvus. It will probably be necessary ultimately to prepare a series of alloys at close composition intervals (say 2 a/o), and then bracket the solvus by heat treating the alloys at a series of temperatures and identifying the phases present by X-ray and metallographic analyses.

APPENDIX I: ARC MELTER

In this work, Nuclear Metals, Inc. has used a newly constructed nonconsumable electrode arc melter. This arc melter has a water cooled copper hearth with seven depressions in it.

The arc melter has a power source that will deliver up to 1,000 amps at 40 volts D.C. This power supply is equipped with a high-frequency, high voltage arc starter which permits the arc to be started without touching the electrode to the hearth or the specimen.

The hearth chamber is approximately 14 inches in diameter by 16 inches high and is evacuated by a Consolidated Vacuum Corp. MC-275 diffusion pump with a Cenco Hypervac mechanical pump. This pump arrangement has a liquid nitrogen cold trap between the diffusion pump and the hearth chamber and permits evacuation to pressures as low as 5×10^{-6} millimeters of mercury.

The arc melter has a gas purification train as auxiliary equipment. Helium or argon is passed through zirconium chips at 800°C and tantalum chips 600°C before being used as an arc-melting atmosphere. This equipment is also fitted with an auxiliary liquid nitrogen cold trap (not used in purifying argon since that gas boils at a higher temperature than nitrogen).

APPENDIX II: OPTICAL PYROMETRY

Since nearly all temperatures encountered were well above 1000°C, optical pyrometry was the most suitable technique for temperature measurement. The instrument used was a Leeds and Northrup Company portable pyrometer (Catalog No. 8622-C), which had been calibrated at the National Bureau of Standards over the temperature range 800 - 4000°C. The maximum temperature uncertainties over this range are given in Table III:11 below.

Table III:11

Accuracy of National Bureau of Standards Pyrometer Calibration

(Leeds and Northrup Pyrometer No. 776555)

Scale	Temperature (°C)	Maximum Uncertainty (°C)
Low	800	± 4
High	1100	± 3
X-High	2800	± 8
XX-High	2500	± 12
	3200	± 15
	4000	± 20

The pyrometer was calibrated by measuring the pyrometer bulb current as a function of temperature (referred to black body radiation). In service, the filament current was measured by determining the voltage drop across an accurately known resistance in series with the bulb. Calibration of the bulb filament current results in more reliable temperature measurement than can be obtained by calibrating the temperature scale of the instrument directly. Black body radiation was approached for all critical temperature measurements in this work. The criteria for the geometry of cavities necessary to obtain black body radiation were taken from DeVas[4].

Twenty-four new pyrex sight glasses of the same batch and the same thickness were ordered for this work and the transmittence temperature correction was determined experimentally for these glasses. This was done by inserting multiple thicknesses of the glass into the light path of the pyrometer and reading the apparent temperature as a function of glass thickness. Using a number of glass discs the same thickness allowed extrapolation back to a single thickness. Hume-Rothery[5] and others have pointed out that the sight-glass correction is directly proportional to the square of the absolute temperature. The experimental procedure outlined above allows the constant of proportionality to be determined experimentally for given sight-glass optical properties.

One problem of considerable importance at temperatures above 2000°C is the deposition of metal vapors on the sight-glass. These deposits behave as filters, effectively changing the transmittence characteristics of the sight-glass. The technique used at NMI to avoid this difficulty was to insert an additional piece of glass held in a steel carrier, between the sight-glass and the sample. This second piece of glass was kept in the path, shielding the external sight-glass while permitting visual observation of the sample. Then when a temperature measurement was to be made, it was moved out of the path by means of a magnet, thus allowing direct readings of the sample through the clean sight-glass. This technique worked well at all but the very highest temperatures, at which rather large quantities of vapor were given off and some deposit on the sight-glass became unavoidable.

APPENDIX III: HIGH TEMPERATURE VACUUM FURNACE

The furnace with which most of this work was carried out consists of a tubular resistance heating element (usually tantalum or tungsten) housed in a water-cooled vacuum chamber. The heating tube, approximately 1 inch in diameter by 12 inches long, is clamped vertically at its ends for electrical contact, and is surrounded by tantalum and molybdenum radiation shields. The vacuum chamber is evacuated by a diffusion pump backed by a rough mechanical pump with a liquid nitrogen cold trap in the line. This system is capable of pressures as low as 5×10^{-6} millimeters of mercury. The furnace has produced temperatures as high as $2950^{\circ}C$, using a tungsten heating element. Samples placed into the tube are observed through sighting ports located along the side of the chamber, or viewed directly through a port at the top of the chamber. Only the top sighting port is equipped with magnetically operated shutters as described in Appendix II.

APPENDIX IV: A.C. ELECTRO-ETCHING

The following technique was found to be satisfactory for practically all of the alloys investigated.

Each sample was held in a steel clamp and polished mechanically. It was then made one electrode of an electrolytic cell, tantalum being used as the other (inert) electrode. The electrolyte found to give the best overall results was a 20% HCl solution saturated with NaCl. Specific values of current density and time varied with the specific alloy composition. All etching was done at room temperature. Two 110 volt Variacs were connected in series to supply finely adjustable, low-voltage A.C. power.

APPENDIX V: SYNTRON VIBRATORY POLISHING

During the early part of the program, the following technique was used in the metallographic preparation of as-cast and homogenized alloys.

Specimens were mounted in bakelite and mechanically polished. They were then placed in a Syntron vibratory polisher at room temperature for 8 to 16 hours. The slurry used in the Syntron consisted of Linde A (approximately 1/4-micron alumina) and a saturated solution of potassium ferricyanide. This technique achieved only limited success, its main shortcoming being that it was slow and did not give a deep enough etch for many alloys. Subsequent etching with heated etchants was sometimes helpful, but frequently the bakelite was attacked rather than the alloys, leaving a badly stained, barely etched surface.

After the A.C. electro-etching technique (described in Appendix IV) was put into use, the vibratory polishing technique was not explored any further for these alloys.

REFERENCES

1. WADD TR-60-132, "Refractory Metal Constitution Diagrams", Table 3, p. 10.

2. Raub, E., "Metals and Alloys of the Platinum Group", J. Less Common Metals, 1, No. 1, Feb. 1959.

3. Greenfield, P. and Beck, P. A., J. of Metals, 8, No. 2, Feb. 1956.

4. DeVas, J. C., "Evaluation of the Quality of a Blackbody", Physica, 20 (1954) p. 669.

5. Hume-Rothery, W., Christian, J. W., and Pearson, W. B., Metallurgical Equilibrium Diagrams, Institute of Physics, London (1952).

IV. CONSTITUTION DIAGRAMS Ta-Zr and W-Ta-Zr (Work done at Massachusetts Institute of Technology by L. F. Pease, J. H. Brophy and J. Wulff)

A. General

During the period covered by this Final Report an extensive investigation of the binary tantalum-zirconium system has been conducted. As an efficient investigation of the ternary tungsten-tantalum-zirconium system is dependent upon the final outcome of the binary system, work on ternary alloys has been limited to preparation of as-cast alloys and a survey of their microstructures.

Three versions of the binary tantalum-zirconium system exist in the literature. Although there are several regions of agreement among these presentations, there are also important differences. It has become the objective of the present research to resolve these differences. Hansen and Anderko[1] report no intermediate phases in the system and give an approximation of the diagram in the high zirconium region. Their results indicate a eutectoid transformation between alpha and beta zirconium in equilibrium with tantalum solid solution at 820°C and 96.5 atom percent zirconium. In this system, liquid-solid equilibrium involves a eutectic reaction between beta zirconium, tantalum solid solution, and liquid at 1850°C with the eutectic point at 89 atom percent zirconium. Emilyanov, Godin, and Evstyukhin[2] also report a eutectic-eutectoid system but differ with Hansen on temperature and composition. They locate the eutectic at 1585°C and 66 atom percent zirconium and the eutectoid at 786°C and 93 atom percent zirconium. The discrepancies between these melting points is significant and extraordinarily large. A third version of the system by Larsen and Williams[3] appears in a summary report of several years' work, and in a thesis by Williams.[4] Larsen's and Williams' results are considerably different from those of previous research. Their melting transformations involve a minimum in liquidus and solidus at 1800°C and 80 atom percent zirconium. This leads to a miscibility gap in the solid state between two body-centered cubic phases. The monotectoid reaction which represents alpha zirconium in equilibrium with these two solid solutions is located at 800°C and 94 atom percent zirconium, in fair agreement with eutectoid locations of the previous work.

In view of these discrepancies, it is well to consider published experiences in niobium-zirconium alloys which might be expected to show similarity to tantalum zirconium alloys. Two versions of the niobium zirconium binary systems have been published.[5,6] These both show a minimum melting point configuration with a monotectoid reaction, but the temperatures of the monotectoid isotherm, the top of the solid state miscibility gap, and the minimum melting point differ by several hundred degrees centigrade. This has been attributed to differences in impurity content affecting the pseudo-binary configuration.[6]

With this experience in mind, the discrepancies in existing tantalum-zirconium diagrams may eventually prove to be due to differences in impurity levels. Each of the previously proposed diagrams could result from relatively small movements of various phase boundaries by variation of impurity levels. This has been observed in the present investigation by inconsistencies from specimen to specimen and even within the same specimen when oxide contamination was encountered.

In the ternary tungsten-tantalum-zirconium system no published phase information exists. With the determination of the tantalum-zirconium system, each of the component binary systems will be known. The tungsten-tantalum system shows complete solid solubility without melting point maximum or minimum (see for example reference 1). The tungsten-zirconium system shows an intermetallic compound, W_2Zr, forming peritectically at 2150°C with a eutectic at 1660°C and 90 atom percent zirconium and a eutectoid at 860°C and 99.7 atom percent zirconium.

The investigation of the tantalum-zirconium system has included direct and indirect melting point measurements, X-ray diffraction and fluorescence, wet chemical analyses, thermal arrest and resistivity measurements, metallography, and electron microprobe analyses of diffusion couples.

B. Materials

Tantalum was used for melted alloy preparation in the form of commercial 99.7 percent pure powder, sheet, and rod. In diffusion couples rod was used exclusively. Zirconium was exclusively in the form of reactor grade (low hafnium) iodide crystal bar. Commercially pure tungsten powder was used in ternary alloy preparation. Table IV:1 shows these sources and nominal analyses.

C. Alloy Preparation

Alloys were prepared for investigation either by non-consumable arc melting, electron beam melting, or from diffusion couples.

Material for arc melting was weighed on an analytical balance to yield charges ranging from 10 grams for general investigation to 15 grams for thermal and resistance analysis. When powders were used, they were pressed and pre-melted. Pressing was accomplished in a hardened steel die at 15,000 psi without a binder. Melting was accomplished on one of six water-cooled copper hearths in a non-consumable tungsten electrode arc furnace. The furnace was evacuated with a mechanical pump to a pressure of about .2 millimeter, flushed with pre-purified helium or argon, and pumped again. This flushing procedure was repeated five times. The final static atmosphere of 500 millimeters pressure was "gettered" by melting a zirconium button for one minute.

The melting procedure called for placing tantalum or tungsten rich pre-melted button on top of a piece of zirconium of suitable weight. In this way the higher melting component melted down over the zirconium. Each button was melted three to eight times on a side with the zirconium getter button being melted between each cycle. Weight changes were recorded for all alloys, and no alloys which showed change above 1 percent were used. It was found that an argon atmosphere reduced blackening of the copper hearths and made a more manageable arc. No systematic differences in weight loss or structure were detectable between alloys prepared in argon and those melted in helium. Electron beam melting was accomplished at 10^{-4} mm. of mercury residual pressure in a commercial welding unit. Specimens were supported on a copper hearth in a manner similar to that employed in arc melting.

Table IV:1

Material Sources and Nominal Analyses

Material	Source	Designation	Analysis, wt. %
Zr (Iodide bar)	Foote Mineral Company	Reactor grade	O .0235, Fe .0220, C .0110, Mg .0006, N .0006, Mn .0005, H .0040, Mo .0010, Al .0040, Ni .0040, Ca .0030, Pb .0010, Cr .0030, Si .0020, Cu .0020, Sn .0008, Hf .0320, Ti .0005, V .0020
Zr (sheet)	Metals and Controls Corporation	Reactor grade	
Ta (powder)	Fansteel Metallurgical Corporation	Type 268	Ta 99.88, Fe .02, C .01, W .04, Cb .05
Ta (sheet and rod)	National Research Corporation	Metallurgical grade	
W	Fansteel Metallurgical Corporation	Type 425	W 99.9, KCl .08, SiO_2 .027, B_2O_3 .027, CaO .027, O_2 .05
W	Westinghouse Electric Company	Pure undoped type "S"	W 99.9, Fe .02, Ni .002, Si .005, Al .0005, Ca .003, Mn .003, Mg .002, C .004, Mo .003

In both the binary and the ternary systems alloys containing more than 20 percent zirconium were macroscopically homogeneous and free of visible oxide in the as-cast condition. On the other hand arc-cast alloys containing less than 20 percent zirconium were internally oxidized when made from either tantalum powder or massive tantalum melted over zirconium. This problem was avoided by electron beam melting.

Diffusion couples were prepared from tantalum rod and crystal bar zirconium. A one-half inch diameter tantalum rod was drilled with a one-eighth inch hole down its center. The faceted surface of zirconium crystal bar was turned off. The resulting cylinder was swaged, finished turned and polished to a slip fit in the tantalum. Mating surfaces were degreased and lightly etched. The two were assembled and swaged from 0.5 to 0.48 inches outside diameter. Small flats were milled on opposite sides of the outer tantalum jacket and the entire assembly was rolled to 66.6 percent reduction in thickness. The resulting specimen was an elliptical cylinder of zirconium extending down the center of a rectangular shaped tantalum bar 0.5" x 0.125". This bar was cut into 0.25" lengths which were heat-treated at desired diffusion temperatures. This geometry did not permit diffusion rate measurements but was adequate for phase analysis.

D. Composition Determination of Melts

A series of alloy specimens was analyzed by wet chemistry for use as standards in X-ray fluorescence and electron microprobe analysis. The results of this analysis are shown in Table IV:2. Since nominal and wet analyses are close, the former was used throughout the investigation. Critical alloys were checked by X-ray fluorescence techniques.

The remaining halves of buttons analyzed by wet techniques were used as fluorescent standards, along with arc-melted pure components. Fluorescence was excited by a tungsten target X-ray tube operated at 45 KVP and 45 ma in a General Electric XRD-5 spectrometer. A LiF analyzing crystal was used. The intensities of tantalum Lα1 at 44.40° 2θ and second order zirconium Kα1 at 45.94° 2θ were measured by recording total counts as the proportional counter moved through an angle of 0.33° across the point of peak intensity. A complete re-calibration was measured each time the instrument was energized. A typical set of data appear in Figure IV:1 for a 1/8-inch diameter specimen mask. The use of an intensity ratio was established empirically to yield a nearly linear plot for ease in interpolation.

Electron microprobe analyses were made by measuring the intensity of the Lα1 lines for both zirconium and tantalum. The zirconium measurement was made in a helium path unit. The intensity ratio versus composition curves used in this investigation are shown in Figure IV:2. It should be noted that the composition scale is atomic percent in this figure. All microprobe measurements were made by Advanced Metals Research Corporation in Somerville, Massachusetts.

Table IV:2

Nominal and Wet Chemical Analyses of

Several Tantalum-Zirconium Alloys

Nominal Composition Atomic % Zr	Wet Chemical Analysis Atomic % Zr
81.0	80.7
81.2	81.0
80.0	80.2
60.0	60.1
40.0	40.4
20.0	20.7

E. Temperature Measurement

For all temperatures above 1100°C a Leeds and Northrup Optical Pyrometer was used for temperature measurement. This unit was calibrated within ± 5°C with a similar unit standardized by the National Bureau of Standards for Nuclear Metals Inc.

Correction was made for the presence of a slight glass in the optical path by using additional glasses of various thicknesses and extrapolating to zero thickness and zero number of surfaces. Empirically it was found that for a 1/4-inch pyrex glass it was necessary to add a correction to the observed temperature. This was found to be approximately equal to one percent of the observed reading in degrees centigrade from 1100 to 3000°C. All reported temperatures include this correction.

Blackbody conditions were obtained for optical pyrometry by using a resistance heated tantalum filament with a specimen chamber at least 6 to 1 in depth-to-opening ratio. The exact configuration used was developed in this laboratory and has been described elsewhere.(7)

Temperatures below 1100°C were measured with chromel-alumel thermocouples making suitable room temperature cold junction corrections. Furnace temperatures were controlled by the couples to ± 2°C by Wheelco Controllers with cold junction compensation.

F. Thermal Treatments

Alloy heat treatments above 1100°C were accomplished in a dynamic vacuum of 4×10^{-5} mm. of mercury in a tantalum resistance filament described in the previous section. When necessary, alloy buttons were separated from the filament by preheated zirconia chips. On occasion it was desirable to let a zirconium-rich specimen alloy with the filament, and this could easily be accomplished in the

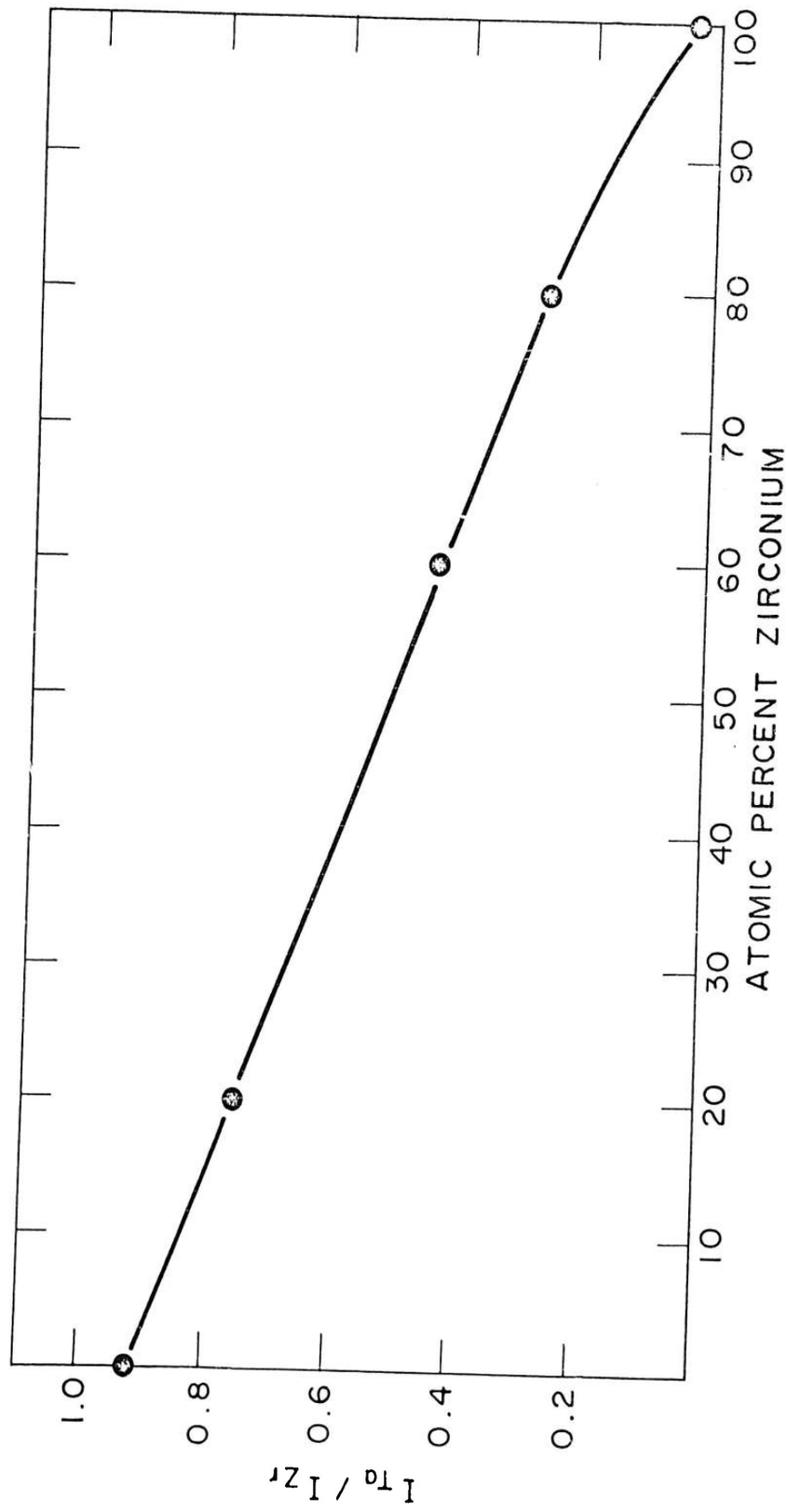

Figure IV:1 - X-ray fluorescent chemical analysis.

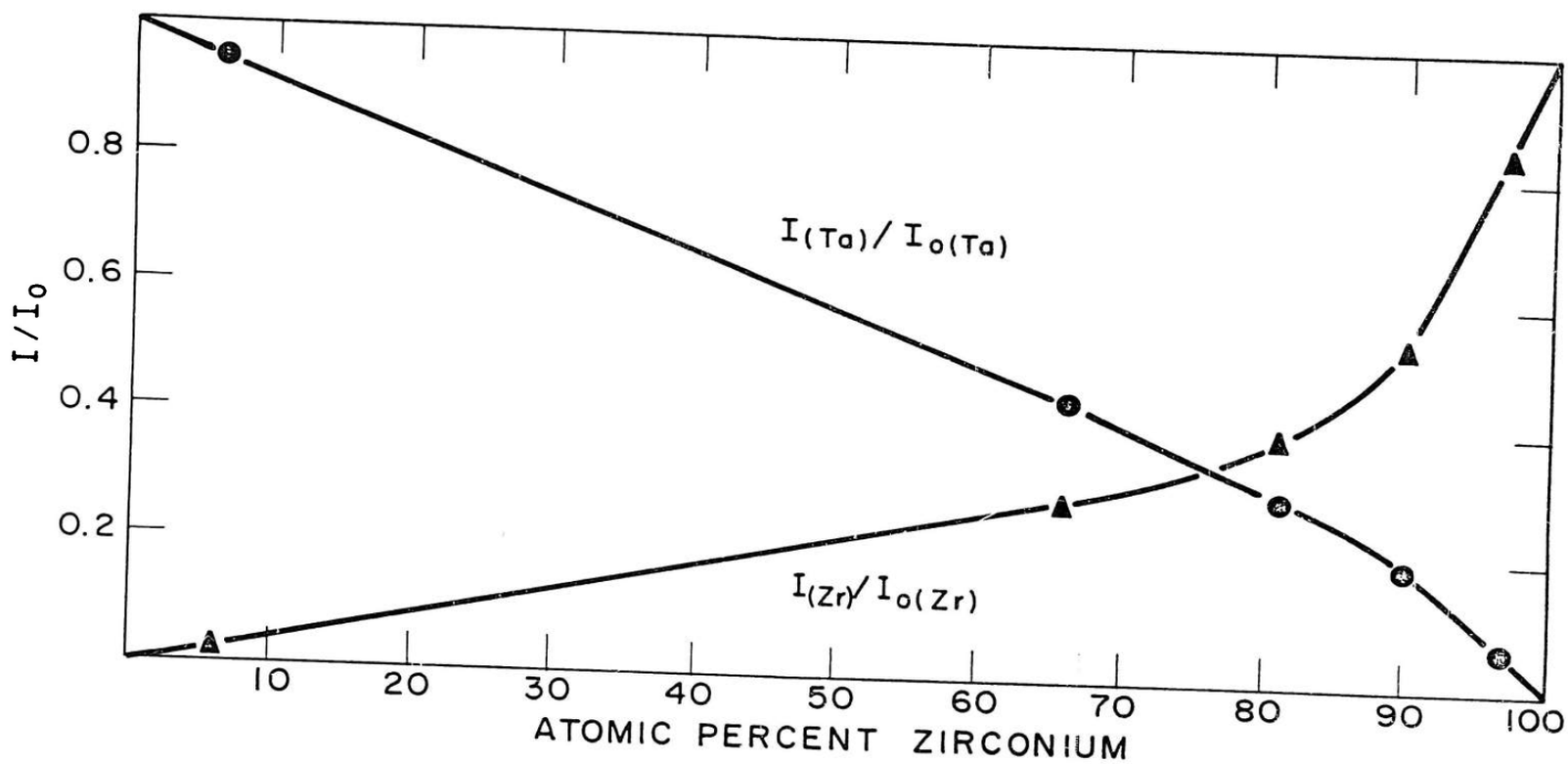

Figure IV:2 - Normalized intensity of characteristic radiation versus composition for Ta-Zr alloys.

normal filament shape. Diffusion couple specimens were heat-treated directly in a boat of this shape. High tantalum alloys frequently showed oxidation of the zirconium-rich phase after heat treatment even when the as-cast button was oxide free. This situation was avoided by wrapping samples in thin zirconium foil before placing them in the tantalum filament.

Homogenization anneals were conducted for 5 hours at 1400°C and the time was doubled for each 50°C interval below. Diffusion couples were heated 20 hours at temperatures above 1200°C and for 120 hours below 1200°C.

G. X-Ray Diffraction Techniques

Powder specimens could be made from all compositions by either crushing or filing. These resulted in patterns for alpha zirconium plus tantalum in all cases since cold working induced transformation in any retained beta phase. Phase identification and limited lattice parameter measurements could be made directly on mounted and polished metallographic specimens. Tantalum solid solution lattice parameter measurements were made by using mounted alloy specimens.

H. Metallographic Techniques

The development of satisfactory polished and etched surfaces for microscopic examination proved to be the most difficult problem in this system. Both terminal solid solutions were easily smeared during polishing. In the observed absence of any intermediate phases, both solid solutions were always present in all but a few alloys. The chemical reactivity of the two solid solutions was considerably different, making the removal of flowed metal difficult. The technique which proved successful was rough polishing through dry 4/0 paper followed by fine polishing with 0.5 micron alumina on a "Syntron" vibratory polisher. This left a surface which was relatively free of relief and of cold work.

Etchants generally required a fluoride ion present. However, satisfactory acid mixtures for high tantalum alloys severely pickled any second phase present. A satisfactory procedure was developed using 2 percent hydrofluosilicic acid and 98 percent concentrated nitric acid for alloys containing more than ten atom percent zirconium. Etching times were varied with tantalum content ranging from a few swabs at low tantalum to 30 seconds near the center of the diagram. Any excess water on the specimen or in the etchant invariably led to pitting. As far as could be detected in this investigation, no surface films were produced which obscured the correct optical activity of the various phases present. For alloys containing less than ten percent zirconium an etchant of 9 parts concentrated H_2SO_4 and 1 part concentrated HF was employed.

I. Solidus and Solvus Measurement

Solidus measurement was complicated by impurity content, large liquidus to solidus span in high tantalum alloys, and difficulty in obtaining homogeneous microstructures. Due to the relatively low diffusivity of tantalum compared to zirconium it was difficult to remove dendritic as-cast structure by heat treatment. Cold working was occasionally helpful, if the as-cast structure was sufficiently ductile to resist fracture on initial breakdown - a common occurrence in Ta-Zr and

Nb-Zr alloys. Since homogenization is a pre-requisite to the metallographic detection of incipient fusion, this method was of limited usefulness.

The melting point results which form the diagram proposed by this research are based on diffusion couple techniques, confirmed by micro-structural results. An alloy heated in a boat of a different metal will apparently melt at the minimum melting point in the binary system between the alloy and the boat metal. While this technique does not show the composition of the minimum nor whether it is a eutectic or congruent melting, it does reveal the temperature.

A variation on the above technique involves careful heating of a tantalum-zirconium diffusion couple above the minimum in the system. At temperatures above the minimum, the interface region can be observed to flow if the specimen is properly located in the heating element. Metallographic examination showed, in some cases, a structure which could only have formed on cooling from a liquid. In most cases macroscopic examination of the sample after removal from the furnace showed evidence of liquid flow at the exposed end of the diffusion couple. The maximum amount of information was obtained in a diffusion couple heated just above the melting point. An electron beam microprobe analysis gave the zirconium-rich solidus, both liquidus lines at the diffusion temperature, and a value for the tantalum-rich solidus. The latter figure may reasonably be in doubt due to "sweeping effect"[8] by which the high diffusivity in the liquid prevents the development of equilibrium solute concentration in the low diffusivity tantalum-rich regions adjacent to it over a distance sufficient to be detected in the microprobe.

Melting observations in diffusion couple specimens as well as between pure zirconium and the tantalum filament were considered to be more dependable than observations by other techniques. Particularly in the swaged and rolled diffusion couple specimens, there was a minimum opportunity for contamination during heating.

Whenever satisfactory microstructures were obtainable, the diffusion couple solvus results were confirmed by metallography of isothermally treated alloy specimens. The lattice parameter technique proved satisfactory for the limit of zirconium solubility in tantalum.

J. Resistance Analysis

The phase diagram in the zirconium-rich region was examined by following the resistance versus temperature behavior of alloys containing 2, 5, 8, 10, and 12 atom percent tantalum. Arc-cast buttons weighing approximately 10 grams were cut into wafers 1/16-inch thick. The wafers were sliced in a maze configuration to lengthen the current path and increase the resistance. Copper current and voltage leads and a chromel-alumel thermocouple bead were spot welded to each specimen. All leads were brought away from the specimen in alundum tubes. A battery-powered current source was employed for the resistance measurement. The voltage drops across the specimen and across a constantan resistor were both measured with a Rubicon potentiometer. The specimen resistance was then computed from the current and voltage data within $\pm$ 0.5%.

The resistance measurements were made in a wire-wound tube furnace in an atmosphere of prepurified helium. Temperature control was $\pm$ 2°C with a Wheelco controller. Readings were taken at 100°C intervals up to 700°C and at 10°C intervals to 900°C. Between temperature changes, 15 to 30 minutes were allowed for thermal equilibrium to be established. Figure IV:3 shows a typical resistance versus temperature curve. The eutectoid isotherm was indicated by the beginning of a sharp decrease in resistance. This decrease continued until the two-phase field above the eutectoid line was crossed. The upper temperature boundary, in some alloys, was indicated by a return to a positive variation of resistance with temperature.

K. Proposed Tantalum-Zirconium Diagram

The proposed binary tantalum-zirconium system appears in Figure IV:4. Where there are inconsistencies in different forms of the data, and composition limits cannot be assigned to better than 5 percent, the system is represented by conventional dashed lines. A more extensive treatment of the data will illustrate the need for this representation.

The existence of a eutectic reaction in this system can be seen in several forms of evidence. Figure IV:5 represents a composition versus distance plot for a pure tantalum-pure zirconium diffusion couple heat-treated for 20 hours at 1575°C. There is clear evidence of an intermediate phase between 72 and 80 atom percent zirconium over a distance in the couple of 25 thousandths of an inch. This intermediate phase was absent in couples heat-treated at 1465°C and below. The fact that the intermediate phase was a liquid was indicated first by a direct observation of flow at the interface while heating a similar couple above 1600°C, and second by its relatively long, flat composition curve. The fact that this liquid was a eutectic composition and not a minimum melting alloy was shown metallographically in the diffusion couple heat-treated at 1575°C. Figure IV:6 shows that this structure consists of rounded tantalum-rich grains surrounded by a fine lamellar eutectic. The eutectic structure was then developed in several alloy specimens. Figure IV:7 shows the structure of an as-cast alloy containing 40 atom percent zirconium. Here primary tantalum and a fine lamellar structure are evident. A coarser form of the eutectic was developed by heating a series of alloys containing 89, 87, 85, 81, 75, and 66 percent zirconium at 1515°C for 20 hours. These were solidified rapidly, and showed increasing amounts of the non-equilibrium eutectiform structure as shown in Figure IV:8. Similarly, solidified alloys containing less than 75 percent zirconium showed a new structure typified by Figure IV:9. This structure is evidently a divorced eutectic whose formation was favored by cooling alloys on the low zirconium side of the eutectic in the resistance filament. Reference should be made to Figure IV:7 for the arc-cast structure of a similar alloy. The possibility that the structure of Figure IV:8 is the result of a eutectoid decomposition may be eliminated by its absence in a similarly treated series at 1190°C.

The eutectic temperature was bracketed with a series of diffusion couples, direct melting observations, and microstructural examination. Diffusion couples heat-treated above 1485°C showed evidence of intermediate liquid phase formation in both structure and analyzed composition, while in those heated below 1465°C this evidence was absent. Several observations of liquid flow between pure zirconium and the tantalum heating filament revealed a minimum melting temperature below 1500°C.

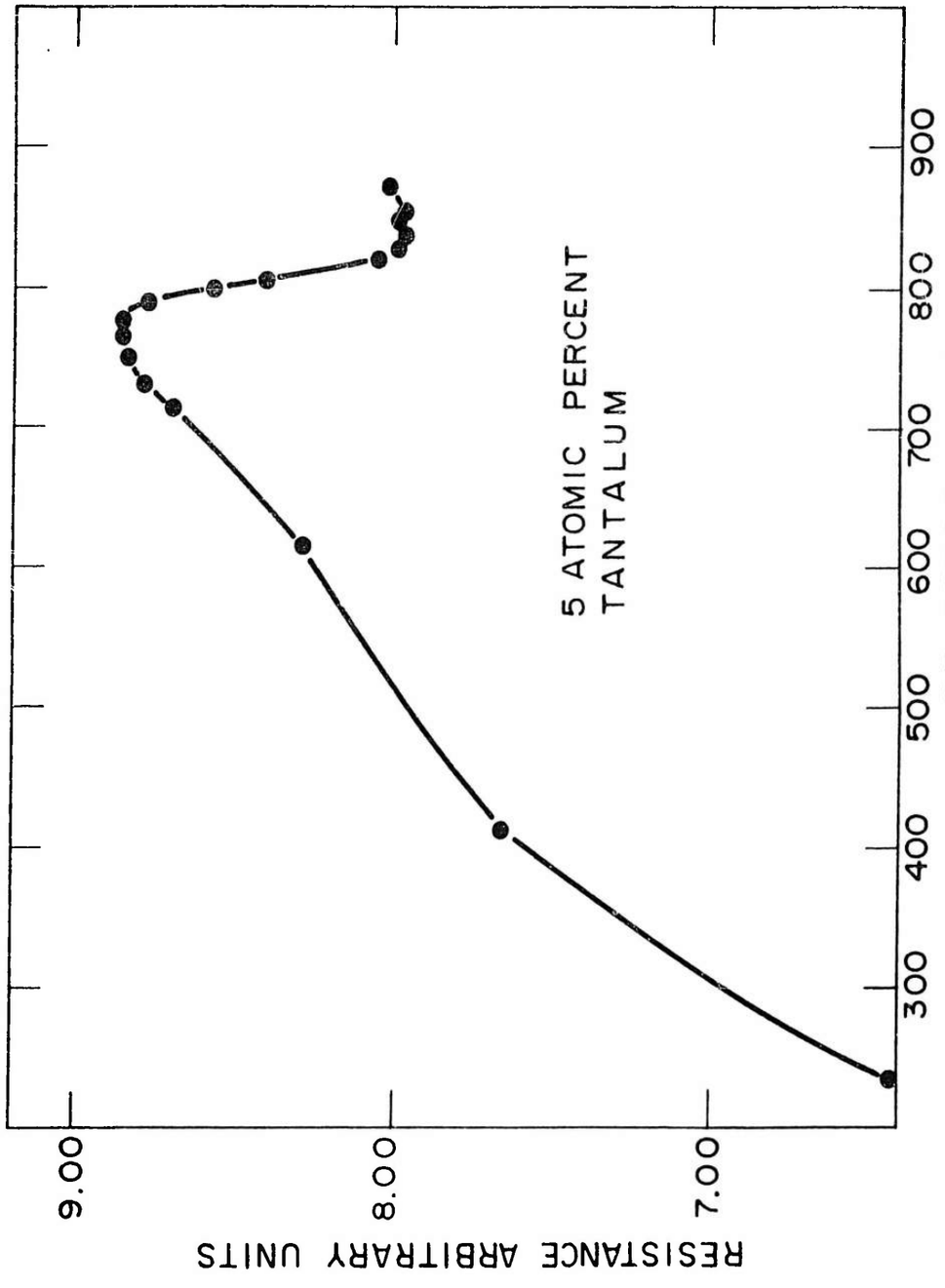

Figure IV:3 - Resistance versus temperature curve for a 95 atom percent zirconium alloy.

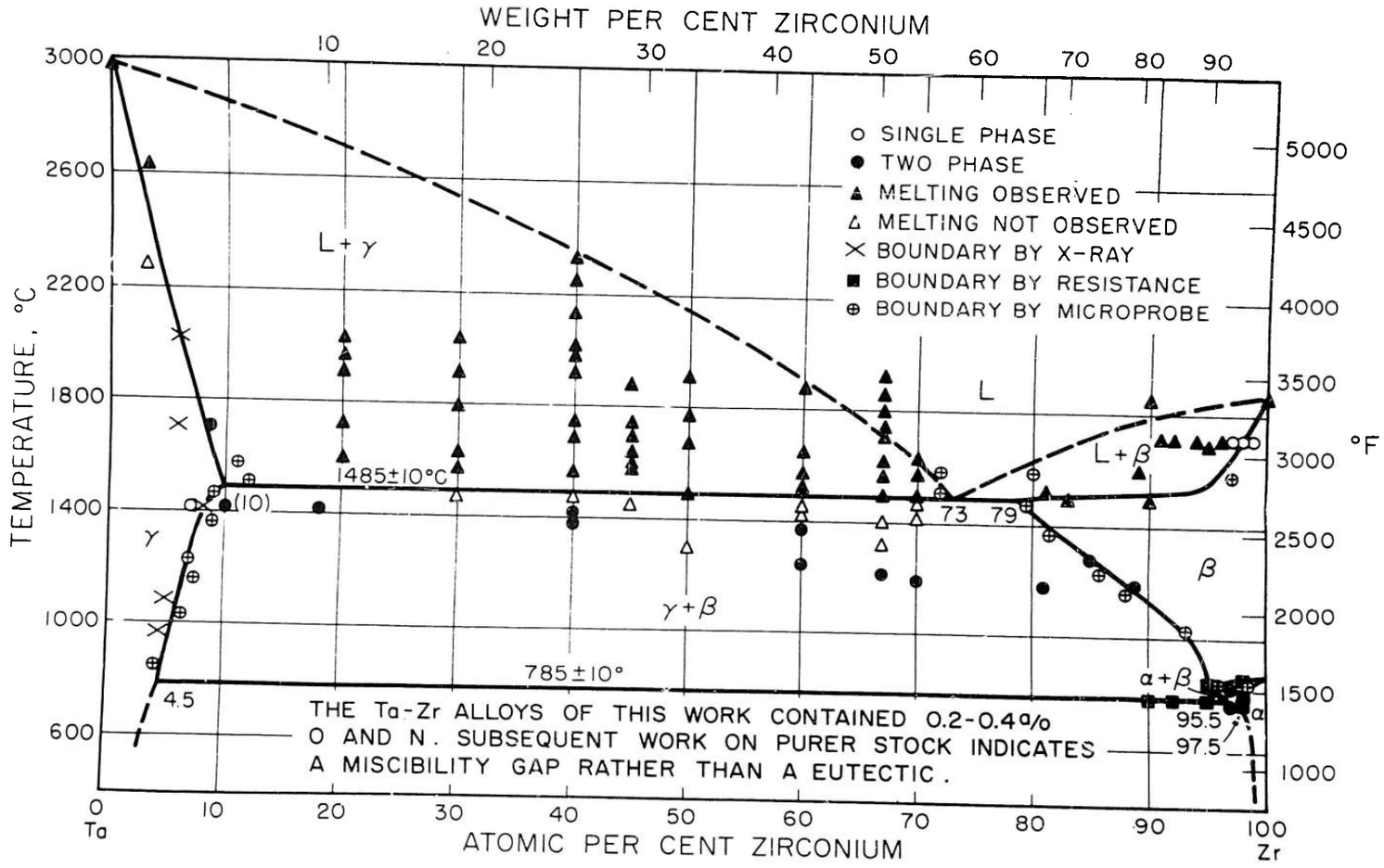

Figure IV:4a - Tantalum-zirconium diagram.

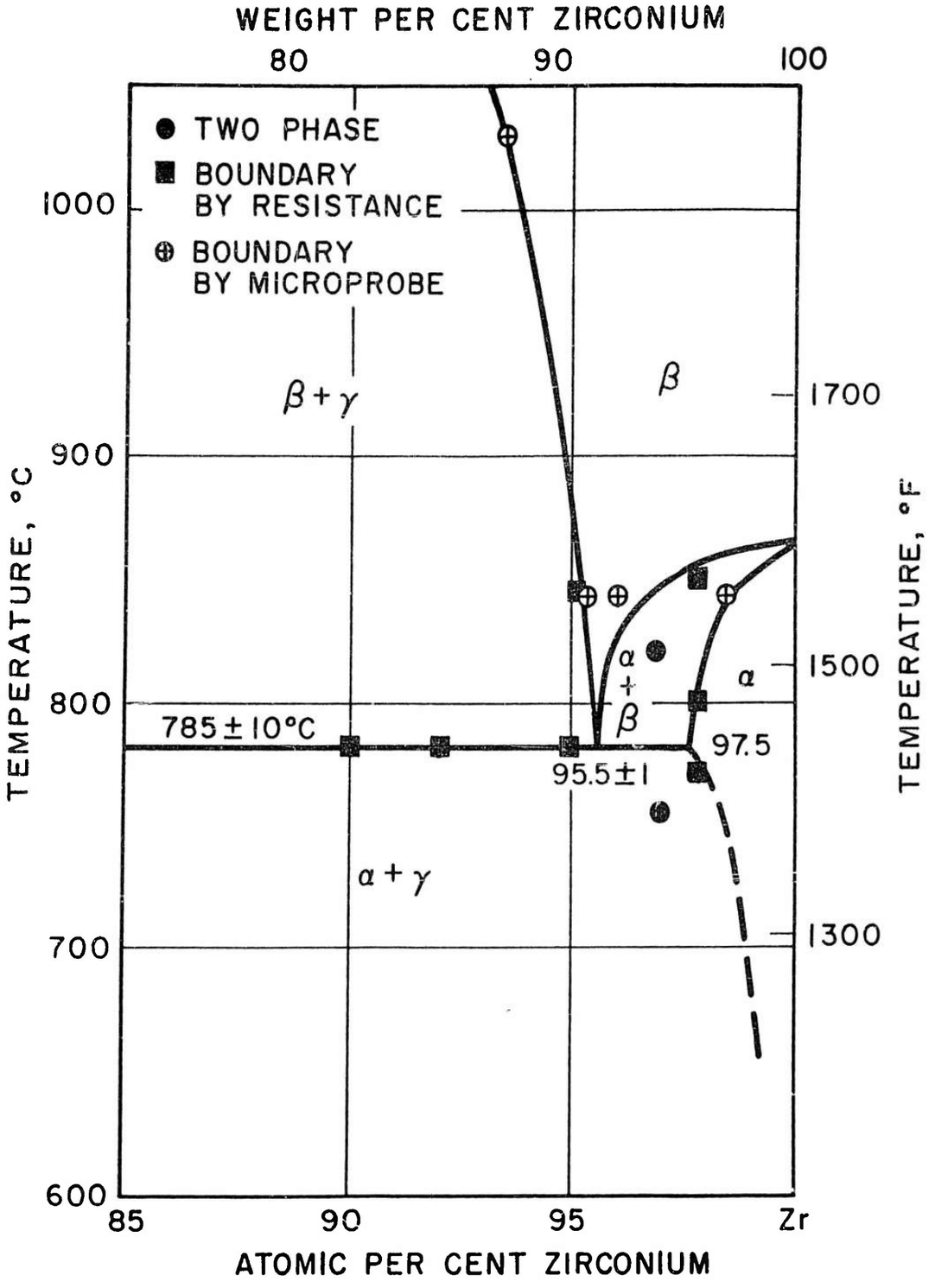

Figure IV:4b - Detailed tantalum-zirconium diagram.

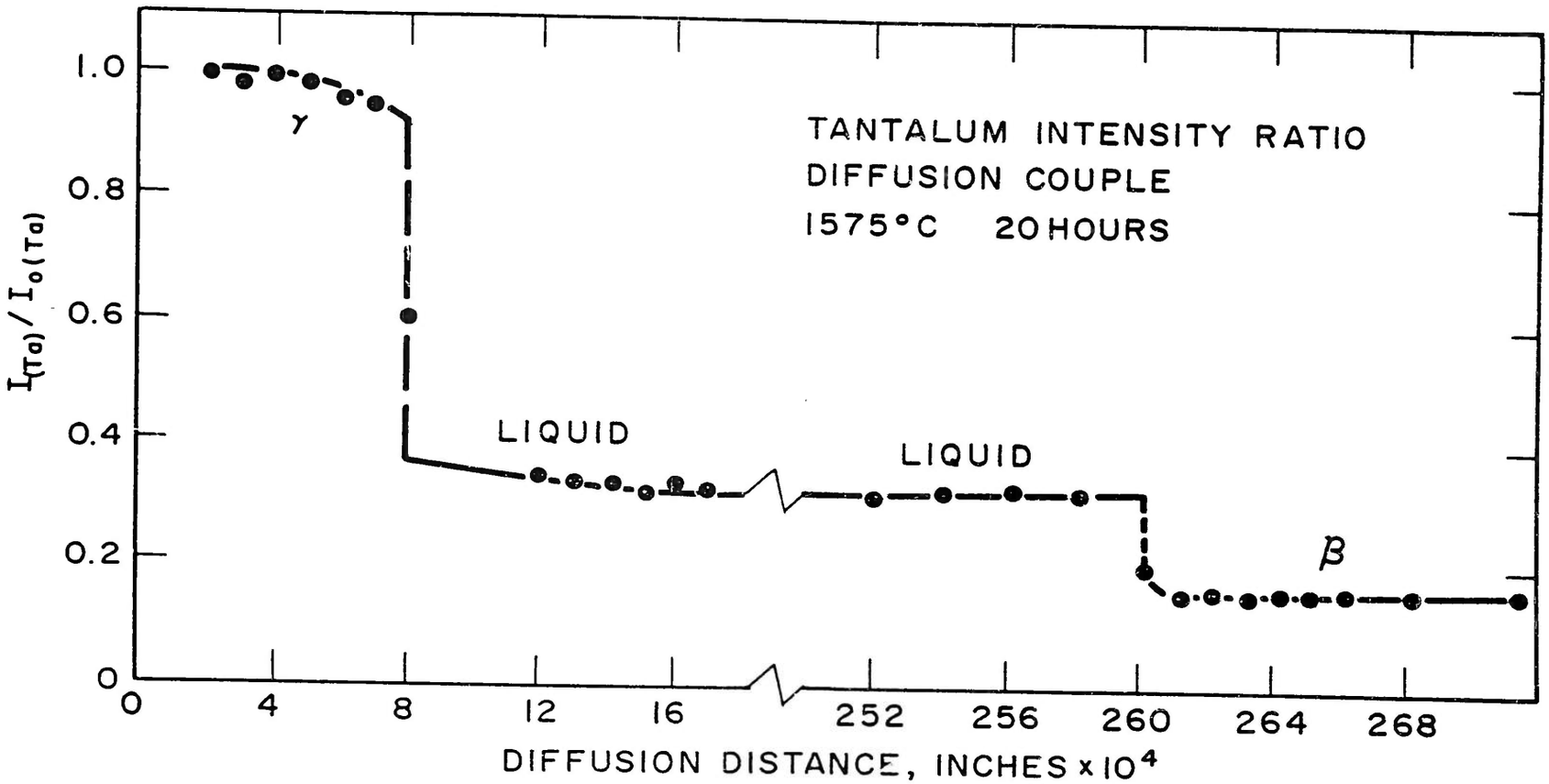

Figure IV:5 - Normalized intensity of tantalum characteristic radiation versus distance for a tantalum-zirconium diffusion couple heat-treated 20 hours at 1575°C.

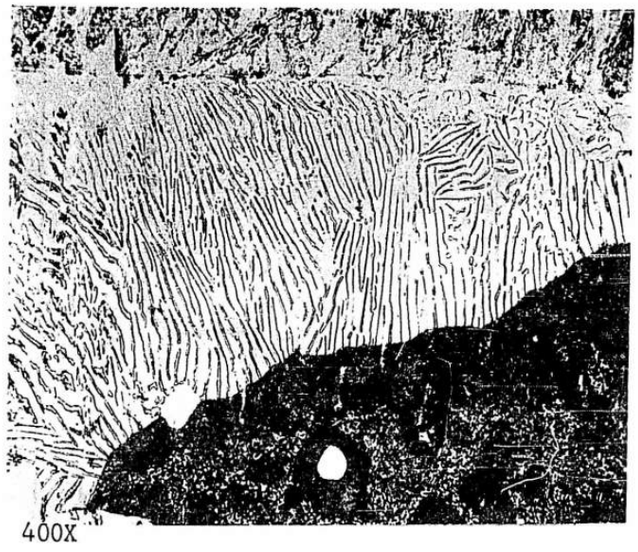

Figure IV:6 - Ta-Zr diffusion couple 20 hours at 1575°C and quenched (γ + eutectic).

1900X

Figure IV:7 - 40 atomic percent zirconium. As-cast. (γ + eutectic)

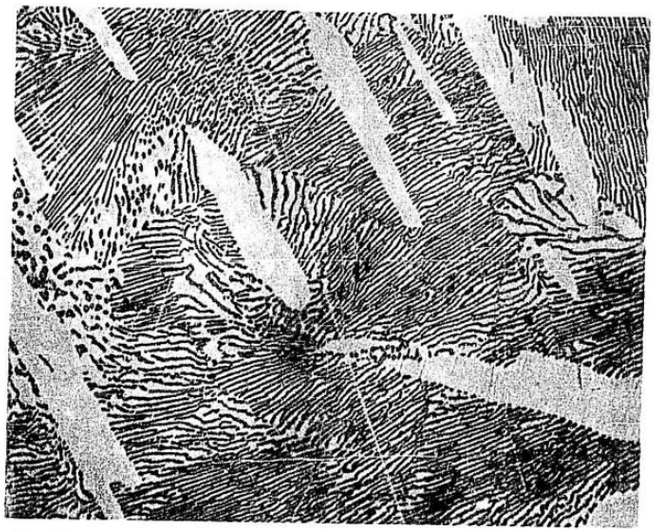

350X

Figure IV:8 - 81 atomic percent zirconium.
20 hours at 1515 °C and quenched.
(α + eutectic)

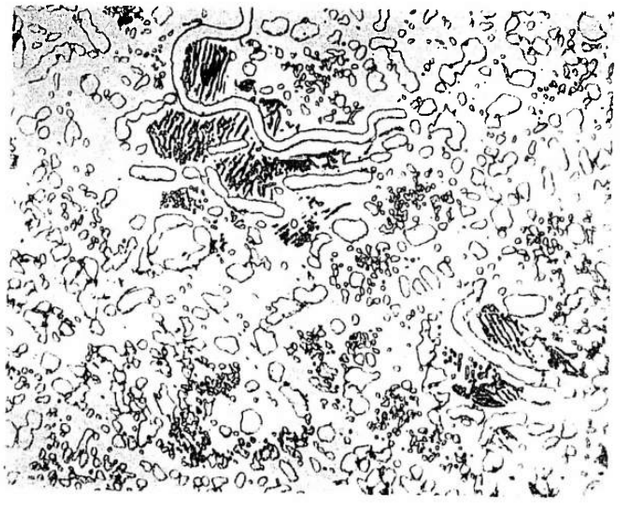

350X

Figure IV:9 - 65 atomic percent zirconium, 25 hours at 1495°C and quenched. (γ + eutectic)

Microstructural evidence of a eutectic reaction at 1475°C may be seen in Figures IV:10, IV:11, and IV:12. These structures all apply to alloys containing 65 to 70 percent zirconium. If heated above the melting point and cooled slowly the eutectiform structure of Figure IV:10 results. If heated below the melting point, the fine precipitate of Figure IV:11 results. Alloys in this same composition range quenched from above the melting point showed an unresolved structure which etched rapidly to reveal large cells, or grains, containing sub cells as shown in Figure IV:12. If this same alloy treatment were etched in 95 percent concentrated H_2SO_4 and 5 percent hydrofluosilicic acid the structure shown in Figure IV:13 results. This latter evidence could easily be erroneously interpreted as retained beta solid solution.

The extent of tantalum solubility in beta zirconium was based largely on diffusion couple data shown in the proposed diagram. These data were confirmed to a limited extent by the observation of isothermal tantalum in a matrix of transformed beta in Figure IV:14 and the complete transformed beta structure of Figure IV:15. The parametric method of solvus determination was unsuccessful in this case since the beta phase could not be retained with any reliability. Several instances of beta retention were observed in as-cast alloys and helium quenched heat-treated alloys at compositions of 85 and 81 atom percent zirconium. This suggests that the tantalum solubility limit is at least this high at the melting point.

The location of the beta zirconium to alpha plus tantalum solid solution eutectoid decomposition was established by resistance measurements, diffusion couples, and metallography. The eutectoid temperature was consistently located at 785°C by resistance evidence such as that of Figure IV:3. This was confirmed by the presence of an intermediate beta phase region in a diffusion couple heated 4 days at 840°C and its absence in a similar couple at 750°C. Metallographic evidence for the eutectoid at 785°C is shown in Figures IV:16 and IV:17. Samples containing 97 percent zirconium were slowly cooled from 900°C to 830, 822, 800, 785, and 750°C and quenched. The structures resulting from the three higher temperatures are typified by Figure IV:16 showing isothermal alpha plus transformed beta. The alloys quenched from below the eutectoid appeared as in Figure IV:17.

The location of the eutectoid composition between 95 and 96 atom percent zirconium is based on the simultaneous extrapolation of resistance and diffusion couple data to the eutectoid temperature. The resistance curves for 92 and 95 percent zirconium alloys showed minima at temperatures of 850 and 830°C. These points combined with solvus locations in the diffusion couple series permitted an accurate extrapolation to 785°C at 95.5 percent zirconium. This composition is further indicated by a change in the beta transformation product as tantalum content increased past the six percent value. This is illustrated by Figures IV:18 and IV:19.

The alpha zirconium single phase field was established by the diffusion couple data indicated on the proposed diagram. It was confirmed by the 98 percent zirconium resistance data which showed inflections at 770, 800 and 860°C. From this it may be concluded that maximum solubility of tantalum in alpha zirconium is between 2 and 3 atom percent tantalum at 785°C.

1300X

Figure IV:10 - 67 atomic percent zirconium, 2 hours at 1545°C, slow cooled to 1250°C, quenched. (γ + transformed β + eutectic)

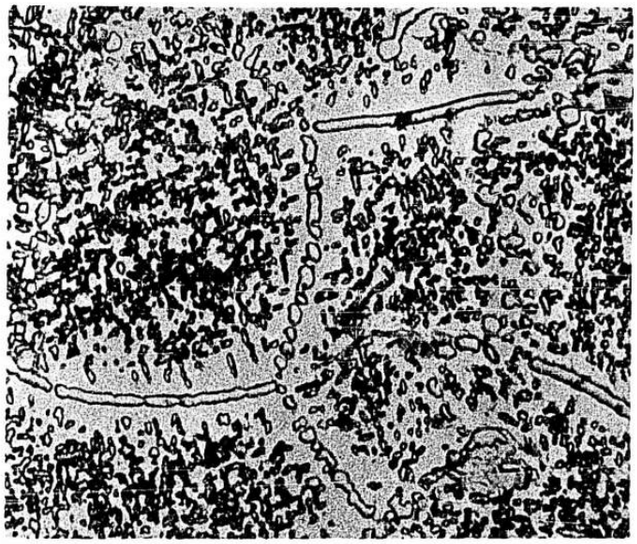

600X

Figure IV:11 - 67 atomic percent zirconium, 2-1/4 hours at 1395°C, slow cooled to 1225°C and quenched. (γ + transformed β)

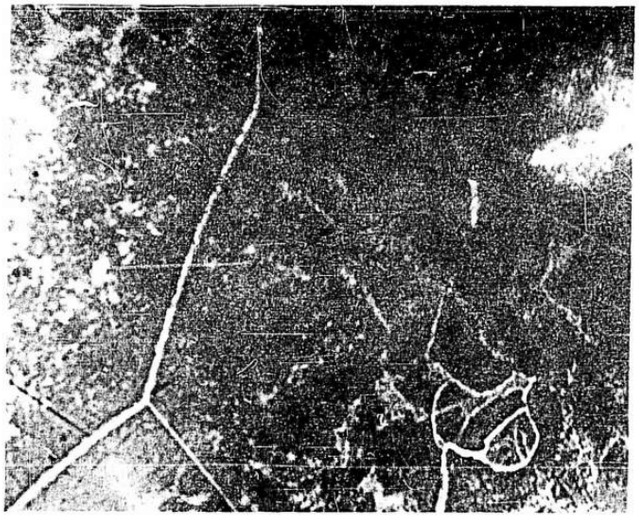

75X

Figure IV:12 - 70 atomic percent zirconium, 2 hours at 1610°C and quenched. (modified eutectic)

300X

Figure IV:13 - 70 atomic percent zirconium, 2 hours at 1610°C and quenched. (modified eutectic)

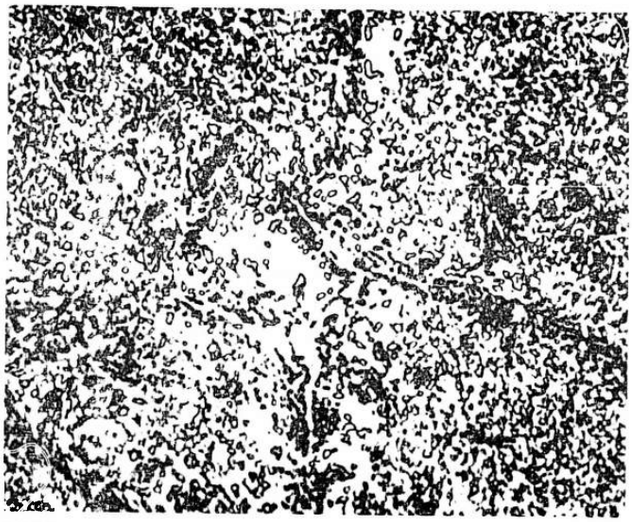

1000X

Figure IV:14 - 85 atomic percent zirconium, 96 hours at 1000°C, slow cooled to 600°C and quenched. (γ + transformed β)

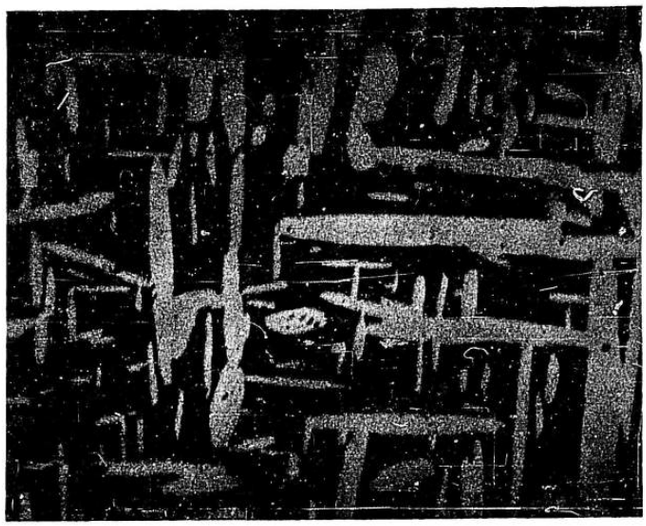

350X

Figure IV:15 - 95 atomic percent zirconium, 15 hours at 1475°C, 14 hours at 1275°C and quenched. (transformed β)

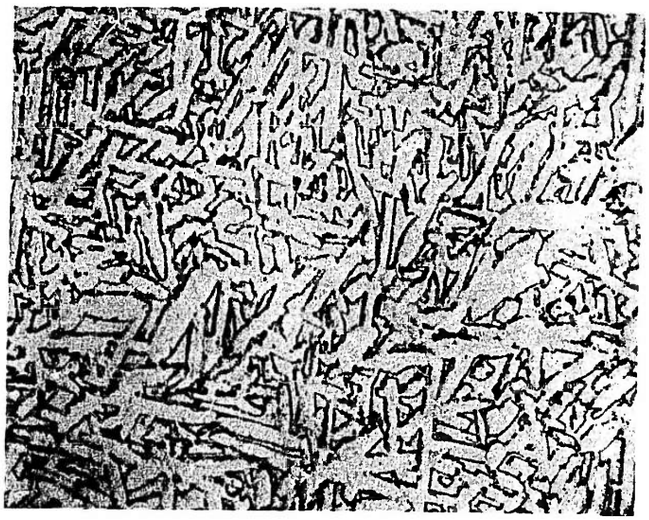

350X

Figure IV:16 - 97 atomic percent zirconium, 3 hours at 1000°C, slow cooled to 822°C. (α + transformed β)

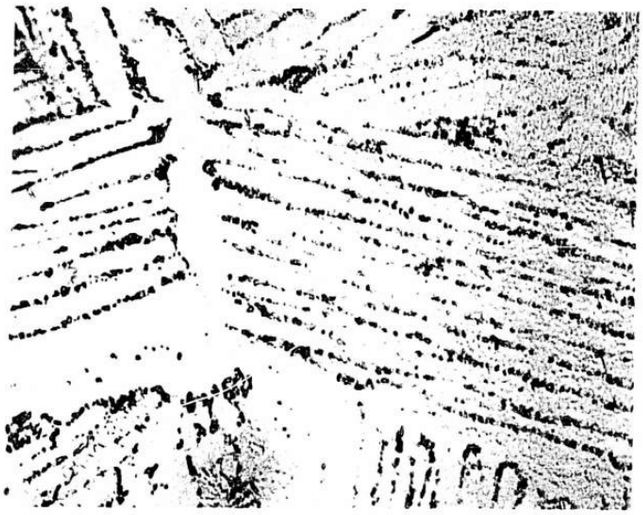

800X

Figure IV:17 - 97 atomic percent zirconium, 3 hours at 1000°C, slow cooled to 758°C, quenched. (γ and transformed β)

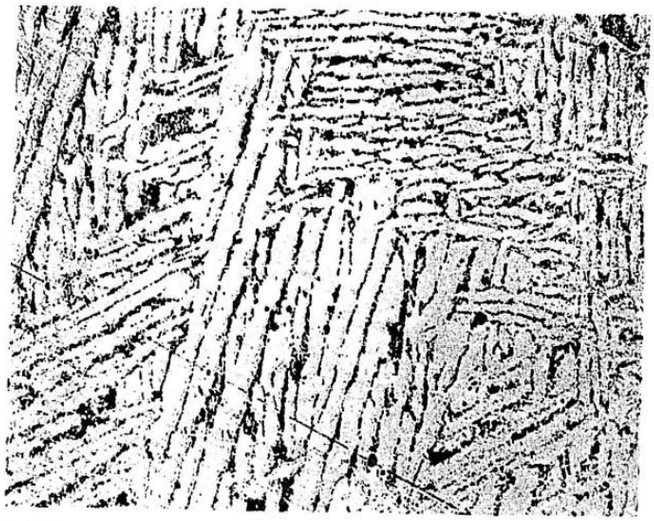

800X

Figure IV:18 - 96 atomic percent zirconium, 24 hours at 1000°C, slow cooled to 600°C, quenched. (transformed β)

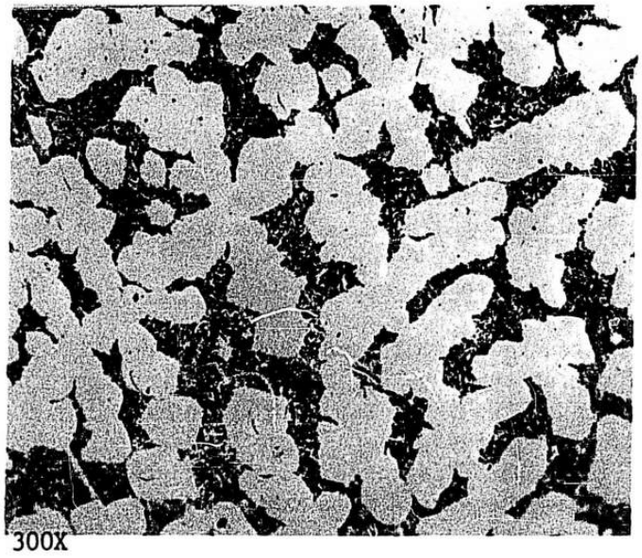

Figure IV:19 - 95 atomic percent zirconium, 24 hours at 1000°C, slow cooled to 600°C and quenched. (α + transformed β)

The extent of the single phase γ tantalum region was based largely on diffusion couple data. As a result of the possibility of errors in this figure due to widely differing diffusivities in adjacent phases,[8] the solubility limit in the proposed diagram represents the minimum amount of zirconium soluble at the various temperatures. More refined techniques should show at least this amount of zirconium soluble, and perhaps more.

Microstructural examination and lattice parameter measurements were of limited usefulness due to the great tendency for internal oxidation in high tantalum alloys. Figure IV:20 shows that a 7 atom percent zirconium alloy contains a single phase at 1415°C, while Figure IV:21 shows that a 10 percent zirconium alloy contains two phases at 1415°C. These results were substantiated by lattice parameter measurements on single phase tantalum base alloys and two phase alloys toward the center of the diagram. These results are shown in Figure IV:22.

L. Investigations in Ternary Tungsten-Tantalum-Zirconium Alloys

Ternary tungsten-tantalum-zirconium alloys were arc-melted at 10 atom percent intervals throughout the system. These were sectioned, polished, and etched by the same techniques as those found to be satisfactory in the tantalum-zirconium system. Phase identification was made by X-ray diffraction and metallographic examination. Table IV:3 indicates the phases present in as-cast alloys in regions of composition which were free from oxide. There is no evidence of new ternary intermediate phases in the as-cast condition.

Table IV:3

Phases Present in As-Cast Ternary Alloys, as Determined by X-ray Diffraction

a/o Zr	a/o W	a/o Ta	α	β	γ	W_2Zr
80	10	10	tr	m	m	tr
70	10	20	tr	l	m	0
70	20	10	l	m	l	0
60	10	30	l	tr	tr	0
60	20	20	m	m	l	0
60	30	10	m	m	l	0
50	20	30	m	0	l	0
50	30	20	m	tr	m	0
50	40	10	m	m	m	0

0 = none
tr = trace
m = medium amount
l = large amount

650X

Figure IV:20 - 7 atomic percent zirconium, 66 hours at 1400°C, and quenched. (γTa)

Figure IV:21 - 10 atomic percent zirconium, 66 hours at 1400°C and quenched. (γTa and transformed β)

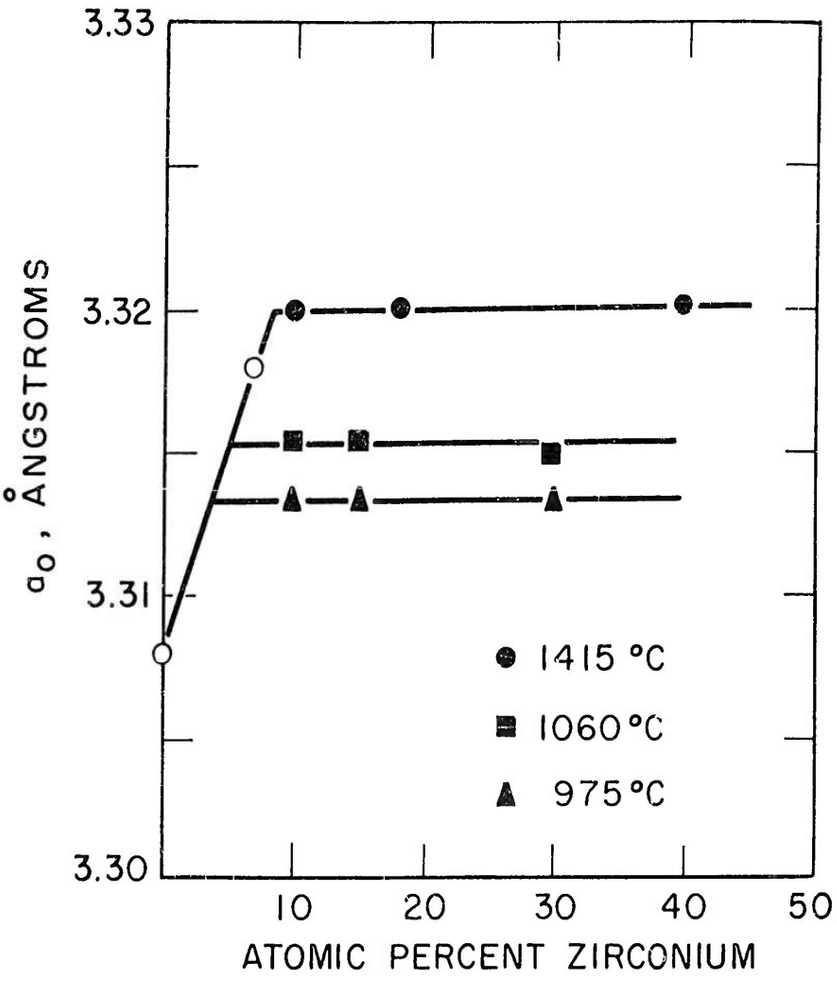

Figure IV:22 - Dependence of the tantalum solid solution lattice parameters on zirconium content.

REFERENCES

1. M. Hansen, K. Anderko, Constitution of Binary Alloys, 2nd Ed., McGraw-Hill, New York (1958) p. 1226.

2. V. S. Emelyanov, Yu. G. Godin, A. J. Evstyukhin, "An Investigation of the Zirconium Tantalum System", Atomnaya Energiya 2 42 (1957), translated by J. Adam, J. Nuclear Energy II (1957) 5, p. 247.

3. W. L. Larsen, D. E. Williams, "Tantalum Zirconium System", Annual Summary Research Report in Metallurgy, Ames Laboratory, Iowa State University, IS-93, December (1960), p. 35.

4. D. E. Williams, "Determination of the Tantalum Zirconium Phase Diagram", M. S. Thesis, Iowa State University, Ames, Iowa (1961).

5. B. A. Rogers, D. F. Atkins, "Zirconium-Columbium Diagram", Trans AIME, 203 (1955) p. 1034.

6. R. F. Domagala, D. J. McPherson, "Discussion of Zirconium-Columbium Diagram", Trans AIME, 203 (1955) p. 1034.

7. J. H. Brophy, P. Schwarzkopf, "Solidus Measurement Technique for the Tantalum-Rhenium System", Trans AIME, 218 (1960), p. 184.

8. N. L. Peterson, R. E. Ogilivie, "Diffusion in U-Nb Alloys", Trans AIME, 218 (1960), p. 439.

V. CONSTITUTION DIAGRAMS Mo-Os and Mo-Re-Hf (Work done at Westinghouse Research Laboratories by Dr. A. Taylor, Mr. N. J. Doyle and Miss Brenda Kagle).

A. General

The contribution of the Westinghouse Research Laboratories to the Refractory Metals Phase Diagram Program is the determination of the constitution diagrams Mo-Os and Mo-Re-Hf, concerning which very little published data are available.

On account of the highly oxidizable nature of the constituent elements and their alloys, coupled with their high melting points and the high temperatures required to produce homogeneity and thermal equilibrium, special furnaces were required. These were available from a previous refractory alloys investigation on the W-Os, Mo-Hf and Re-Hf systems contained in WADD Technical Report 60-132 with the exception of a specially designed tungsten tube annealing and melting point furnace capable of operating at 3000°C. This furnace will be described in the present report.

B. Materials

The alloying elements were of the highest purity obtainable. These consisted of the following:

1. Molybdenum

This was prepared by the Technology Department of the Westinghouse Research Laboratories by the hydrogen reduction of ammonium molybdate at 1100°C. Analysis of the reduced powder gave, in parts per million, Cr 100, Fe 10, Al 30, Mg 50, Co 30, Mn 50, Si 80.

No other sources of supply were considered. The powder was stored in sealed air-tight tins. Before alloying, however, it was found beneficial to compress the powder into small slugs weighing from 5 - 10 grams and degas in an induction furnace at 1200°C in a vacuum of 10^{-5} - 10^{-6} mm Hg.

2. Osmium

Pure osmium sponge supplied by Baker, purity given as 99.99 percent. No N_2; C not detected; O_2 negligible.

No other source of supply considered.

3. Rhenium

Rhenium was supplied by the Chase Brass and Copper Company, Pittsburgh. The purity was 99.99 percent with the following impurities: Fe 0.0011 percent; Cu, Mg, Ca, Al and Si, 0.0001 to 0.001 percent; K approximately zero (by flame photometry); O_2 probably 10 ppm; C and N not analyzed.

Alternate source of 99.99 percent pure rhenium: Varlacoid, New York City.

As in the case of molybdenum, the rhenium was degassed prior to alloying.

4. Hafnium Crystal Bar

Hafnium was supplied by the Foote Mineral Company and obtained from the AEC, Pittsburgh Naval Reactors Office via Nuclear Metals Inc. The specification and grade was POS-11553. A typical analysis of the material in parts per million was as follows: N 20, C 40, Al 50, Cu 20, Ti 35, W 20, Fe 150, Zr 23,000 (2.3 percent), Cl 300.

C. Alloy Preparation

Usually alloys were made as 30 gram buttons. After carefully weighing the powdered ingredients, or fine turnings in the case of the crystal hafnium bar, the mixtures were compressed into small slugs at a pressure of about 10 ton/in.^{2}. In the case of Mo-Os alloys, the slugs were sintered and degassed in a high frequency induction furnace operating at 1200^{o}C and 10^{-5} - 10^{-6} mm Hg. Melting of all the alloys was carried out in a Kroll type furnace having a water-cooled copper hearth, non-consumable tungsten electrode, and a purified argon atmosphere.

Previous experience with alloys in the W-Os, Mo-Hf and Re-Hf systems had shown that weight losses during melting were exceptionally small. This proved to be the case in the present series of alloys, so that, in general, it may be assumed that the final compositions of the alloys correspond very closely to the original weighed-out values.

In the arc melting process, care was taken first to evacuate the system to 10^{-4} mm Hg by means of a mechanical oil pump. The furnace was then flushed four times with research grade argon, pumping down to 10^{-4} mm each time. It was then filled with argon to one half atmosphere pressure and the gas carefully scavenged by melting a 15 gram titanium button which was held molten for about 3 minutes. The arc was then shifted over to the sample until the whole mass was completely molten. After cooling, the alloy was turned over without opening the furnace and remelted. This operation was repeated at least three times and sometimes as many as six, according to the appearance of the button. Not only was this remelting process desirable to ensure complete homogeneity of the finished sample, but it was found that an arc current of more than 350 amperes was absolutely essential to ensure freedom from unmelted particles and segregated areas. Samples prepared in this manner usually had an excellent, clean, mirror-like, and silvery appearance. Any alloy showing signs of possible contamination was discarded. The rapid cooling from the molten state on the water-cooled hearth conferred a typical "as-cast" structure on the alloy samples.

D. Composition Determination of Melts

In conformity with past experience with analogous alloys made and heat treated under similar conditions, the weight losses sustained are so trivial and the X-ray and micrographic results so self-consistent, that little would be gained

by chemical analysis, except in a few isolated cases. In general, it was found more expedient to repeat an alloy of dubious composition or faulty heat treatment.

Some losses were sustained when annealing under vacuum for long periods near the solidus temperature. As shown by micrographic examination, such losses were invariably confined to a sharply delineated layer, the thickness of which was, at most, only a few thousandths of an inch. This impoverished layer was always removed prior to the preparation of powder samples for X-ray diffraction analysis, so that the X-ray results were always representative of the weighed out compositions and the microstructures.

E. Temperature Measurement

All temperature measurements were made with the same Leeds and Northrup disappearing filament optical pyrometer which was calibrated at the Bureau of Standards to temperatures in excess of 4000°C. According to them the maximum uncertainties in the temperatures reported for the low, high and extra-high ranges decrease from about $\pm 4^{\circ}$ at 800°C to about $\pm 3^{\circ}$ at 1063°C, and then increase to about $\pm 8^{\circ}$ at 2800°C. For the extra high range, the maximum uncertainties were about $\pm 12^{\circ}$ at 2600°C, $\pm 15^{\circ}$ at 3200°C, and about $\pm 20^{\circ}$ at 4000°C.

When using the tungsten tube annealing furnace a correction had to be applied to the pyrometer reading to take into account the size of the hole through which the observation was made to simulate black body conditions and the reflections from the double-quartz windows. Observations were made through a 1/8-inch diameter sight hole on to the rear inner surface of the tungsten furnace tube using one, two, ... six clear quartz windows (2 ... 12 reflecting surfaces) and recording the observed temperatures. These values plotted as an almost straight line which was extrapolated back to zero sight glasses. Some typical pyrometer readings with 1 ... 6 sight glasses were 2505°, 2480°, 2455°, 2430°, 2395°, and 2365°C, with an extrapolated value at zero sight glasses of 2539°C. Curves for temperatures in the range 1245° to 2850° C ran almost parallel to this.

The emissivity of the 1/8-inch diameter spy hole was estimated to be 0.994, so that any errors resulting from this slight departure from unity could be neglected. A calculation of the temperature difference between the sample and the walls of the furnace tube showed it to be of the order of 1 or 2 degrees and this was also neglected. The corrections required to account for reflections from the surfaces of the quartz windows, is as we have seen, far from negligible. The corrections obtained experimentally for the double windows (4 reflecting surfaces) tit in with the theoretical values computed using Planck's law are a value of 0.835 for the transmittance.

The corrected temperature T_{true} is given by the expression

$$T_{true} = \frac{C_2}{\lambda\{\log_e 1 + t\ [\exp\ (C_2/\lambda T_{obs}) - 1]\}}$$

where C_2 = 14384.7 micron-degrees,

λ = 0.6500 microns,

and t = 0.835, the transmittance.

In Table V:1 are given the corrections to be applied in the case of a single pyrex window (t = 0.91) and a double quartz window (t = 0.835), the former values being required for correcting the temperatures observed in the induction furnace used for the lump annealing of certain specimens.

Table V:1

Corrections for Various Values of Transmittance

$T_{obs.}$ °C	Correction to be added °C for transmittance t	
	One Pyrex or Quartz Window t = 0.91	Double Quartz Window t = 0.84
1500	14	26
1600	15	29
1700	17	32
1800	19	36
1900	20	39
2000	22	43
2100	24	47
2200	26	50
2300	29	54
2400	31	59
2500	33	63
2600	36	68
2700	38	72
2800	41	77
2900	43	82
3000	46	88

F. Melting Point Determinations and Thermal Treatment of Solid Ingots

Because of the extremely high temperatures required for melting point determinations and thermal treatment, conventional wire-wound ceramic tube furnaces were completely inadequate. A special tungsten tube furnace capable of operating at 3000°C with a vacuum of 10^{-5} - 10^{-6} mm Hg was constructed for melting point determinations and occasional heat treatment work, while most long-term thermal annealing was carried out in a conventional induction furnace.

Figures V:1 and V:2 illustrate the construction of the furnace and its general layout. The working element consists of a vertical tungsten tube 9-1/2 inches long and 1-1/4 inch diameter, the wall thickness being 0.020 inch. The tube is surrounded by three concentric tantalum radiation shields resting on a tantalum support which also serves as the lower electrical connection to the tungsten tube. This connector is, in turn, supported by two hollow water-cooled stainless steel conductors connected in parallel and capable of carrying a current of 3000 amperes. The upper connection to the tungsten tube is likewise supported on water-cooled stainless steel conductors arranged at 90° to the lower ones, but the final connection is made via a laminated flexible cantilever consisting of several layers of 0.005 inch thick tantalum strip. This provides sufficient flexibility for the expansion of the furnace tube on heating.

The specimen itself is normally suspended on a thin wire which may be of tungsten, rhenium, molybdenum, tantalum or hafnium according to the nature of the material being heat treated and its tendency to form low temperature eutectics with the suspension. The latter is itself hung from a thin tungsten wire bridge which may be shorted across a power transformer and fused to enable the specimen to fall through the furnace and be instantaneously quenched in a bath of molten tin.

The specimen may be observed during heat treatment via a 1/8-inch diameter spy hole drilled in the wall of the tube, or from above. Since radiation through the spy hole conforms closely to black-body conditions, the hole is used for temperature measurements by means of an optical pyrometer, the sighting of the instrument being made on the rear inner wall of the heater element, corrections being applied, as described above, for the transmittance of the double quartz windows in the viewing port. In order to ensure that condensed metal on the viewing port does not seriously affect the temperature reading, the innermost window is made rotatable to ensure a perfectly clean surface for each observation. Finally, to ensure freedom from contamination by carbonaceous products from conventional pump oils, the furnace was evacuated by means of a mercury vapor pump fitted with a suitable baffle and liquid nitrogen traps.

The high frequency furnace employed for the bulk of the long term heat treatments operated with a vacuum of 10^{-5} - 10^{-6} mm pressure using a mercury vapor pump and liquid nitrogen trap similar to that used for the tungsten tube furnace. Inside the coil was a cylindrical susceptor of either tungsten or molybdenum, according to circumstances, its length being 4 inches and outside diameter 1-3/4 inches, the wall thickness being approximately 3/16 inch. This was closed by a

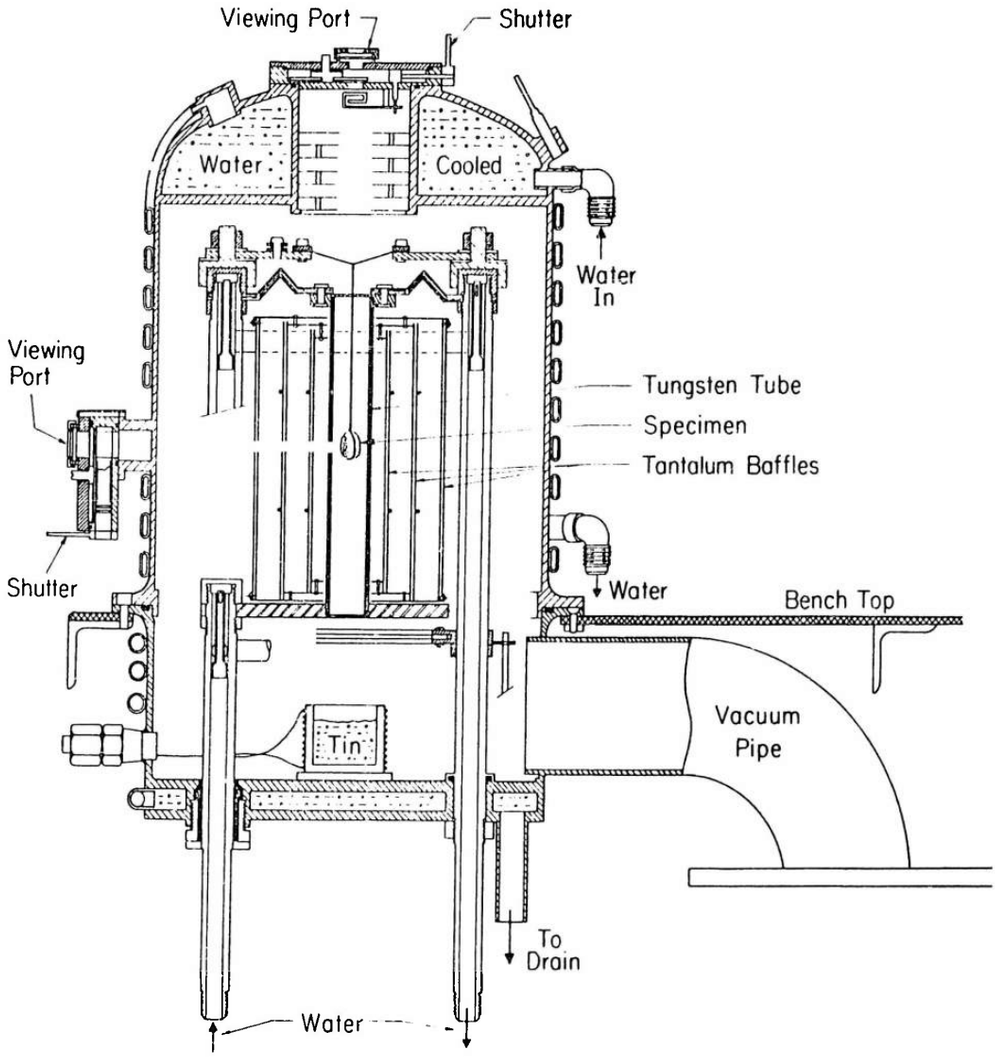

Figure V:1 - Tungsten tube high temperature furnace.

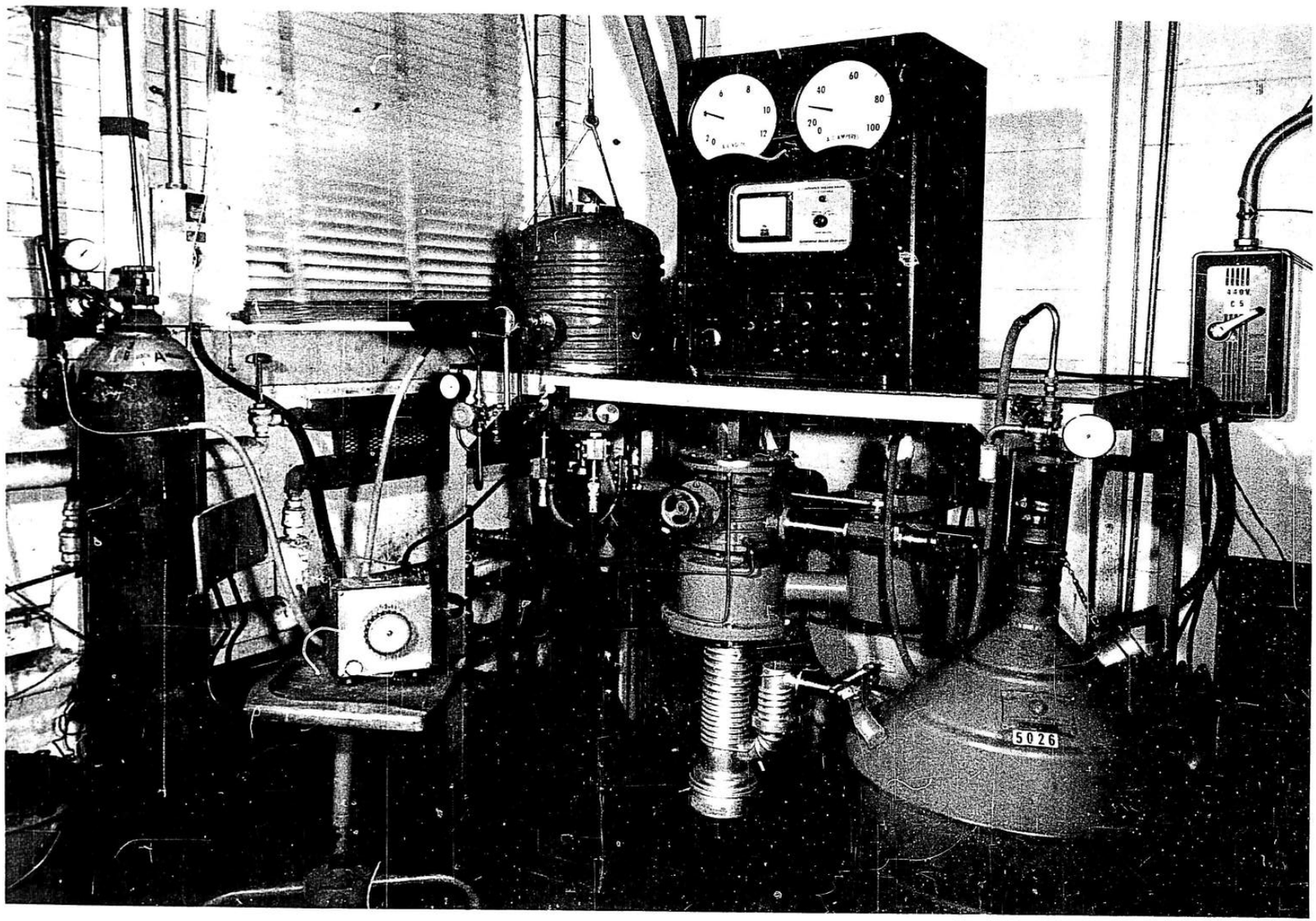

Figure V:2 - Tungsten tube furnace assembly.

tungsten (or molybdenum) disc, 3/16 inch in thickness and in whose center was drilled a 1/8-inch diameter spy hole for observing the specimens inside. The latter were arranged in vertical layers by means of spacers of thin tungsten (or molybdenum) sheet. A similar arrangement was successfully employed with the tungsten tube furnace, by using a 1-inch diameter tungsten tube as the spacer support, and fixing the tube in an alumina insulating base which stood on the hearth where the tin quenching bath is normally placed.

Both the induction furnace and the tungsten tube furnace proved to be remarkably steady in operation and would run for days without serious fluctuation in temperature or vacuum conditions. The temperature in the long-term heat treatments was checked every 2 hours during the working day with the optical pyrometer and was found to remain between $\pm$ 10° of the original setting at 2500°C. The vacuum maintained a steady value of 10^{-5} - 10^{-6} mm throughout each run.

On the basis of experience, homogenization anneals of 40-50 hours duration were employed at as high a temperature possible consistent with the characteristics of the specimen. In the case of molybdenum-osmium alloys, for example, annealing at 2300° for 48 hours produced coarse-grained homogeneous single phase alloys or two phase alloys having a well defined microstructure. The equilibrium condition at lower temperatures was obtained by annealing for three days or more, but always after the ingot had been initially homogenized at the requisite high temperature. Details of individual heat treatments are given in the appropriate tables.

G. Techniques for Phase Boundary Determination

The solidus temperatures of alloys in the Mo-Os and Mo-Re-Hf systems were determined by means of the incipient melting technique using the tungsten tube furnace and the optical pyrometer. Prior to the solidus determinations a rough idea of the melting point was obtained by heating alloys in the as-cast condition until obvious melting occurred. These preliminary experiments gave an idea of the maximum homogenizing temperatures permissible. The actual solidus temperatures were then determined after carefully homogenizing the specimens and preparing photomicrographs of them for subsequent structural comparison.

In general, specimens weighing about 10 grams were cut from the homogenized 30 gram ingots and suspended on 5-mil diameter wire within the tungsten tube furnace where they could be observed through the 1/8-inch diameter spy hole drilled in the tube. The temperature was slowly raised to the vicinity of the solidus, the outset of a slight swaying motion of the alloy "pendulum" serving as a warning that melting was imminent. After holding the specimen at temperature for at least 5 minutes, the thin horizontal tungsten support wire was electrically fused and the alloy caused to fall into the molten tin quenching bath.

After sectioning, and examining the microstructure of the alloy, the process was repeated until signs of incipient melting were clearly evident. This was taken to correspond to the solidus temperature. Instrument readings could be repeated to within $\pm$ 5° although the over-all accuracy varies with temperature, the uncertainty reaching as high as $\pm$ 15° at 3200°C as stated above in Section V-E.

The wire on which the alloys were suspended were chosen to suit the system. Rhenium and hafnium rich alloys were normally suspended on rhenium and hafnium wires. In the case of Mo-Os alloys, it proved satisfactory to employ tungsten wire except at the extreme osmium end of the system on account of the formation of a tungsten-osmium eutectic at 2725°C. In these cases (namely 80 atomic percent Os, and 100 percent Os, respectively) the specimens were rested within a small cavity in a thin disc of pure thoria, which in turn was held in a cradle of tungsten sheet.

With the techniques available, no attempt was made to determine the liquidus temperatures. While such information is of interest mainly from a thermodynamic point of view, the solidus, which can be determined quite accurately, is of more immediate interest and importance.

The individual single phase fields were identified by the X-ray powder diffraction method, details of which will be presented later, and by micrographic examination. The former technique is much more positive because of the unique nature of the individual diffraction spectra; uncertainties in the micrographic method are caused by difficulties in obtaining sufficiently discriminating etching reagents. An approximate evaluation of the solid solubility limits could be made both by the microscope and the disappearing phase method with the aid of X-ray diffraction. Usually, once the phases were identified, the microscope proved more satisfactory than the X-ray method which often tended to favor one phase at the expense of the other on account of differential absorption affects and unfavorable structure-factor values. On the other hand, the X-ray method proved more satisfactory in establishing solid solubility limits when lattice parameters vs composition curves could be drawn, the discontinuities in the curves being capable of establishing the limits to $\pm$ 0.5 atomic percent.

H. The Molybdenum-Osmium Constitution Diagram

The final molybdenum-osmium diagram is shown in Figure V:3. Four single phase fields are of primary interest. These consist of (1) the α-Mo primary solid solution, (2) the narrow intermediate β phase based on Mo_3Os, (3) the extensive σ phase centered round Mo_2Os, and (4) the extremely wide terminal solid solution based on θ-Os. Except for the addition of the β-Mo_3Os phase, the Mo-Os system is closely analogous to that of W-Os[1].

1. The α-Mo Phase Field

As shown by the constitution diagram in Figure V:3, the body centered cubic α-Mo primary solid solution extends from pure molybdenum to approximately 19.5 atomic percent osmium at 2380°C, narrowing down to 7.0 atomic percent at 1000°C. The high temperature solid solubility limit was fixed by microscopical methods, while at 2000° and 1400°C it was fixed by X-ray lattice parameter measurements and confirmed micrographically. The lattice parameter curve for the α-Mo phase field is shown in Figure V:4. Heat treatment data and hardness measurements for the α-Mo phase are presented in Table V:2.

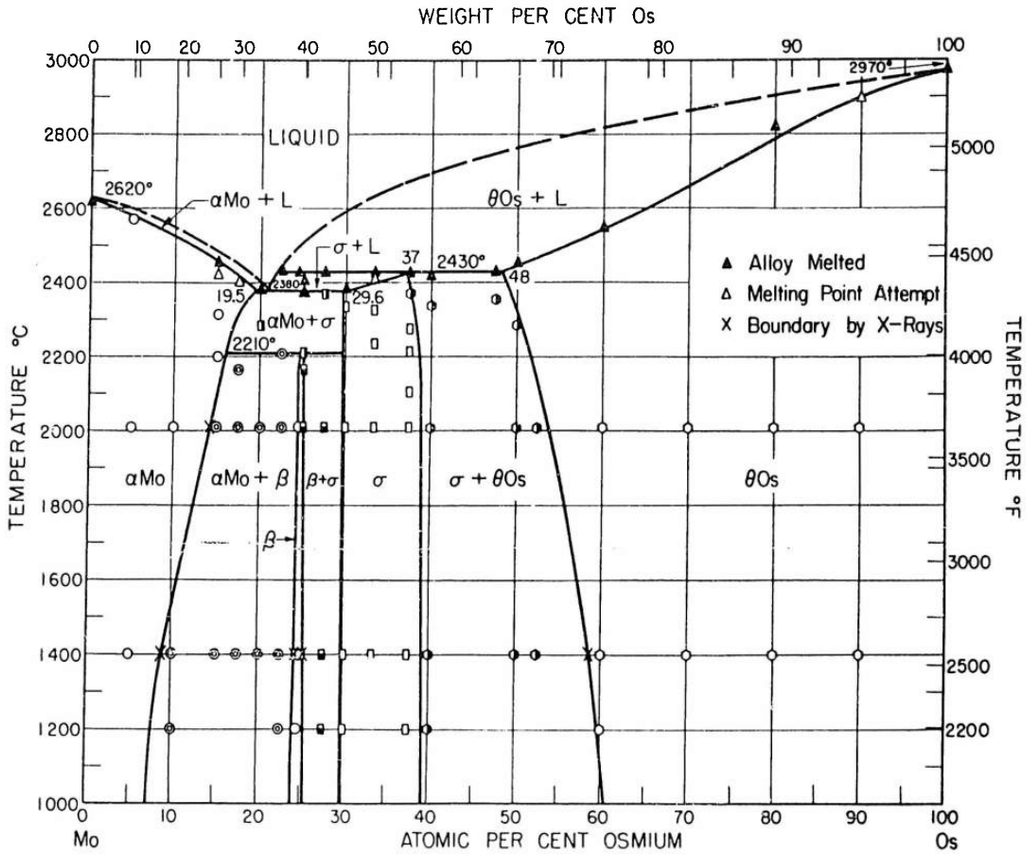

Figure V:3 - The molybdenum-osmium constitution diagram.

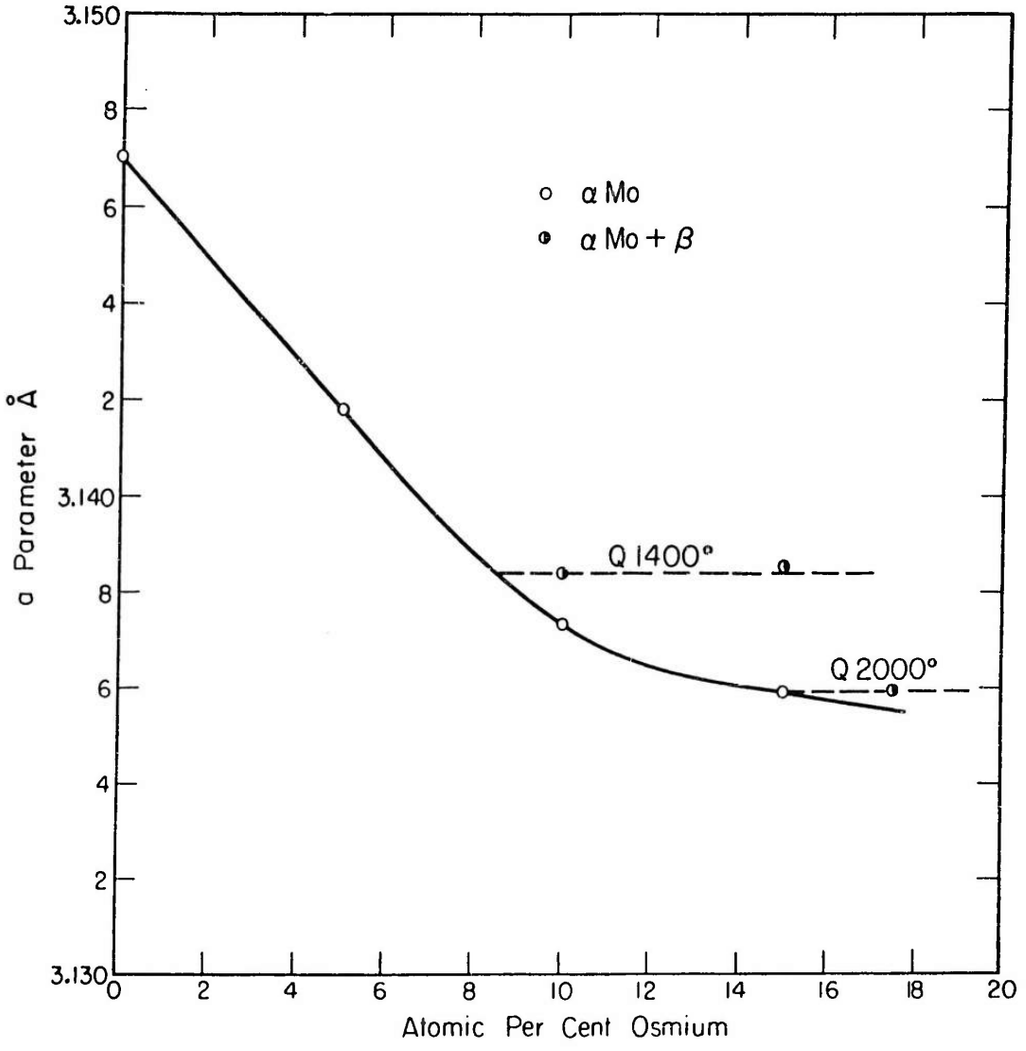

Figure V:4 - Lattice parameters of αMo Mo-Os Alloys.

Table V:2

Collected Data on the Mo-Os System

Alloy Number	Osmium Atomic %	Melting Observed	Heat Treatment °C *	Observed Structure	Lattice Parameter Å	Atomic Volume Å 3	Vickers Hardness
--	0.0			α Mo	3.1470	15.5833	180
1B	5.0		48 hr 2010° R.Q.	α Mo			332
			+ 2010° SC 29 hr 1400° 72 hr R.Q.	α Mo	a = 3.1418	15.5062	
			+ 5 min 2570° R.Q.	α Mo			
2	10.0		51 hr 2010° R.Q.	α Mo	a = 3.1372		454
			+ 2000° SC 29 hr 1400° 72 hr R.Q.	α Mo + Tr β	a = 3.1384		
			+ 140 hr 1200°C R.Q.	α Mo + Tr β			
3	15.0	2455°C	56 hr 2010° R.Q.	α Mo + Tr β			542
			+ 5 min 2425° Q	α Mo			
			+ 2000° SC 48 hr 1400° 48 hr R.Q.	α Mo + β	a = 3.1386		
			+ 2 hr 2200°Q	α Mo			
			+ 1 hr 2313°Q	α Mo	a = 3.1360		
23	17.5		48 hr 2010° R.Q.	α Mo + β			579
			+ 2000° SC 48 hr 1400° 48 hr	α Mo + β			
			+ 1 hr 2165° Q	α Mo + β			
			+ 10 min 2405° Q	α Mo			

* R.Q. = radiation quench
SC = slow cool to equilibrium temperature
Q = quenched into molten tin

Table V:2 (Continued)

Alloy Number	Osmium Atomic %	Melting Observed	Heat Treatment °C *	Observed Structure	Lattice Parameter Å	Atomic Volume Å 3	Vickers Hardness
4	20.0	2385°C	51 hr 2010° R.Q.	α Mo + β	a = 3.1361		
			+ 2000° SC 36 hr 1400° 48 hr R.Q.	α Mo + β			
			+ 15 min 2285° Q	α Mo + σ			
21	22.5	2434°C	48 hr 2010° R.Q.	α Mo + β			
			+ 2000° SC 29 hr 1400° 72 hr R.Q.	α Mo + β	β phase a = 4.9723	15.3667	
			+ 1 hr 2209° Q	α Mo + β	a = 4.9717	15.3612	
			+ 140 hr 1200° R.Q.	α Mo + β			
24	24.5	2431°C	48 hr 2010° R.Q.	β			1231
			+ 2000° SC 48 hr 1400° 48 hr R.Q.	β	a = 4.9712	15.3566	
			+ 140 hr 1200° R.Q.	β			
5	25.0	2405°C	51 hr 2010° R.Q.	β + Trσ			
		2380°C	+ 2000° SC 48 hr 1400° 48 hr R.Q.	β	a = 4.9693	15.3390	
			+ 15 min 2211°	α Mo + σ			
			+ 1 hr 2165°	β + Trσ	a = 4.9690	14.3362	

* R.Q. = radiation quench
SC = slow cool to equilibrium temperature
Q = quenched into molten tin

Table V:2 (Continued)

Alloy Number	Osmium Atomic %	Melting Observed	Heat Treatment °C *	Observed Structure	Lattice Parameter Å	Atomic Volume Å^3	Vickers Hardness
22	27.5	2430°C	48 hr 2010° R.Q.	β + σ	a = 9.63_5 c = 4.96_0		1206
			+ 2000° SC 29 hr 1400° 72 hr R.Q.	β + σ	a = 4.9685		
			+ 20 min 2370°C Q	α Mo + σ			
			+ 140 hr 1200° Q	β + σ			
6	30.0	2385°C	51 hr 2010°R.Q.	σ	a = 9.63_2 c = 4.95_0	15.3079	
			+ 2000° SC 36 hr 1400° 48 hr R.Q.	σ			
			+ 15 min 2335° Q	σ			
			+ 140 hr 1200° R.Q.	σ			
20B	33.33	2429°C	56 hr 2010° R.Q.	σ	a = 9.62_4 c = 4.94_4	14.2578	1434
			+ 2000° SC 48 hr 1400° 48 hr R.Q.	σ			
			+ 45 min 2325° Q	σ			
			+ 30 min 2235° Q	σ			
			+ 10 min 2415° Q	σ			

* R.Q. = radiation quench
SC = slow cool to equilibrium temperature
Q = quenched into molten tin

Table V:2 (Continued)

Alloy Number	Osmium Atomic %	Melting Observed	Heat Treatment °C *	Observed Structure	Lattice Parameter Å	Atomic Volume Å 3	Vickers Hardness
25	37.5	2430°C	48 hr 2010° R.Q.	σ	a = 9.61$_3$ c = 4.93$_5$	15.1982	
			+ 2000°SC 48 hr 1400° 48 hr R.Q.	σ			
			+ 20 min 2370° Q	σ + Tr θ			
			+ 15 min 2275° Q	σ			
			+ 5 min 2215° Q	σ			
			+ 2 hr 2105° Q	σ			
			+ 140 hr 1200° R.Q.	σ			
8	40.0	2423°C	51 hr 2010° R.Q.	σ + θ	a = 9.60$_9$ c = 4.93$_6$	15.2012	
			+ 2000° SC 48 hr 1400° 48 hr R.Q.	σ + θ			
			+ 2 min 2339° Q	σ + θ			
			+ 140 hr 1200° R.Q.	σ + θ			
26	47.5	2434°C	5 hr 2355° Q	σ + θ			
10	50.0	2455°C	56 hr 2010° R.Q.	σ + θ			566
			+ 2000° SC 48 hr 1400° 48 hr R.Q.	σ + θ			
			+ 45 min 2285° Q	θ + Tr σ			

* R.Q. = radiation quench
SC = slow cool to equilibrium temperature
Q = quenched into molten tin

Table V:2 (Continued)

Alloy Number	Osmium Atomic %	Melting Observed	Heat Treatment °C *	Observed Structure	Lattice Parameter Å	Atomic Volume Å 3	Vickers Hardness
27	52.5		48 hr 2010° R.Q.	θ + Tr σ			
			+ 2000° SC 48 hr 1400° 48 hr R.Q.	θ + σ	a = 2.7605 c = 4.4205	14.5864	
12	60.0	2545°C	56 hr 2010° R.Q.	θ		14.5726	492
			+ 2000° SC 48 hr 1400° 48 hr R.Q.	θ	a = 2.7601 c = 4.4176		
			+ 140 hr 1200° R.Q.	θ			
14	70.0		48 hr 2010° R.Q.	θ			584
			+ 2000° SC 29 hr 1400° 72 hr R.Q.	θ	a = 2.7555 c = 4.3898	14.4327	
16	80.0	2823°C	48 hr 2010° R.Q.	θ			635
			+ 2000° SC 29 hr 1400° 72 hr R.Q.	θ	a = 2.7505 c = 4.3632	14.2932	
18	90.0		48 hr 2010° R.Q.	θ			551
			+ 2000° SC 29 hr 1400° 72 hr R.Q.	θ	a = 2.7434 c = 4.3414	14.1485	
Os 1	100.0	2970°C			a = 2.7341 c = 4.3199	13.9831	530

* R.Q. = radiation quench
SC = slow cool to equilibrium temperature
Q = quenched into molten tin

2. The β-Mo_3Os Phase Field

The β-Mo_3Os phase forms via a peritectoid reaction between α-Mo and σ at 2210°C (see below). The field is very narrow, ranging from about 24 to 25.5 atomic percent osmium at 1000°C. The phase has the β-W A15 type of structure with a lattice parameter ranging from 4.971_2 Å at 24.5 atomic percent Os to 4.969_3 Å at 25 atomic percent.

3. The σ-Mo_2Os Phase Field

A peritectic reaction occurs at 2430°C between liquid containing approximately 22 atomic percent osmium and θ-Os primary solid solution containing 48 atomic percent to form the σ-phase structure at 37 atomic percent osmium. The σ phase broadens rapidly and from 2200° down to 1000°C it extends approximately from 30 to 39 atomic percent osmium. The structure of the σ phase is typical of σ-FeCr which has the atomic arrangement of tetragonal β-U. The lattice parameters of the structure decrease with added osmium from a = 9.632 and c = 4.950 Å at 30 atomic percent osmium to a = 9.613 and c = 4.934 Å at 37.5 atomic percent. Thermal and hardness data on σ-phase alloys are presented in Table V:2.

4. The θ-Os Phase Field

This extends from pure osmium to 48 atomic percent osmium at 2430°C, the temperature of the peritectic horizontal, the boundary sloping to a solid solubility limit at 60 atomic percent osmium at 1100°C. The high temperature solid-solubility limits are fixed essentially by micrographic methods while the 1400° limit of the θ-Os phase was fixed by lattice parameter determinations on quenched alloys and verified micrographically. Increasing the amount of Os produces a decrease in the lattice parameters and c/a ratios, the parameter values falling from a = 2.7605, c = 4.4205 Å at 60 atomic percent Os to a = 2.7341 and c = 4.3199 Å at 100 atomic percent. The changes on crossing the θ-Os phase field are shown in Figure V:5 and are remarkably similar to those occurring in the θ-Os phase of the W-Os system.

In order to bring the cell dimensions for the different phases to a common basis for comparison purposes, it is essential to plot the lattice parameter data in the form of atomic volumes (vol. of unit cell/No. of atoms per unit cell) as a function of composition. This plot for the Mo-Os system is given in Figure V:6. Although the general trend is a decrease in atomic volume with increasing osmium content, there is a marked volume expansion for the β-Mo_3Os and the σ-Mo_2Os phase structures. A similar expansion is also observed for the σ-phase in the W-Os system. This is somewhat unusual, the normal trend in alloy systems being towards a contraction in atomic volumes in both the primary and intermediate phase fields.

Figure V:7 presents a series of X-ray powder diffraction patterns of the various phases in the Mo-Os system and includes patterns of Mo_3Os quenched from below and above the peritectoid reaction at 2210°C to illustrate the decomposition of β-Mo_3Os to αMo + σ on heating. Photomicrographs of Mo_3Os are also shown in Figures V:8-11. Figure V:8 shows the "as cast" structure obtained from a melting point determination sample and reveals crystals of σ phase embedded in an eutectic of α-Mo + σ. Figure V:9 shows single phase β-Mo_3Os (with a small trace of σ) obtained after annealing for 51 hours at 2010°C. Figure V:10 shows the retention

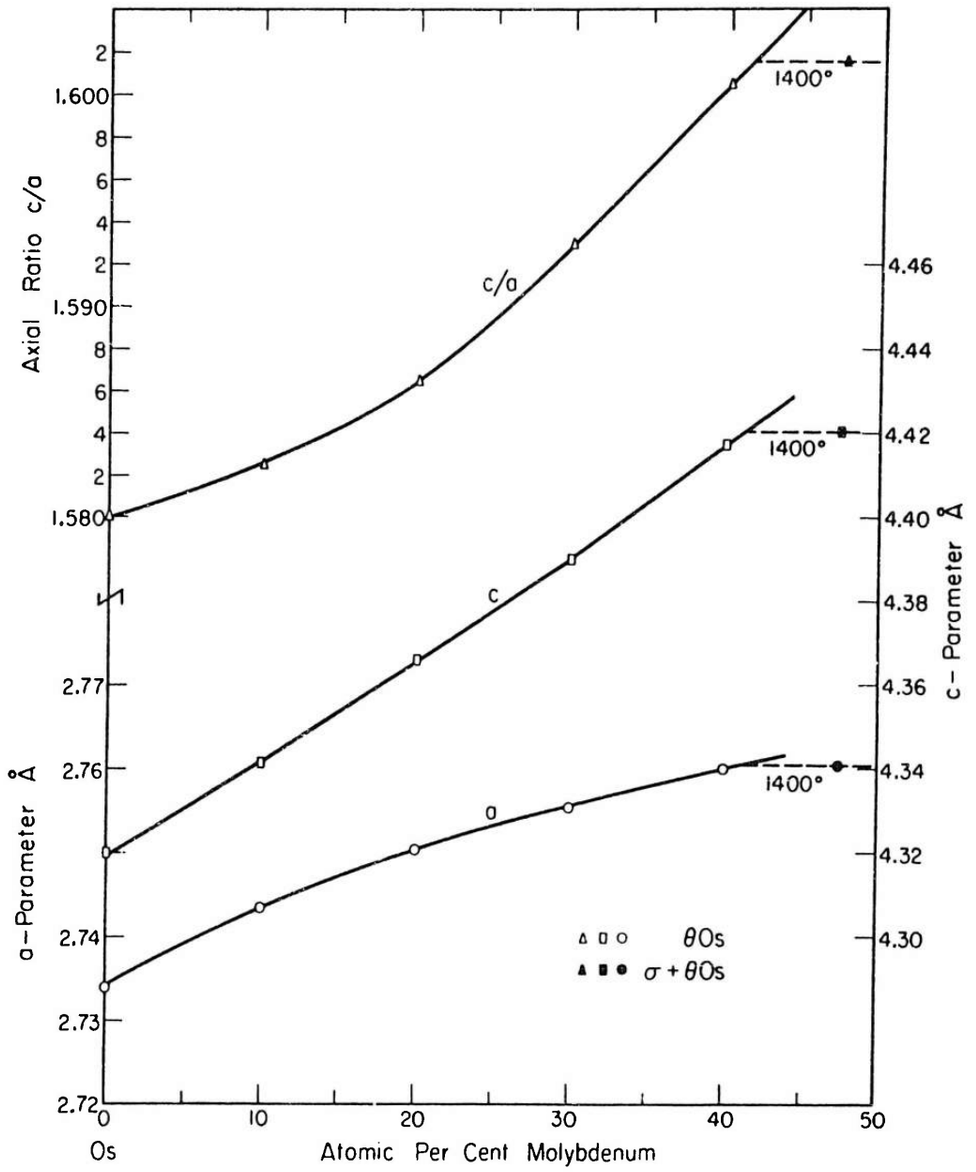

Figure V:5 - Lattice parameters and axial ratios vs composition for θ-phase molybdenum-osmium alloys. Alloys quenched 1400°C.

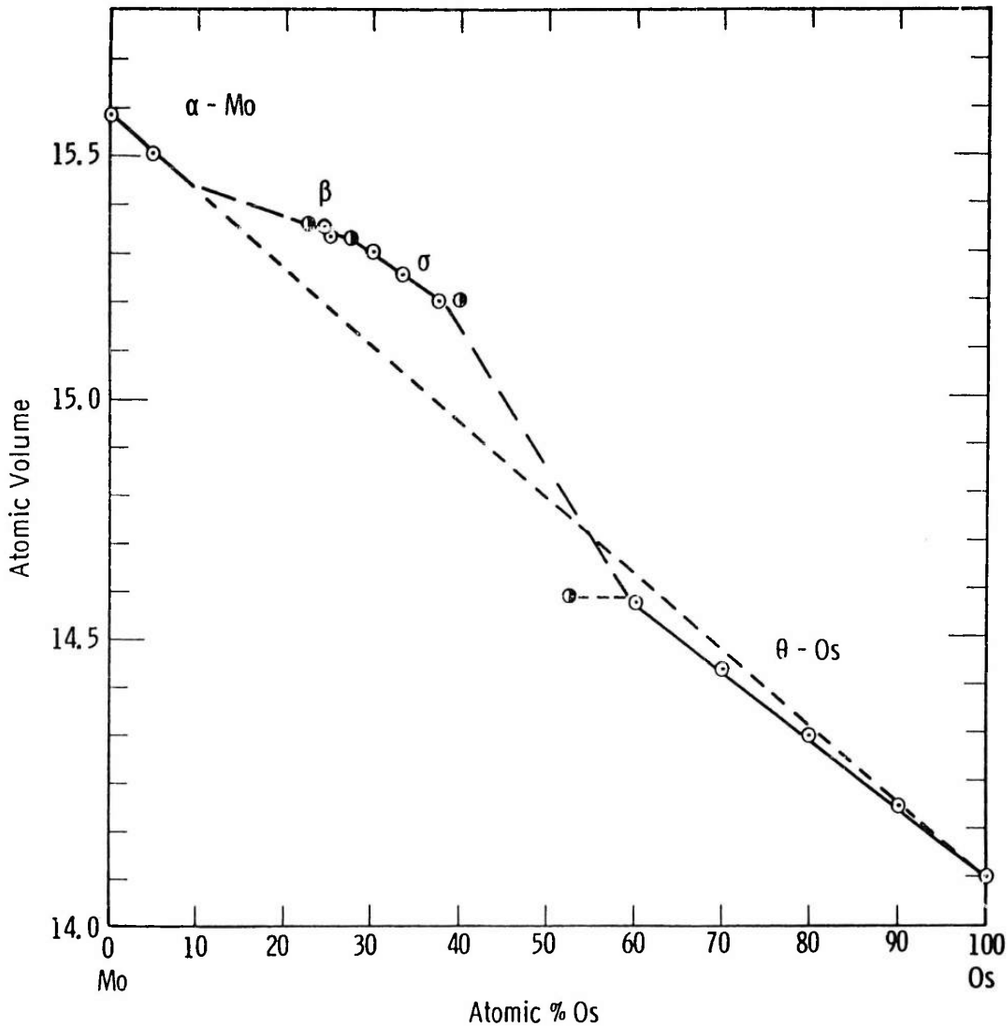

Figure V:6 - Atomic volumes of Mo-Os alloys.

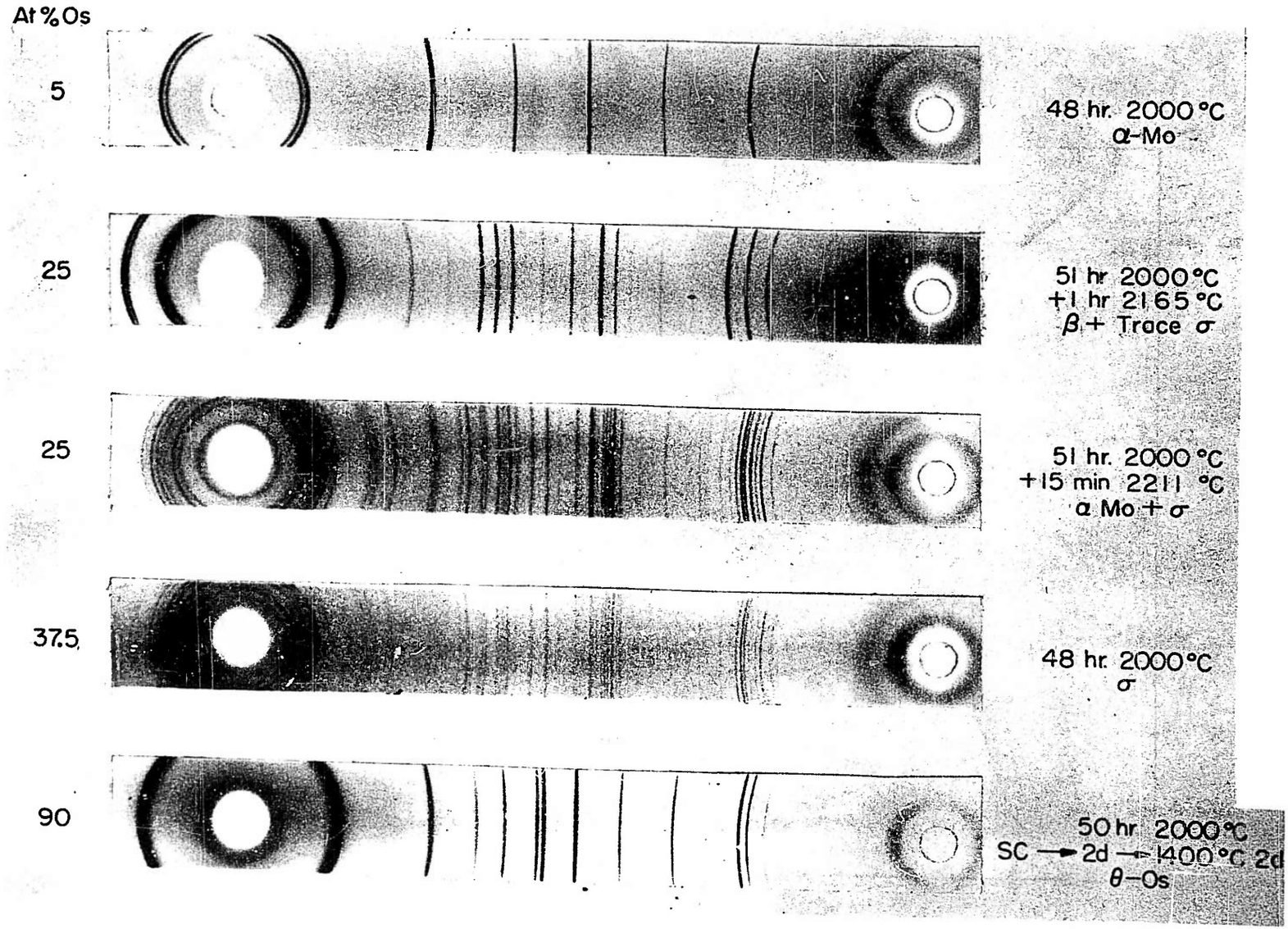

Figure V:7 - Debye Scherrer patterns of molybdenum-osmium alloys.

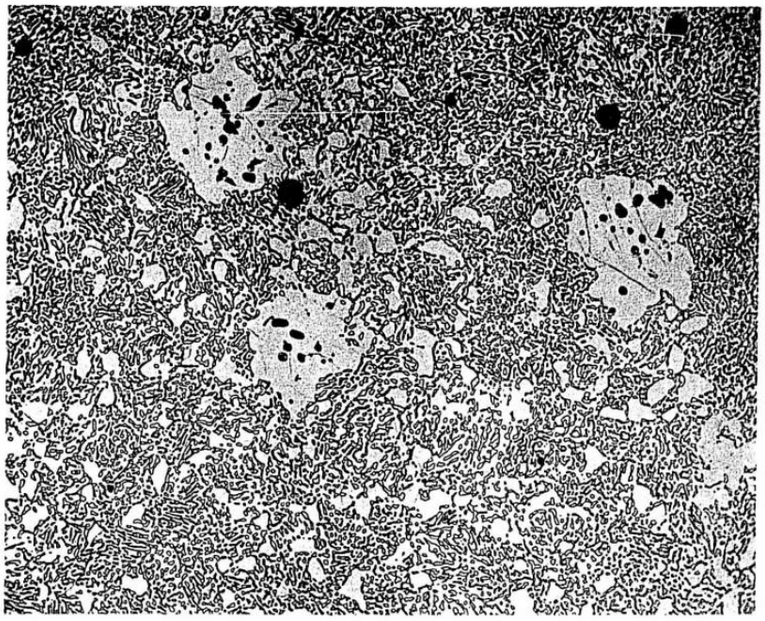

1000X

Figure V:8 - Photomicrograph of Mo-Os alloy.
25 ^{a}/o Os as cast (σ + eutectic)

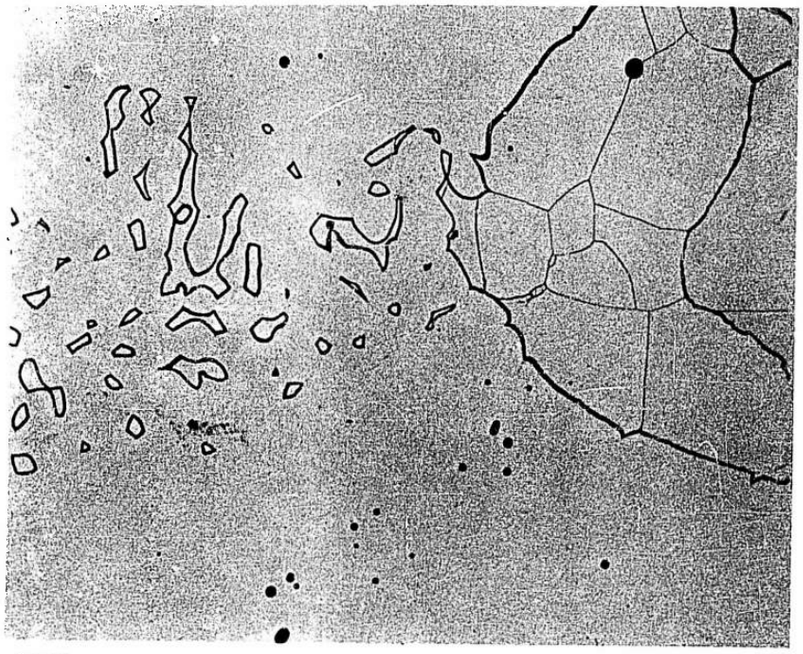

200X

Figure V:9 - Photomicrograph of Mo-Os alloy.
25 a/o Os 51 hr 2010°C (β + trace σ).

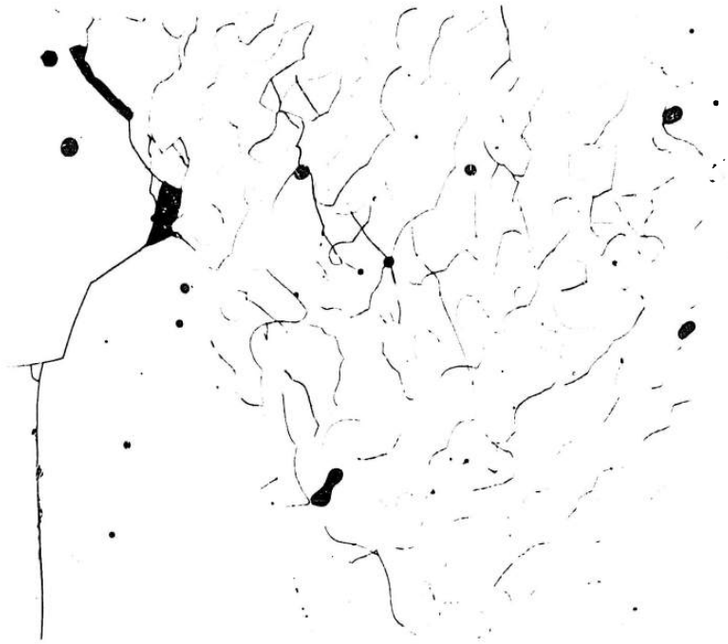

200X

Figure V:10 - Photomicrograph of Mo-Os alloy.
25 ^{a}/o Os lump annealed + 1 hr 2165^{o}C.
(β + trace σ)

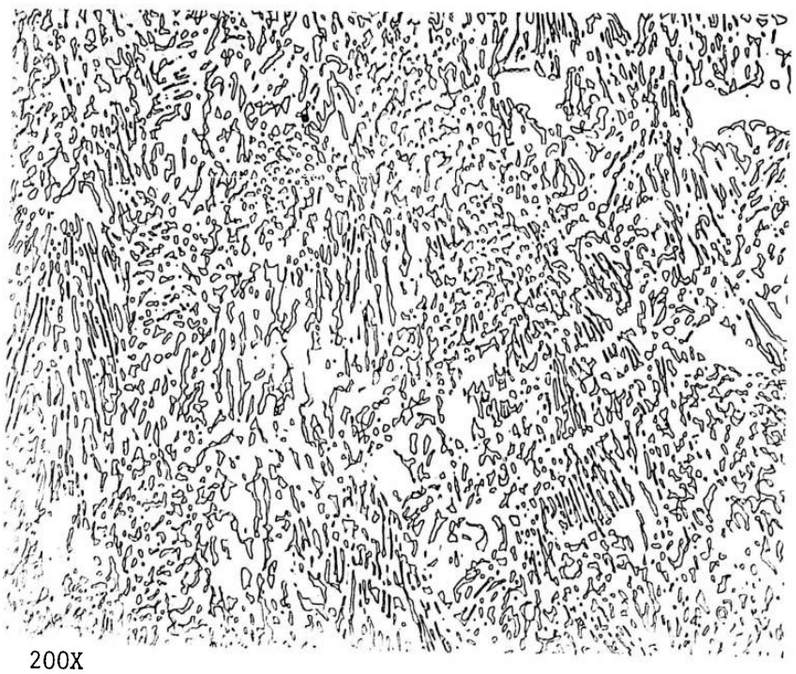

200X

Figure V:11 - Photomicrograph of Mo-Os alloy.
25 ^{a}/o Os lump annealed + 15 min 2211^{o}C.
(α Mo + σ)

of β-Mo_3Os at 2165°C while the breakdown of β to $\alpha Mo + \sigma$ is clearly seen to occur in the specimen annealed at 2211°C and quenched (Figure V:11).

I. Molybdenum-Rhenium-Hafnium Constitution Diagram

The phase fields extending across the molybdenum-rhenium-hafnium ternary system are based entirely on those present in the three constituent binaries, Mo-Re, Mo-Hf, Re-Hf, no ternary intermediate phases of different structure being present. Therefore, before describing the ternary system in detail, a brief description will be given of the constituent binaries.

1. Molybdenum-Rhenium System

The phase diagram shown in Figure V:12 is based principally on the work of Dickinson and Richardson[2] and Knapton[3]. The single phase fields of interest in this system are (1) the wide phase field consisting of body centered cubic α-Mo primary solid-solution, containing up to 40 atomic percent rhenium, (2) a wide σ-phase region ranging from approximately 50 to 70 atomic percent rhenium which forms via a peritectic reaction at 2645°C, (3) a narrow χ-phase field, alloys of which have the same structure as α-Mn, and which decomposes peritectoidally at about 2162°C, and (4) a terminal α-Re primary solid solution which narrows down from about 80 atomic percent Re at 2645°C to 99 atomic percent Re at 1000°C.

Lattice parameter data for the α-Mo, σ, χ, and α-Re phases have been given by Knapton. Our own α-Mo phase parameter results, based on alloys which have been given much longer homogenizing and equilibrating anneals are in substantial agreement with those of Knapton and are shown in Figure V:13.

2. Molybdenum-Hafnium System

This system, which is illustrated in Figure V:14, has been fully explored by Taylor, Doyle and Kagle.[4] The body centered cubic α-Mo primary solid solution extends to approximately 16.5 atomic percent Hf at 1000°C and 28 atomic percent Hf at 2165°C, at which temperature it reacts peritectically with liquid to form E_1-Mo_2Hf, a hexagonal Laves phase of the C36-$MgNi_2$ type which may be retained on quenching and which has the lattice parameters a = 5.341, c = 17.347 Å, c/a = 3.248. Between 1850° and 1816°C, the structure changes to E_2-Mo_2Hf which is intermediate between the C36-$MgNi_2$ and C14-$MgZn_2$ structural types and which has the lattice parameters a = 5.349, c = 17.490, c/a = 3.270. This, in turn, transforms to the cubic C15-$MgCu_2$ modification, denoted by η-Mo_2Hf, with a = 7.560 Å on annealing for 24 hours at 1752°C.

Both Mo_2Hf and $Mo_{65}Hf_{35}$ remain cubic down to 900°C, but below this temperature, the slight compositional difference reveals itself by a difference in behavior. On annealing for 2 weeks at 700°C and quenching, $Mo_{65}Hf_{35}$ remains cubic, but surprisingly enough Mo_2Hf transforms to E_3, which possesses the original hexagonal C36-$MgNi_2$ structure of the E_1 high temperature phase. The high-order reflections in the diffraction pattern of the low temperature hexagonal modification of Mo_2Hf are extremely diffuse and indicate the presence of lattice strain and the absence of any extensive grain growth at 700°C.

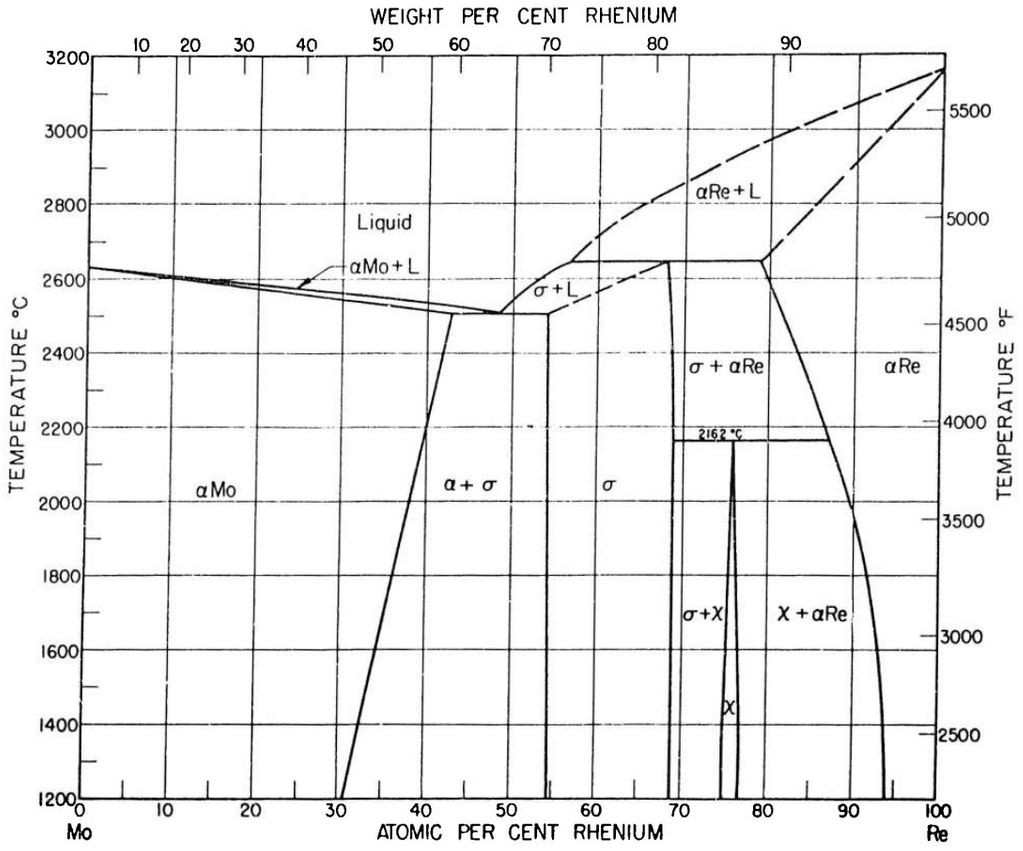

Figure V:12 - Mo-Re constitution diagram.

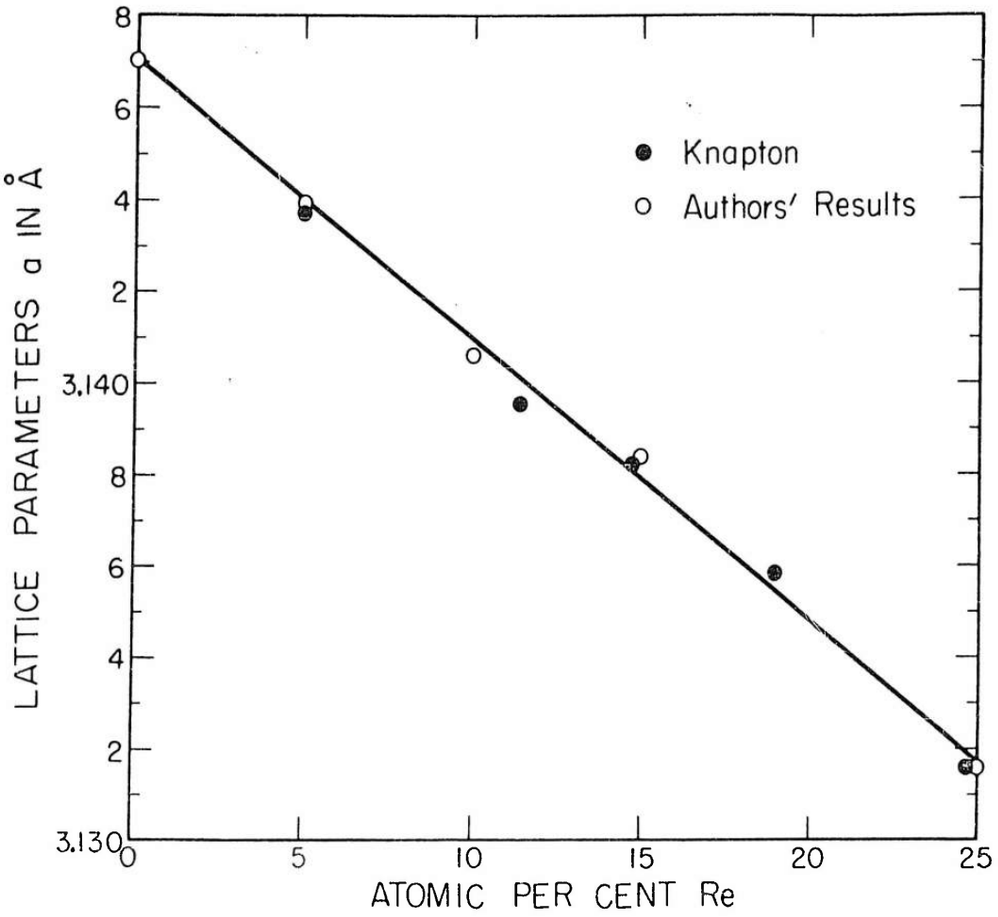

Figure V:13 - Lattice parameters of αMo phase Mo-Re alloys.

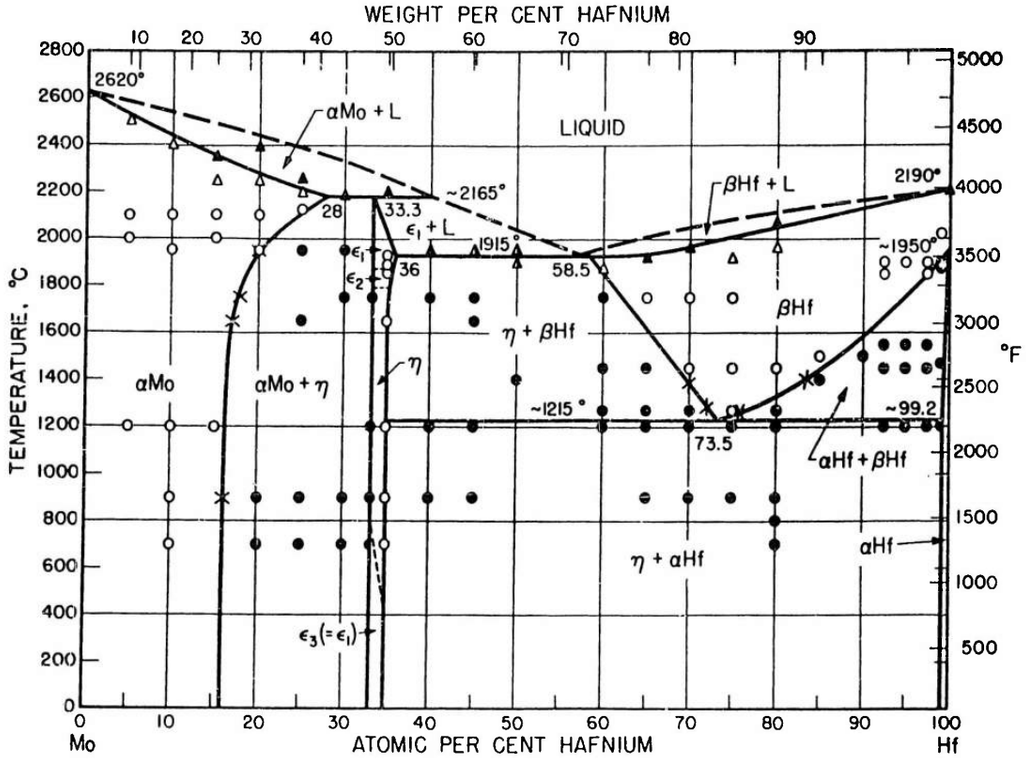

Figure V:14 - The Mo-Hf system.

The transformations occurring in the Mo_2Hf phase extend into the ternary system and influence the equilibrium relationships along the line joining Mo_2Hf with the analogous Laves phase Re_2Hf. Diffraction patterns of the η phase structure and of the various E modifications are presented in Figure V:15.

At the hafnium end of the Mo-Hf system, we have the extensive body-centered cubic β-Hf phase field which can be retained in the cubic form on quenching when containing more than about 7.5 atomic percent molybdenum in solution. Below this amount, the transformation from the β to the hexagonal close packed α-Hf modification becomes increasingly rapid and cannot be completely suppressed, the process being analogous to the martensitic transformation from the body centered β phase to the hexagonal close-packed α phases in zirconium[5] and titanium[6] alloys. β-Hf transforms martensitically to hexagonal α-Hf at 1950°C, the α-Hf phase field being very narrow, ranging from approximately 99.2 to 100 atomic percent Hf. At 73.5 atomic percent Hf, β-Hf decomposes eutectoidally at 1215°C to form η-Mo_2Hf + α-Hf.

3. The Rhenium-Hafnium System

Although the main features of this system have been worked out,[7] detailed work is required fully to elucidate the precise solidus temperatures and the extents of the various single phase fields. The tentative phase diagram presented in Figure V:16 reveals the following single phase regions of interest: (1) the primary solid solution θ-Re with a solid solubility limit at approximately 2.5 atomic percent hafnium; (2) an intermediate χ-phase having the α-Mn structure ranging from 12.0 to 15.8 atomic percent Hf and with a lattice parameter of $a = 9.6612$ Å; (3) a narrow intermediate Laves phase based on E-Re_2Hf ranging from 32.0 to 35.0 atomic percent hafnium, approximately, and which, according to Compton and Matthias[8], has the C14-$MgZn_2$ type of structure with $a = 5.239$, $c = 8.584$ Å, $c/a = 1.638$; (4) a narrow single phase field ϕ, the structure of which is tetragonal with $a = 8.90$, $c = 13.97$ Å, and which forms peritectically at 2745°C and 47.5 percent hafnium approximately. A similar phase has since been discovered in the Ti-Mn system by P. Beck[9]. (5) Finally, as in the Mo-Hf system, there is a fairly extensive terminal solid solution based on the high temperature body centered cubic β-form of hafnium which decomposes eutectically at about 87 atomic percent hafnium to φ + α-Hf, the hexagonal α-Hf phase having a solid-solubility limit of less than 1 atomic percent of rhenium in solid solution. As in the case of the Mo-Hf system, alloys containing more than about 95 percent of hafnium cannot be retained in the β form on quenching, but transform martensitically to α-Hf. Debye Scherrer patterns of the Re-Hf system are illustrated in Figure V:17.

4. The Ternary System, Molybdenum-Rhenium-Hafnium

Isothermal sections through the Mo-Re-Hf ternary system at 1600°, 2000° and 2400°C are illustrated in Figures V:18, 19, and 20 respectively, while a section taken across Mo_2Hf to Re_2Hf is shown in Figure V:21. The most detail and greatest accuracy is possessed by the 1600°C section, while that drawn for 2400° is somewhat speculative. Although a number of melting point determinations have been made, these are insufficient in number fully to establish the precise locations of the solidus surfaces.

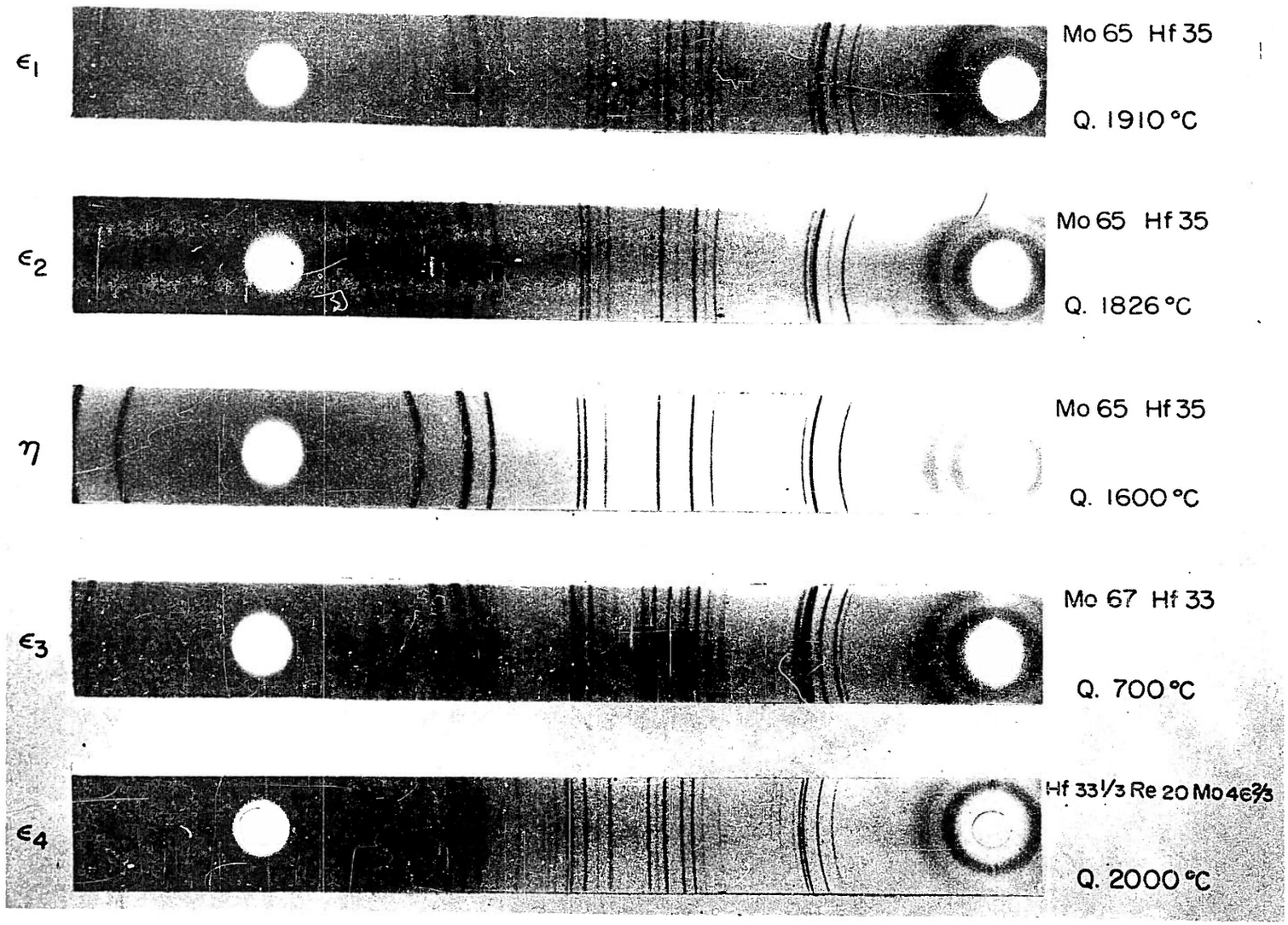

Figure V:15 - Debye Scherrer patterns of laves phases in Mo-Re-Hf system.

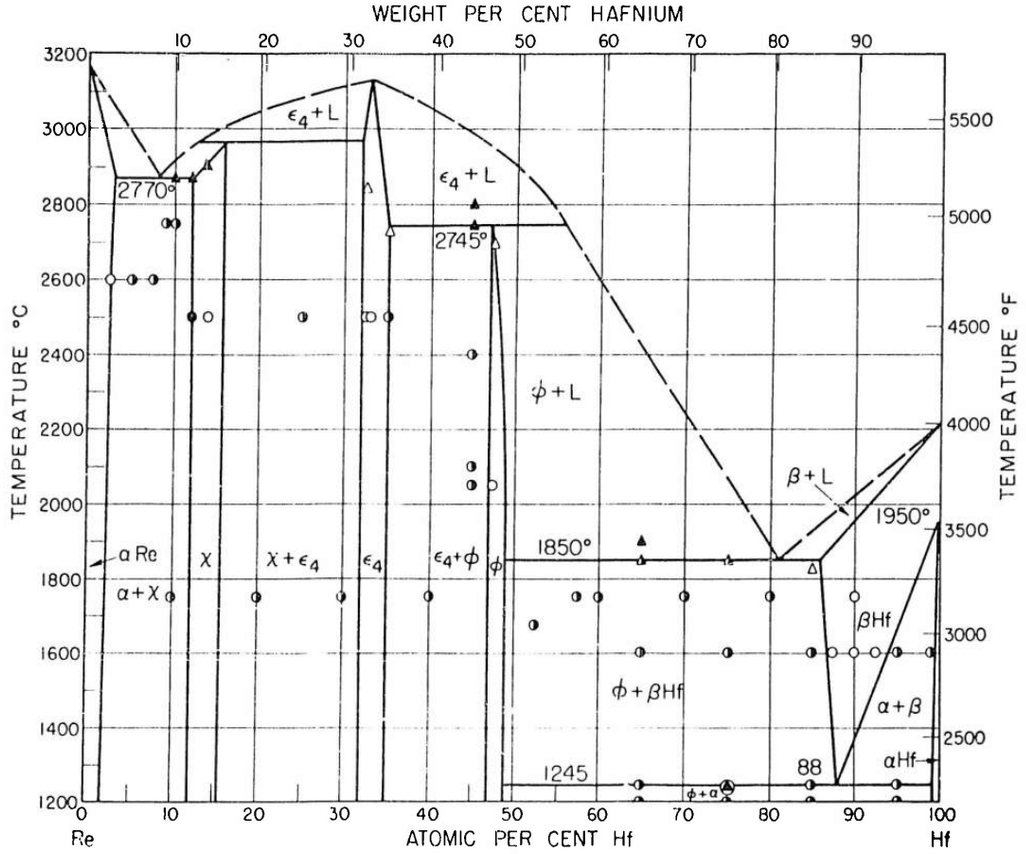

Figure V:16 - Tentative Re-Hf constitution diagram.

Ⅴ Fig.17- X-ray photographs of Re-Hf alloys.

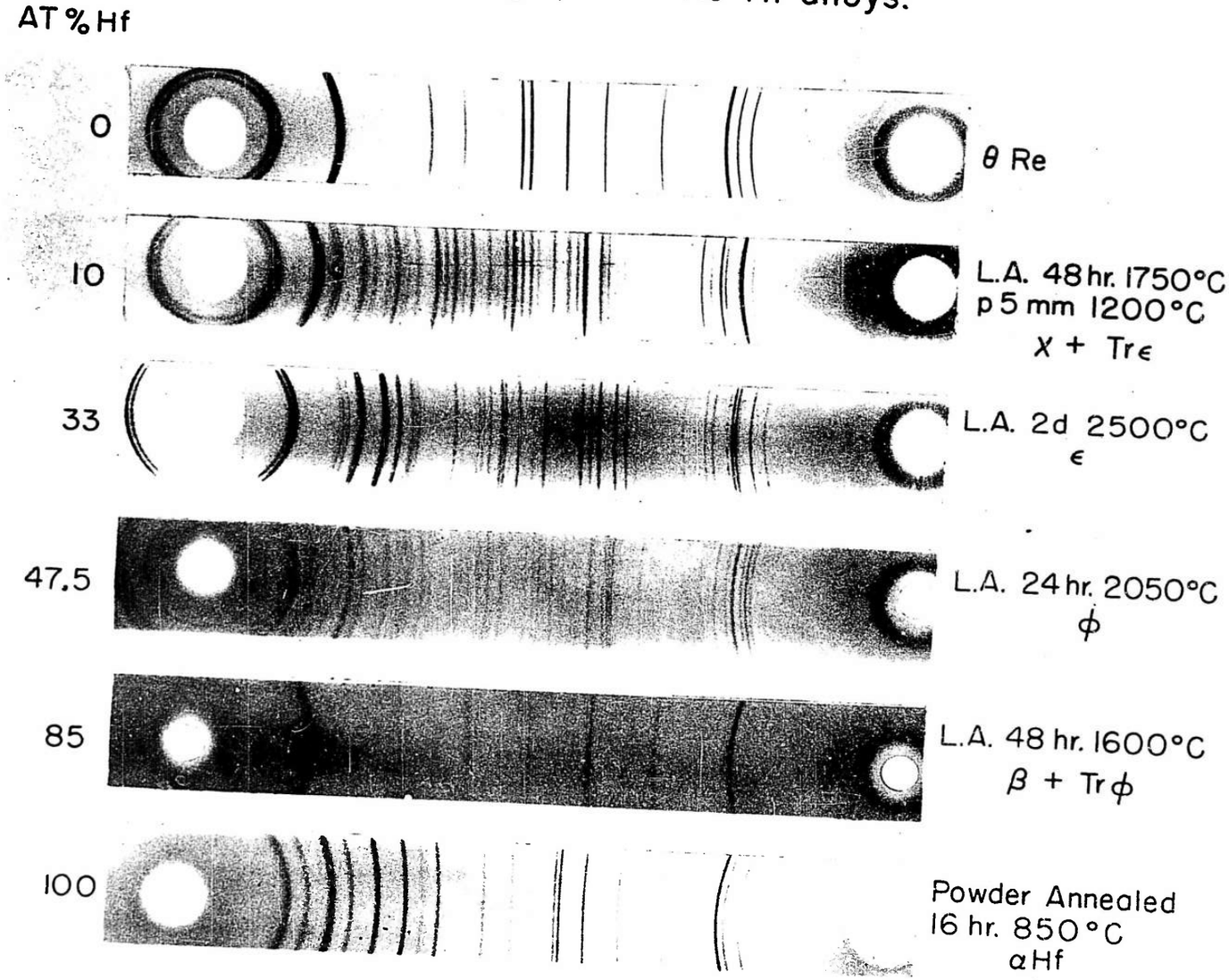

Figure V:17 - X-ray photographs of Re-Hf alloys.

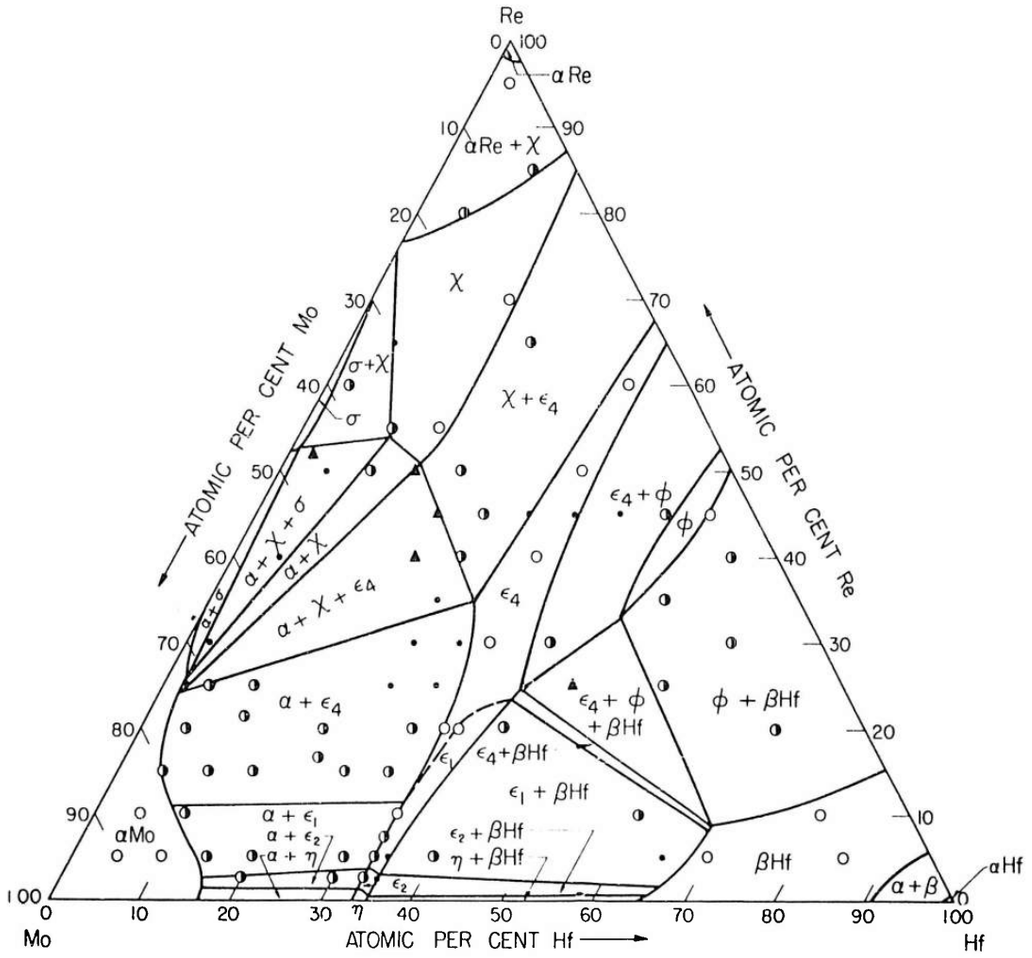

Figure V:18 - Tentative Mo-Re-Hf diagram 1600°C.

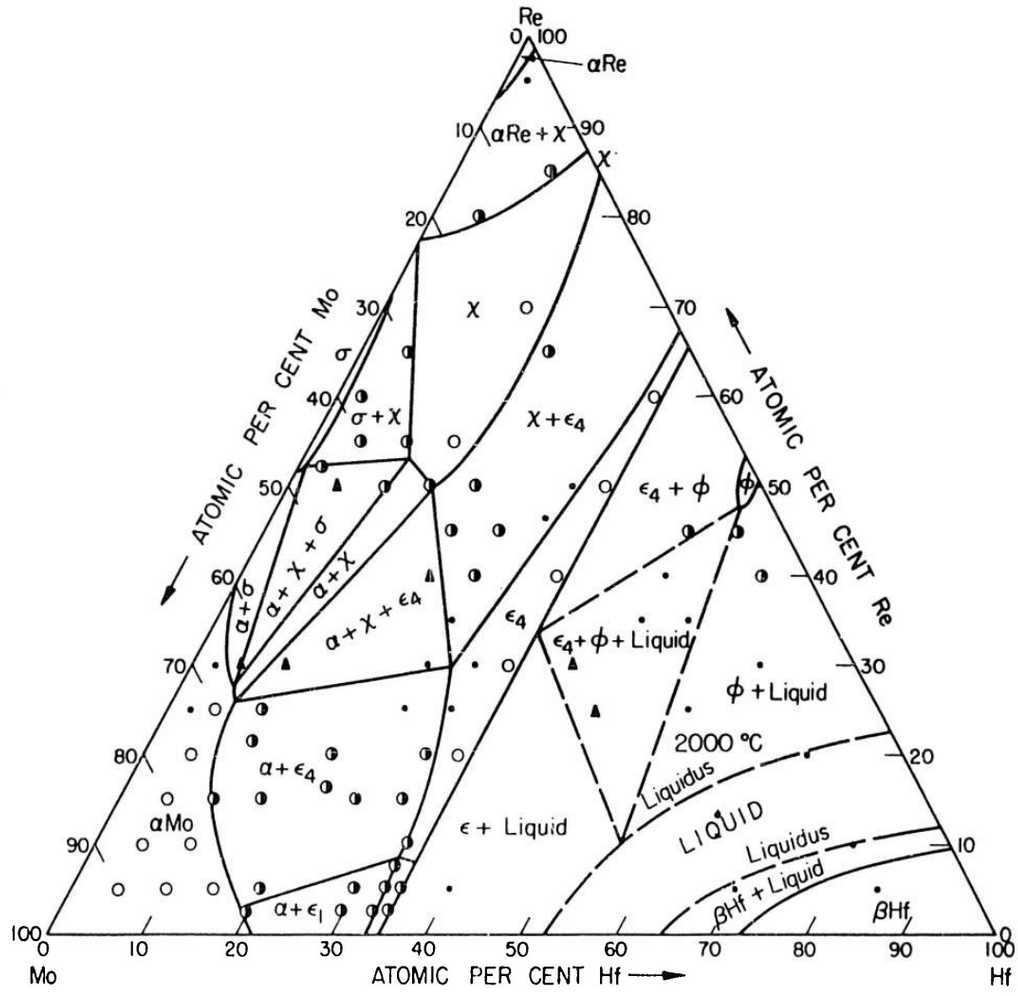

Figure V:19 - Tentative Mo-Re-Hf diagram 2000°C.

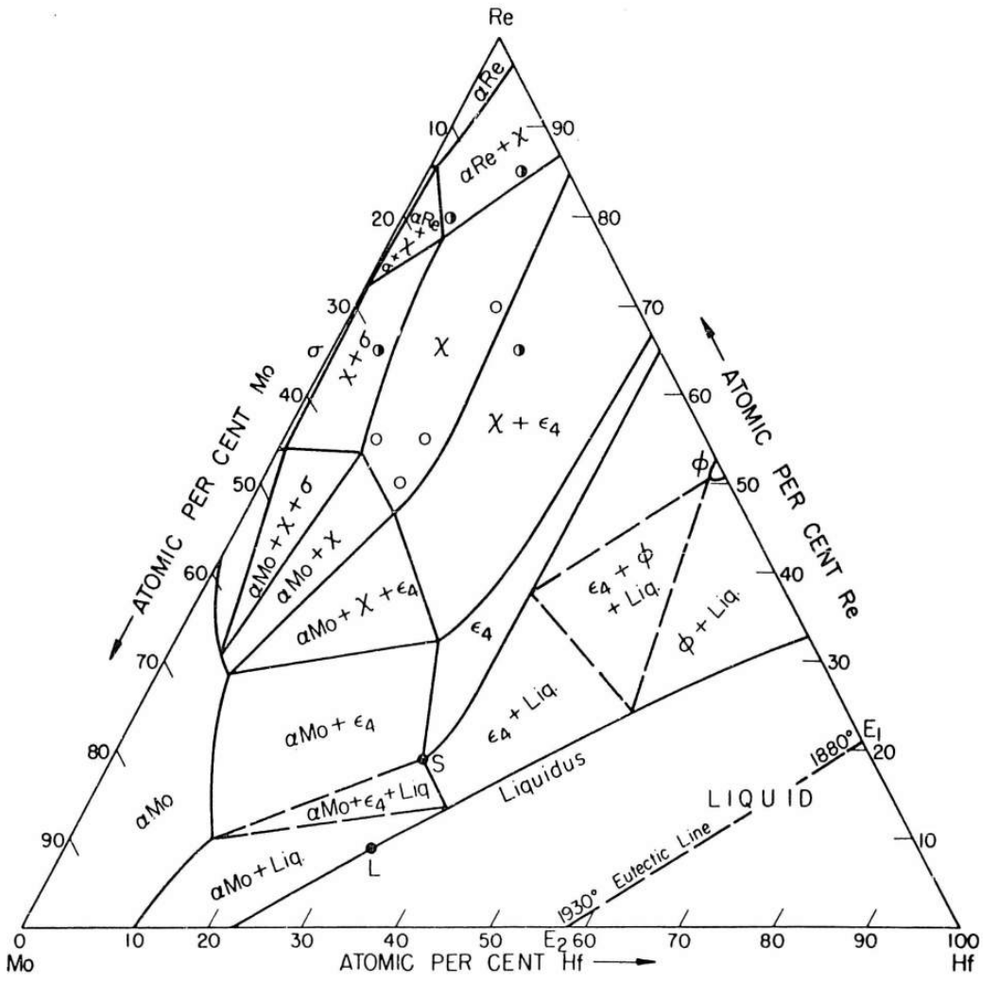

Figure V:20 - Tentative Mo-Re-Hf diagram 2400°C.

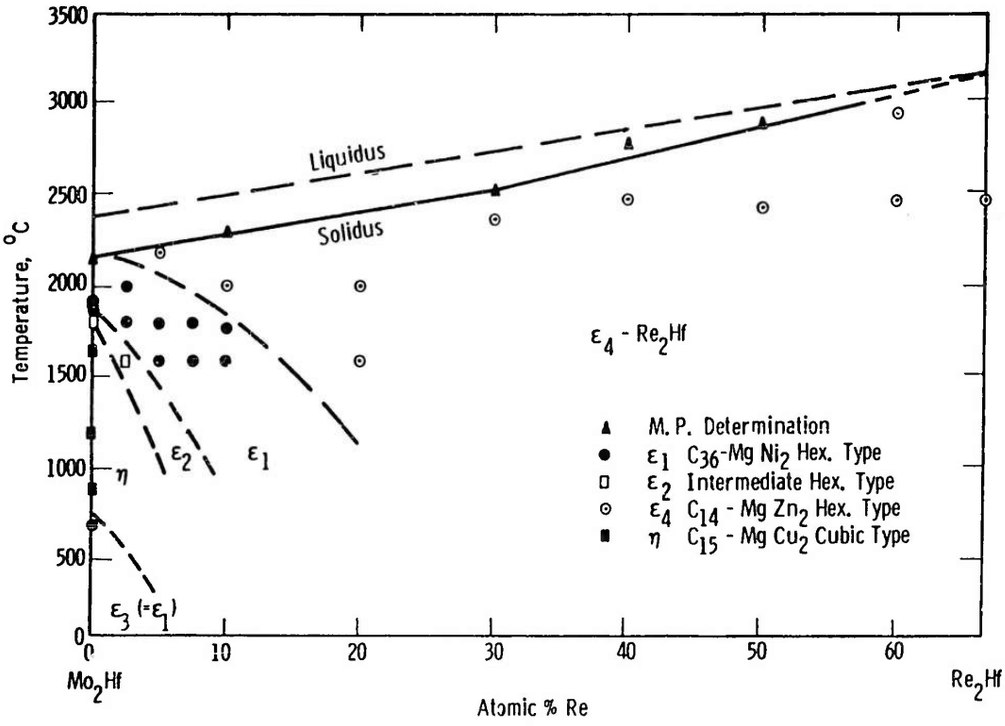

Figure V:21 - Vertical section of the Mo-Hf-Re system through Mo_2Hf-Re_2Hf.

Since no new ternary intermetallic compounds form within the system, the phases present are merely ternary extensions of the existing phases in the Mo-Re, Mo-Hf and Re-Hf systems described above. The chief points of interest with respect to the individual phase fields are described below.

a. The α-Mo Phase

This phase field, which is extensive in both the Mo-Re and Mo-Hf binary systems, extends well into the ternary diagram, as may be seen from Figures V:18-20. X-ray diffraction patterns taken across this phase field only show lines of the body centered cubic form, there being no trace of a pattern corresponding to a face centered cubic form with a lattice parameter of 3.70 Å as suggested by McHargue and Maynor[10] for an alloy with the composition Mo_3Re examined in the form of a wire which had been sintered and swaged at about 1000°C and vacuum annealed at 2000°C.

The lattice parameter of α-Mo falls with the addition of rhenium and rises with the addition of hafnium. Isoparametric contours cross the α-Mo field of the ternary system in the manner illustrated in Figure V:22, it being possible to interpolate an isoparametric line through the Mo corner on which ternary alloys would have a lattice parameter identical with that of pure molybdenum.

b. The σ-Phase Field

Although the σ-phase extends from approximately 50 to 70 atomic percent rhenium in the binary system Mo-Re, the addition of hafnium seems to inhibit the formation of the phase within the ternary system. As a result, the σ-phase field is confined to an extremely narrow region, less than one atomic percent Hf wide along the Mo-Re side of the Mo-Re-Hf composition triangle, and the α + σ two phase field is correspondingly restricted.

c. The χ-Phase Field

The χ-phase, based on the α-Mn structure, offers an interesting contrast to the σ-phase field. Although the χ-phases centered round $MoRe_3$ and Re_9Hf in their respective binary systems are extremely narrow, they link together and broaden out enormously in the ternary system, the addition of hafnium seemingly encouraging the formation of the phase, presumably because its free energy is lower than that of σ.

On account of the peritectoid decomposition of the χ-phase which takes place at 2162°C in the Mo-Re system, according to the equation

$$\chi \longrightarrow \alpha\text{-Re} + \sigma \ ,$$

raising the temperature of ternary alloys in this region causes them to decompose in a similar manner, thus giving rise to the α-Re + σ + χ three-phase triangle, shown in the 2400°C isothermal.

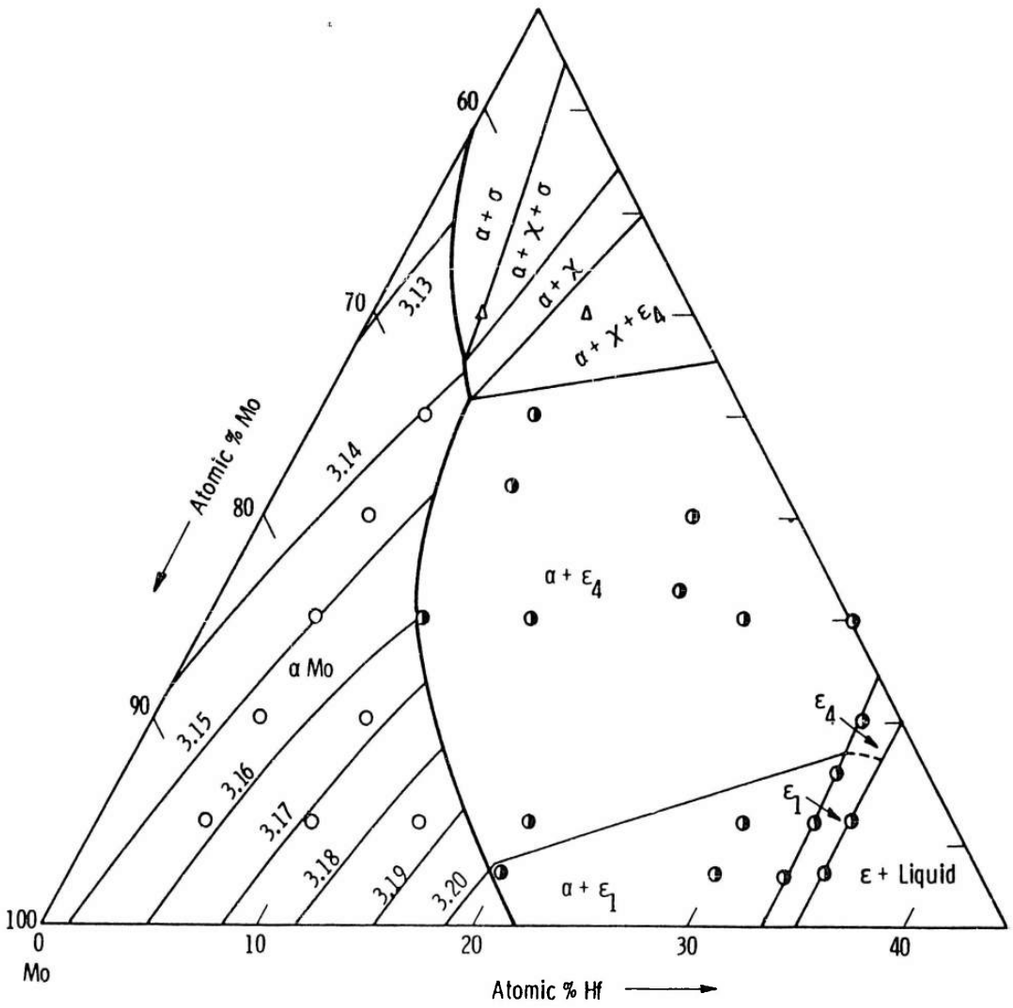

Figure V:22 - Lattice parameters of αMo phase of the Mo-Hf-Re system. Quenched 2000°C.

The variation in the position of the $\chi/\chi + \sigma$ phase boundary is illustrated by the series of photomicrographs shown in Figures V:23-26 for 10 Hf, 55 Re, 35 Mo, for the alloy in the "as cast" and heat treated condition at 2400°, 2000° and 1600°C respectively.

It will be noted that the "as cast" photomicrograph indicates a ternary eutectic between dendrites of substantially χ-phase. The amount of ternary eutectic increases as we proceed towards the center of the diagram, as shown by the photomicrograph of "as cast" 20 Hf, 50 Re, 30 Mo shown in Figure V:27. The exact position of the ternary eutectic has yet to be located. Another interesting feature, illustrated in Figure V:28 by the photomicrograph of as cast 20 Hf, 65 Re, 15 Mo is the geometrical pattern of equilateral triangles and "stars" presumably formed by the epitaxial formation of E_4 on the (111) planes of the cubic χphase, which breaks down, as shown in Figure V:29 by annealing at 2400°C.

Isoparametric contours have been established for the χ-phase as shown in Figure V:30. These are a set of curves which lie almost parallel to the Mo-Re edge of the ternary triangle and simulate the isoparametric contours across the α-Mo phase field, shown in Figure V:22.

d. The Laves Phase Fields E_1 - E_4 and η

On account of their similarities in atomic arrangement, it would be expected that E_1-Mo_2Hf with its Laves C36-$MgNi_2$ structure would spread across the diagram and link up with E_4-Re_2Hf which possesses a C14-$MgZn_2$ atomic arrangement. This is precisely what has been found to take place, the actual relationships between the structural types being, at first, somewhat difficult to elucidate on account of the structural changes taking place in the region of Mo_2Hf with temperature and with composition, and because of the formation between 1850° and 1812°C of a new structural type E_2, which intermediate between the E_1 C36-$MgNi_2$ type and the E_4 C14-$MgZn_2$ type. The situation was further complicated by the transformation of E_2 to $\bar{\eta}$ C15-$MgCu_2$ between 700°C and 1812°, and a reversion to E_1 below 700°C.

In order to establish the relationships between the various structures in the Laves phase, a series of quenches was made across the section Mo_2Hf-Re_2Hf and the ranges of the isostructural regions ascertained by means of X-ray diffraction patterns (cf Figure V:15). As shown by the broken lines in Figure V:21, the region occupied by E_4, the structure denoted by C14-$MgZn_2$ type, is by far the largest. So far, no experiments have been carried out to ascertain whether Re_2Hf itself transforms at lower temperatures.

From the positions of the X-ray lines in the Laves phase patterns, it was immediately evident that a very large increase takes place in the lattice parameters in proceeding from Re_2Hf to Mo_2Hf. In order to place the results on a common basis, the data are plotted in Figure V:31 in the form of atomic volumes.

In addition to the structural data, a series of melting point determinations was made across the section Mo_2Hf - Re_2Hf, the resulting solidus being indicated in Figure V:21. By extrapolation, an approximate value of 3120°C was obtained for

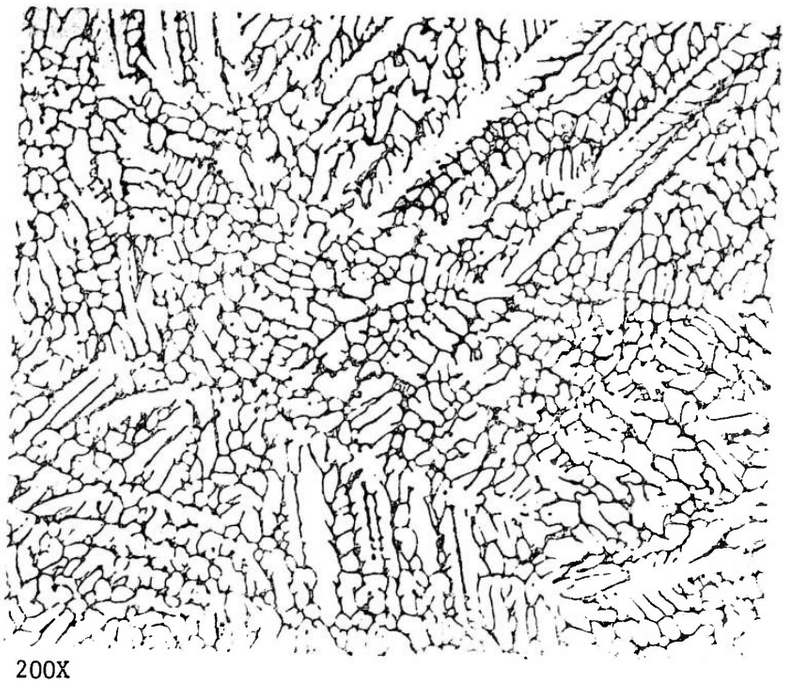

200X

Figure V:23 - Photomicrograph of hafnium-rhenium-molybdenum alloy. No. 50 Hf 10 Re 55 Mo 35. As cast (χ + eutectic).

200X

Figure V:24 - Photomicrograph of hafnium-rhenium-molybdenum alloy. No. 50 Hf 10 Re 55 Mo 35. 24 hr 2400°C and quenched. (X)

Figure V:25 - Photomicrograph of hafnium-rhenium-molybdenum alloy. No. 50. Hf 10 Re 55 Mo 35. Lump annealed 24 hr 2400°C and quenched + 48 hr 2000°C and quenched. (χ + trace σ)

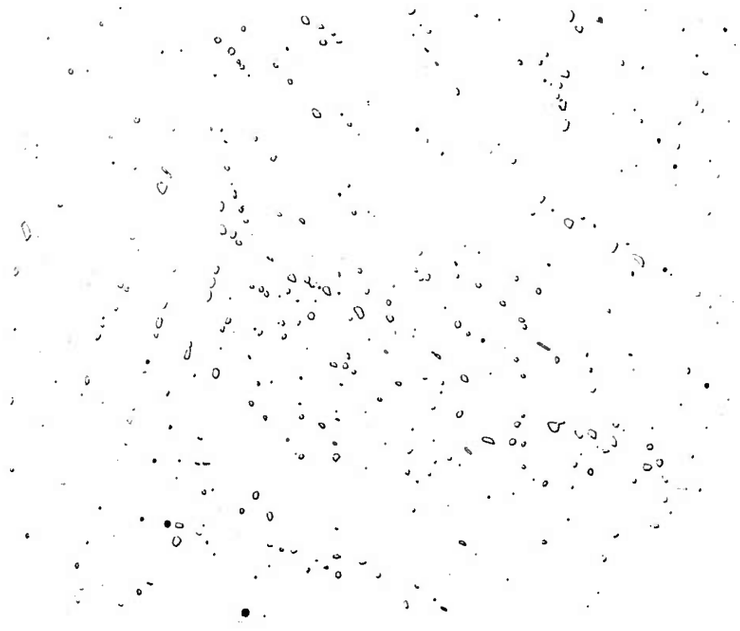

200X

Figure V:26 - Photomicrographs of hafnium-rhenium-molybdenum alloy. No. 50. Hf 10 Re 55 Mo 35. Lump annealed 24 hr 2400°C, + 48 hr at 2000°C + 72 hr at 1600°C, and quenched. (χ + σ)

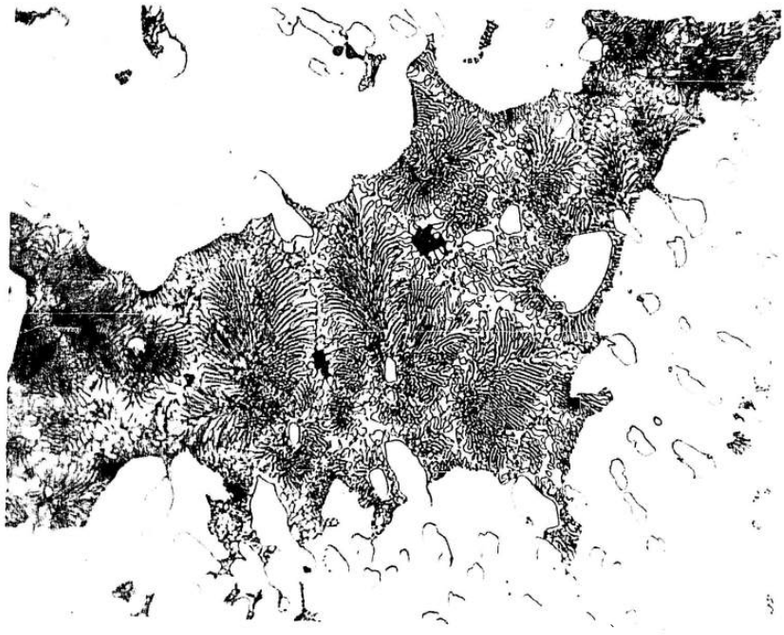

500X

Figure V:27 - Photomicrograph of hafnium-rhenium-molybdenum alloy. No. 12. Hf 20 Re 50 Mo 30. As cast (χ + E + eutectic).

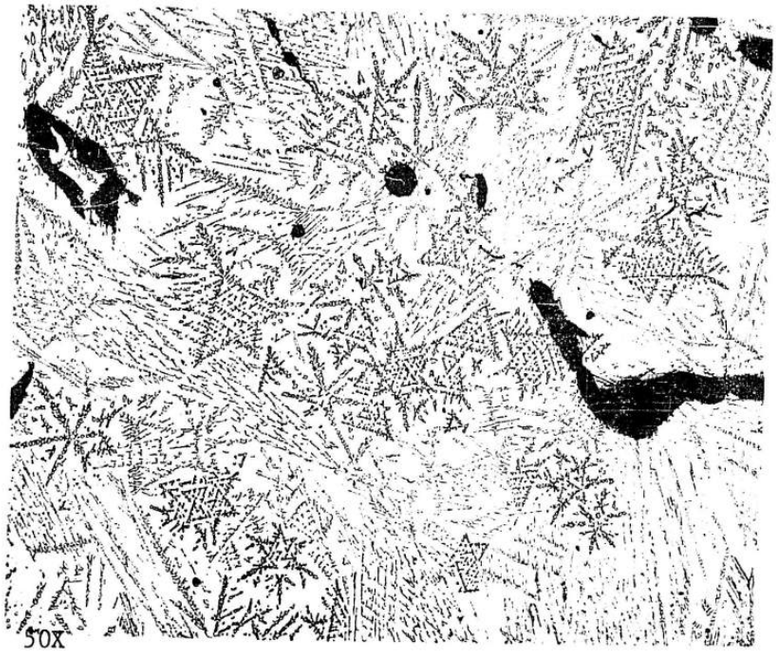

Figure V:28 - Photomicrograph of hafnium-rhenium-molybdenum alloy. No. 60. Hf 20 Re 65 Mo 15. As cast.

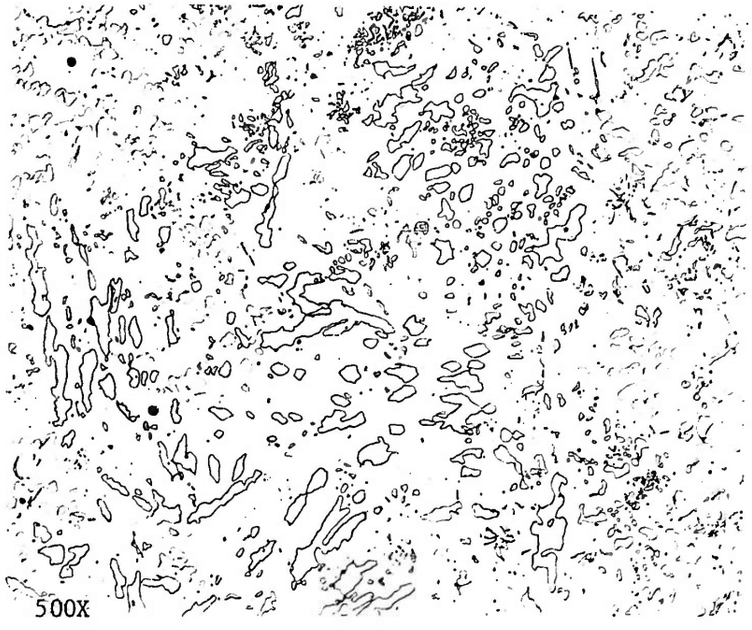

Figure V:29 - Photomicrograph of hafnium-rhenium-molybdenum alloy. No. 60. Hf 20 Re 65 Mo 15. Lump annealed 24 hrs at 2400°C and quenched. ($\chi + E_4$).

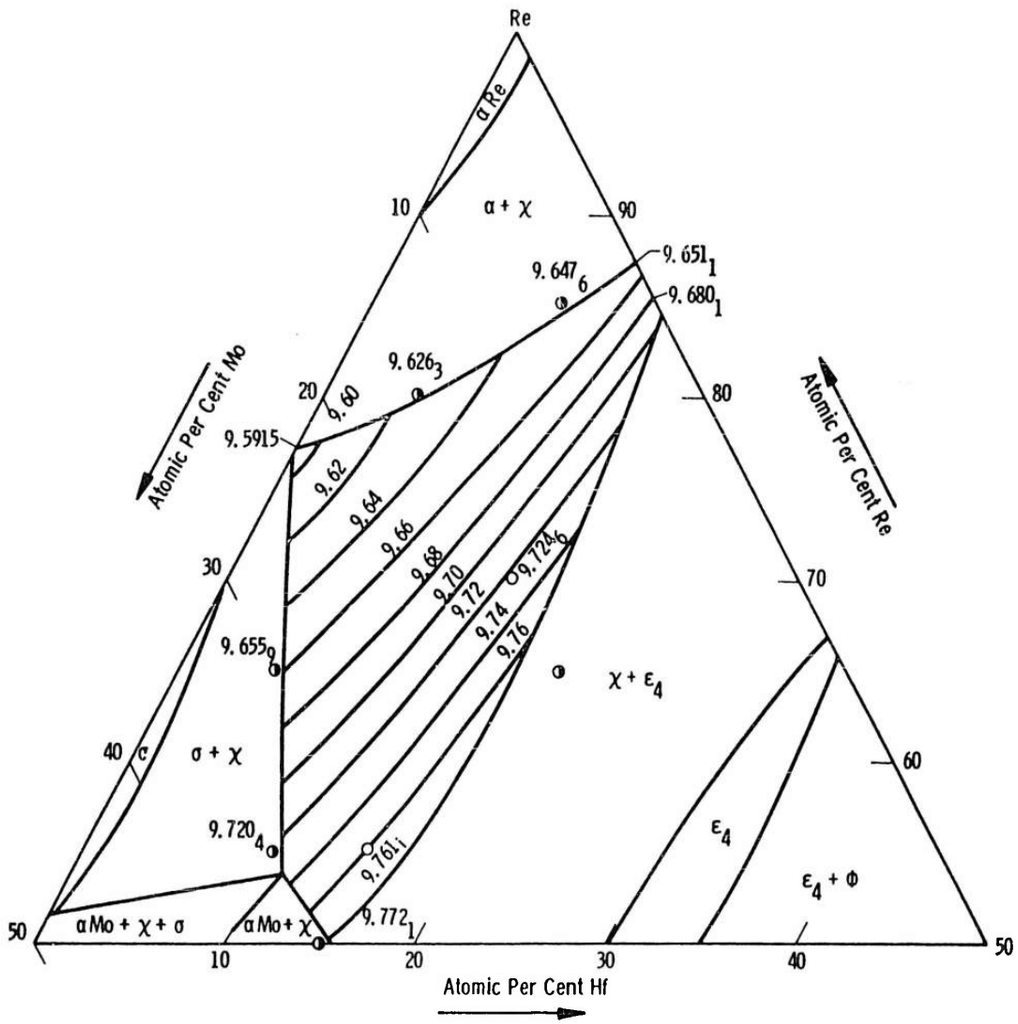

Figure V:30 - Isoparametric contours of χ-phase of Hf-Re-Mo alloys. 2000° isothermal.

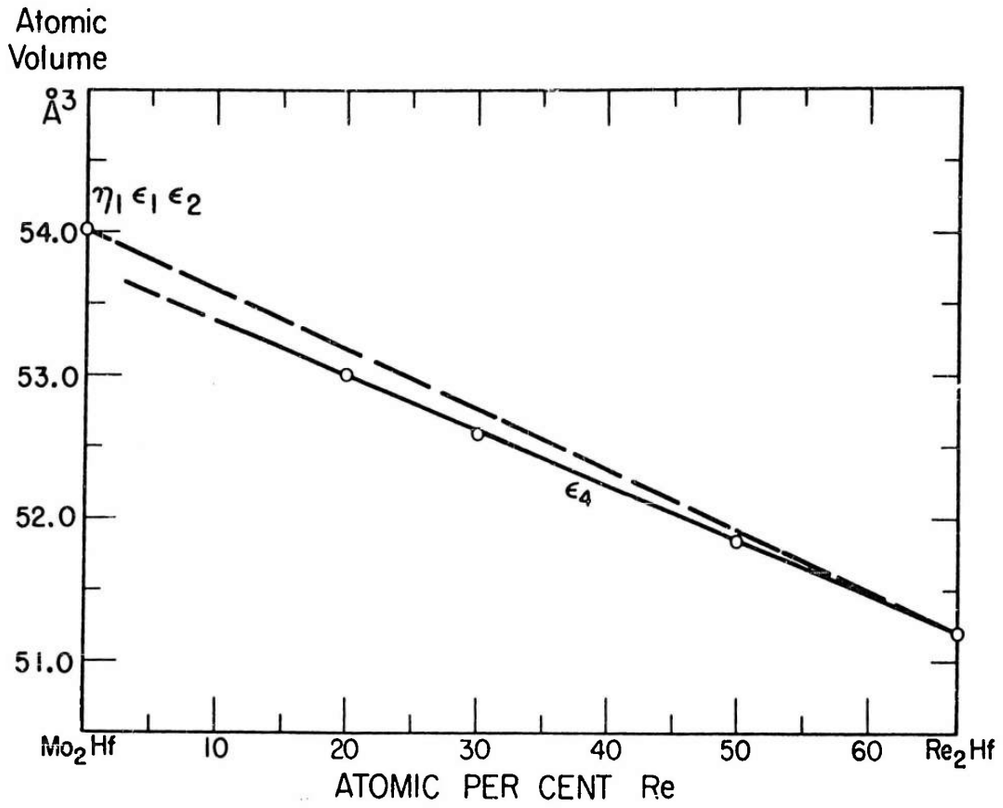

Figure V:31 - Atomic volumes from Mo_2Hf to Re_2Hf.

the melting point of Re_2Hf, it being too high for determination in the tungsten-tube furnace described above without risk of damage. By joining the liquidus and peritectic temperatures corresponding to Mo_2Hf to the melting point of Re_2Hf, as shown in Figure V:20, it was possible to obtain a tentative composition for alloys whose respective solidus and liquidus temperatures lay at 2400°C. These compositions are indicated by S and L along the line Re_2Hf - Mo_2Hf in the ternary diagram shown in Figure V:20, the point S being the extreme limit of the E_4 phase at 2400°C.

e. The ϕ Phase

As far as present results indicate, the tetragonal ϕ-phase, which in the binary system Re-Hf extends from approximately 50 to 52.5 atomic percent Re stretches, at 1600°C, into the ternary diagram, as far as Mo 22, Re 32, Hf 46. The amount of molybdenum in solid-solution decreases rapidly as the temperature is raised until, at 2400°C, the phase contains less than 4 atomic percent in solid solution.

f. The β- and α-Hf Phase Fields

The extents of the β- and α-Hf phase fields at 1600°C are substantially as drawn. At 2000°C only the β-Hf phase field can exist on account of the α-β Hf transformation occurring at 1950°C. Furthermore, the positions of the liquidus in the Mo-Hf and Re-Hf systems indicate a broad band of liquid phase separating the E and ϕ phases from β. At 2400°C, the Hf phase is now completely liquid and the liquidus line extends from approximately 23 Hf-Mo to 33 Re-Hf, only about 2/3 of the E_4 phase now being solid.

Thermal, Micrographic, X-ray and Hardness Results for the Mo-Re-Hf system are listed in Table V:3.

J. Miscellaneous Properties of Mo-Os and Mo-Re-Hf Alloys

1. Hardness and Cold-Working

a. Mo-Os

On homogenizing at 2000°C, alloys in the region of 85 Mo 15 Os became extremely coarse grained, the individual crystals being visible to the naked eye. They work-harden extremely rapidly on filing, wearing out the files and making it virtually impossible to produce powder specimens for X-ray diffraction work by the conventional filing technique. On the other hand, a hammer blow will cause the alloy to separate at the grain boundaries and the individual grains will flatten, the malleable behavior presumably being accounted for by a readiness to form mechanical twins.

Table V:3A

Hafnium-Rhenium-Molybdenum Alloys which are Predominantly α Mo

Alloy Number	Composition a/o %			Quenching Temp. °C	Phases Present	Lattice Parameters Å	V.D.H.
	Hf	Re	Mo				
1	10	15	75	2000	α Mo + E_4		
				1600	α Mo + E_4		
2	10.79	21.58	67.63	2000	α Mo + E_4		
				1600	α Mo + E_4		
3	10	25	65	2000	α Mo + E_4		
				1600	α Mo + E_4		
4	10	30	60	2000	α Mo + χ + E_4		
				1600	α Mo + χ + E_4		
5	15	15	70	2000	α Mo + E_4		
				1600	α Mo + E_4		
16	5	5	90	2000	α Mo	a = 3.1577	373
				1600	α Mo		
17	5	10	85	2000	α Mo	a = 3.1538	387
				1600	α Mo		
18	5	15	80	2000	α Mo		
				1600	α Mo + Tr E_4	a = 3.1496	394

Table V:3A (Continued)

Alloy Number	Composition [a] a/o %			Quenching Temp. °C	Phases Present	Lattice Parameters Å	V.D.H.
	Hf	Re	Mo				
19	5	20	75	2000	α Mo	a = 3.1458	
				1600	α Mo + E_4		
20	5	25	70	2000	α Mo	a = 3.1405	429
				1600	α Mo + E_4		
21	5	30	65	2000	α Mo + χ + σ		450
22	10	5	85	2000	α Mo	a = 3.1717	483
				1600	α Mo		
23	10	10	80	2000	α Mo	a = 3.1654	483
				1600	α Mo + E_4		
24	15	5	80	2000	α Mo	a = 3.1856	579
				1600	α Mo + E_1		
25	20	5	75	2000	α Mo + E_4	a = 3.1896	642
37	20	2.5	77.5	2000	α Mo + Tr E_1		634
				1600	α Mo + E_2		

Table V:3B

Hafnium-Rhenium-Molybdenum Alloys which are Predominantly χ Phase

Alloy No.	Composition a/o %			Quenching Temp. °C	Phases Present	Lattice Parameters Å
	Hf	Re	Mo			
10	5	50	45	2000	α Mo + χ + σ	
11	10	50	40	2000	α Mo + χ	
				1600	α Mo + χ	
12	20	50	30	2000	χ + E_4	
14	5	80	15	2400	χ + α Re	
				2000	χ + α Re	a = 9.6263
				1600	χ + α Re	
15	10	85	5	2400	χ + α Re	
				2000	χ + α Re	a = 9.6476
				1600	χ + α Re	
35	20	45	35	2000	χ + E_4	
				1600	χ + E_4 + α Mo	
36	20	40	40	2000	χ + E_4 + α Mo	
				1600	χ + E_4 + α Mo	
46	15	55	30	2400	χ	
				2000	χ	a = 9.7611
				1600	χ	

Table V:3B (Continued)

Alloy No.	Composition [a]/o %			Quenching Temp. °C	Phases Present	Lattice Parameters Å
	Hf	Re	Mo			
47	5	55	40	2000	$\sigma + \chi$	
48	2.5	52.0	45.5	2000	$\sigma + \chi$	
				1600	$\sigma + \chi + \alpha$ Mo	
49	2.5	60.0	37.5	2000	$\sigma + \chi$	
50	10	55	35	2400	χ	
				2000	χ + Tr σ	a = 9.7204
				1600	$\chi + \sigma$	
51	5	65	30	2400	$\chi + \sigma$	a = 9.6559
				2000	$\chi + \sigma$	
52	15	70	15	2400	χ	
				2000	χ	a = 9.7246
				1600	χ	
60	20	65	15	2400	$\chi + E_4$	
				2000	$\chi + E_4$	
				1600	$\chi + E_4$	
64	15	50	35	2400	χ	
				2000	α Mo + χ	a = 9.7721
				1500	α Mo + $\chi + E_4$	

Table V:3C

Hafnium-Rhenium-Molybdenum Alloys which are Predominantly E Phase

Alloy No.	Composition [a] a/o %			Quenching Temp. °C	Phases Present	Lattice Parameters Å
	Hf	Re	Mo			
6	21.53	16.14	62.33	2000	α Mo + E_4	
				1600	α Mo + E_4	
7	25	15	60	2000	α Mo + E_4	
				1600	α Mo + E_4	
8	20	20	60	2000	α Mo + E_4	
				1600	α Mo + E_4	
9	30	5	65	2000	α Mo + E_1	
				1600	α Mo + E_1	
13	45	25	30	2000	E_4 + ϕ + Liq.	
				1800	E_4 + ϕ + β	
				1600	E_4 + ϕ + β	
26	30	20	50	2000	α Mo + E_4	
				1600	α Mo + E_4	
27	30	15	55	2000	α Mo + E_4	
				1600	α Mo + E_4	

Table V:3C (Continued)

Alloy No.	Composition a/o %			Quenching Temp. °C	Phases Present	Lattice Parameter Å
	Hf	Re	Mo			
28	33.33	10	56.67	2000	E_4 + Tr α Mo	
				1600	E_1 + Tr α Mo	
				1780	E_1 + Tr α Mo	
				2310	melting observed	
29	33.33	20	46.67	2000	E_4	$a = 5.319_0$ $c = 8.652_7$
				1600	E_4	
30	33.33	30	36.67	2380	E_4	$a = 5.296_5$ $c = 8.658_0$
				2588	melting observed	
31	33.33	40	26.67	2485	E_4	
				2785	melting observed	
32	33.33	50	16.67	2445	E_4	$a = 5.266_8$ $c = 8.633_0$
				2900	melting observed	
33	33.33	60	6.67	2485	E_4	
				2960	E_4	
34	40	30	30	2000	E_4 + ϕ + Liq.	
				1600	E_4 + ϕ	
36	20	40	40	2000	E_4 + χ + α Mo	
				1600	E_4 + χ + α Mo	

Table V:3C (Continued)

Alloy No.	Composition [a] a/o %			Quenching Temp. °C	Phases Present	Lattice Parameter Å
	Hf	Re	Mo			
38	30	2.5	67.5	2000	α Mo + E_1	
				1600	α Mo + E_2	
39	33.33	7.50	59.17	1800	E_1 + Tr α Mo	
				1600	E_1 + Tr α Mo	
40	33.33	5.00	61.67	2183	E_4 + Tr α Mo	
				1800	E_1 + Tr α Mo	
				1600	E_1 + Tr α Mo	
41	33.33	2.50	64.17	2000	E_1 + Tr α Mo	
				1800	E_1 + Tr α Mo	
				1600	E_2 + Tr α Mo	
42	35	5	60	1800	E_1 + Tr β	
43	35	2.5	62.5	1800	E_1 + Tr β	
44	25	40	35	2000	E_4 + χ	
				1600	E_4 + χ	
45	25	40	35	2000	E_4 + χ	
				1600	E_4 + χ	

Table V:3C (Continued)

Alloy No.	Composition [a]/o %			Quenching Temp. °C	Phases Present	Lattice Parameter Å
	Hf	Re	Mo			
55	40	5	35	1600	$E_1 + \beta$	
67	45	45	10	2000	$E_4 + \phi$	
				1800	$E_4 + \phi$	
				1600	$E_4 + \phi$	
73	40	20	40	1800	E_1	
				1600	E_1	
74	35	20	45	1800	E_1	
				1600	E_1	

Table V:3D

Hafnium-Rhenium-Molybdenum Alloys which are Predominantly β Hf and ϕ Phase

Alloy Number	Composition [a] /o %			Quenching Temp. °C	Phases Present
	Hf	Re	Mo		
54	55	40	5	1600	ϕ + β
				2000	ϕ + Liq.
56	70	5	25	1600	β
57	50	45	5	2000	ϕ + Liq.
				1800	ϕ + Liq.
				1600	ϕ
58	85	5	10	1600	β
59	80	10	10	1600	β
68	50	35	15	1600	ϕ + β
				1800	ϕ + Liq.
69	[illegible]	30	10	1600	ϕ + β
70	70	20	10	1600	ϕ + β
71	60	10	30	1600	β + E_1
72	55	25	20	1600	ϕ + β

b. Mo-Re-Hf

As shown by Sims[11] and by Savitskii, Tylkina and Povarova[12], the addition of 6 atomic percent rhenium lowers the Vickers hardness number of molybdenum from approximately 190 to 150 and then increases it again to about 375 at the solid solubility limit of 37.5 atomic percent Re. The addition of hafnium also increases the hardness[4] of molybdenum to a value of approximately 600 with 20 atomic percent hafnium in solution.

Hardness measurements have been made on single phase α-Mo alloys in the ternary system Mo-Re-Hf, the results being shown in the form of iso-hardness contours in Figure V:32.

Alloys in the immediate vicinity of the ϕ phase, which are extremely brittle, also reveal an interesting phenomenon on being shattered under a hammer blow, in that sparks are seen to form on the parting surfaces during the impact. This is presumably due to the pyrophoric nature of the clean surfaces.

2. Superconductivity

As is well known, certain phases having the σ and α-Mn structures indicate marked superconductivity as the absolute zero is approached.[13] As an interesting offshoot of the present research, certain alloys in the Mo-Hf-Re system have been examined for superconductivity[14]. In the Mo-Re system, the α-Mo phase exhibits superconductivity, the critical temperatures ranging from 1.2°K to 12°K at 37.5 atomic percent rhenium. The σ phase becomes superconducting at approximately 6°, χ at about 9.7° while the α-Re phase ranges from 8° to 1.8°K for pure Re.

In the Mo-Hf binary system the only phase to show superconductivity is β-Hf, which has a constant critical temperature at about 2.4°K, while in the Re-Hf system, the critical temperature of the β phase ranges from 1.0 to 1.7°K, that of ε is 5.6° while the critical temperature of the χ-phase lies at around 6°K. The ϕ phase does not become superconducting. The critical temperature of the α-Re phase ranges from 1.75°K for rhenium to a maximum value of 7.3°K at the phase boundary.

K. Prior Work

1. Molybdenum-Osmium

Very little data are available in the literature on molybdenum-osmium alloys. Based on the fact that molybdenum-rhenium alloys have good room-temperature ductility and high temperature strength, Baird, Geach and Knapton[15] investigated the comparable molybdenum side of the Mo-Os system. Their tentative diagram, incorporating some results previously published by Raub[16] is given in Figure V:33 and shows an intermediate Mo_3Os phase which has the β-W structure and which is formed at about 2100°C by the peritectoid reaction of α-Mo solid solution containing 14 atomic percent osmium with a σ-phase. They also reported that the addition of osmium to molybdenum raises the room temperature hardness continuously

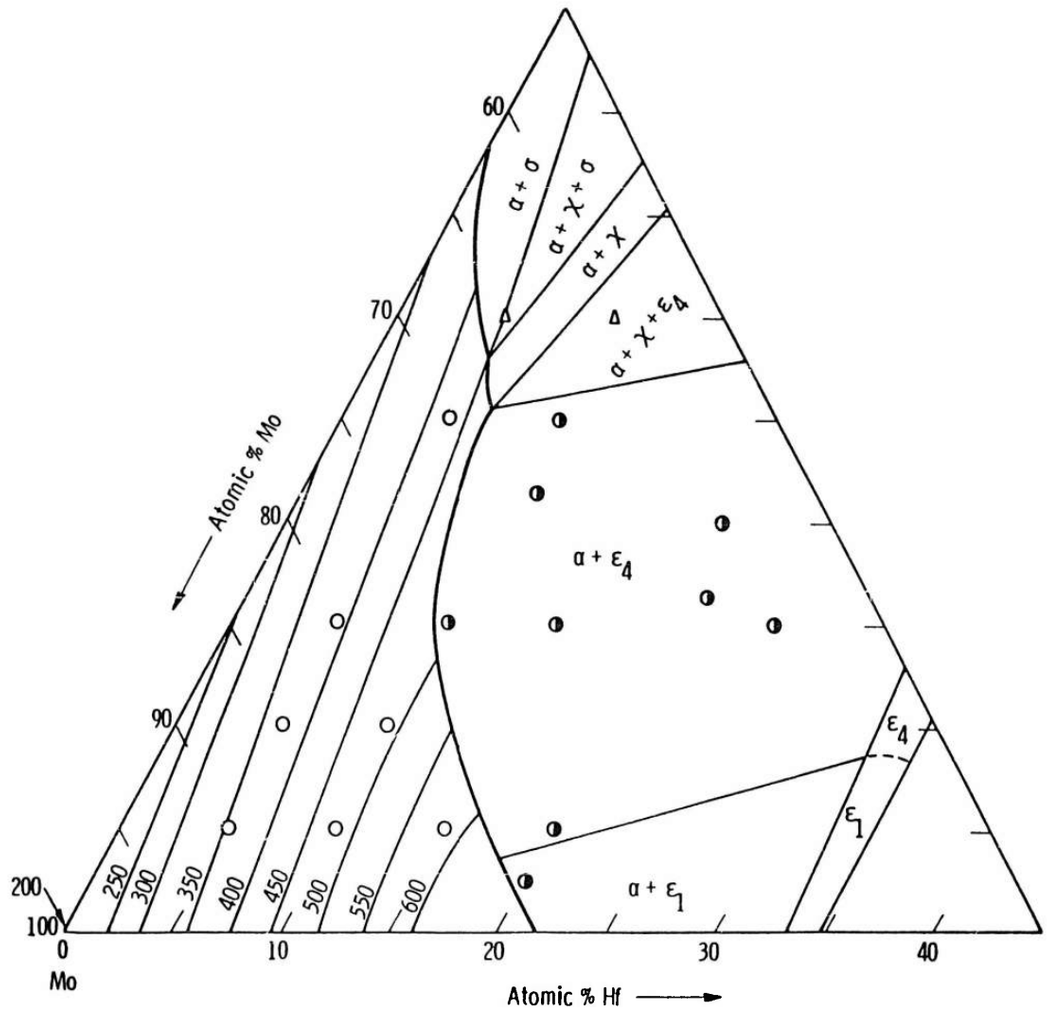

Figure V:32 - Vickers hardness of αMo phase of the Mo-Hf-Re system. Quenched 2000°C.

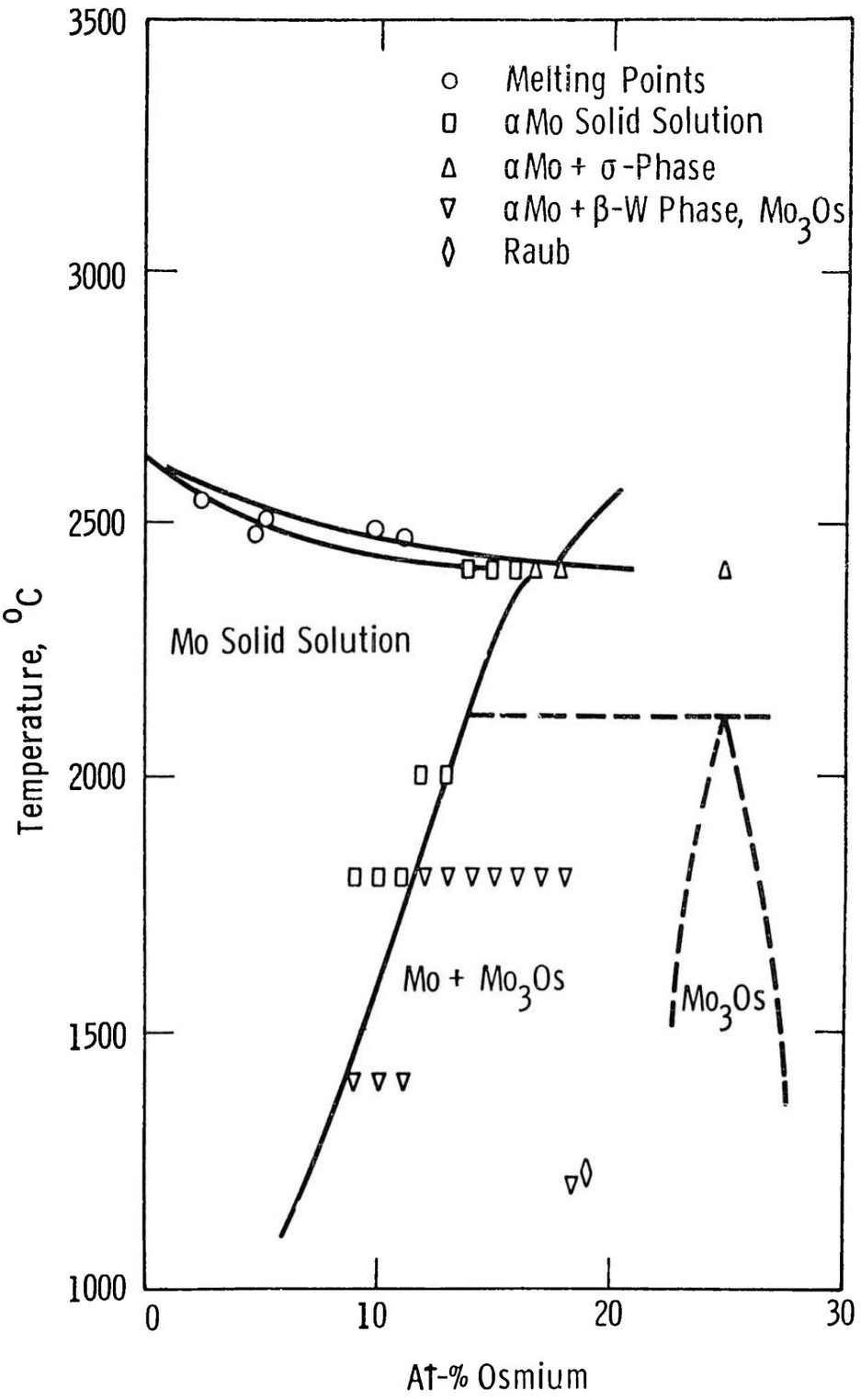

Figure V:33 - Molybdenum-osmium system (according to Baird, Geach and Knapton).

from 180 to 450 VDH at 14 atomic percent osmium. The 14 percent alloy did not work harden severely and retained its hardness well up to 1200°C, the deformation proceeding mainly by twinning.

The present, more detailed, investigation has confirmed the peritectoid reaction of α-Mo solid solution with σ-phase to form β-Mo_3Os but places the reaction temperature at 2210°C.

2. Molybdenum-Hafnium

Except for a brief reference to the crystal structure and melting point of Mo_2Hf by Elliott[17], the only detailed investigation of the Mo-Hf has been that of Taylor, Doyle and Kagle[4], reference to which has been made above.

3. Molybdenum-Rhenium

This system has been investigated in detail by Dickinson and Richardson[2], Knapton[3] and by Savitskii, Tylkina and Povarova[12]. All three groups of workers agree on the presence of the phase fields α-Mo, σ, χ and α-Re but differ in details. Savitskii, et al., show a minimum in the solidus at about 32 atomic percent rhenium which is not shown by Dickinson and Richardson, or by Knapton, while Knapton shows the eutectoidal decomposition of σ into Mo + χ at about 1100°C which is not shown by the others. In contrast to the present investigation, which places the peritectoidal decomposition of the χ -phase at about 2162°C, Dickinson and Richardson place it at about 2080°, Knapton at 1800-1850°, while Savitskii, et al., place it below 1850°C in agreement with Knapton.

4. Rhenium-Hafnium

Except for a description of the hexagonal structure of Re_2Hf by Compton and Matthias[8], the only extensive investigation of the Re-Hf system is that of Taylor, Doyle and Kagle[7], the phase diagram of which is presented in revised form in the present report. The main revision is to place the ϕ phase between 47.5 and 50 atomic percent hafnium. A tetragonal unit cell has been tentatively attributed to the ϕ phase. Details are given in the Appendix II.

APPENDIX I: SPECIAL X-RAY TECHNIQUES

X-ray diffraction patterns were taken with a Philips 114.6-mm diameter camera and a high intensity, rotating anode X-ray tube. For the most part, filtered CoKα radiation was employed. In the case of hexagonal θ-Os alloys it was found advantageous to employ ZnKα radiation on account of the (0006) reflection lying at a Bragg angle of greater than 80 degrees, thus yielding an exceptionally precise value of the c-spacing.

Lattice parameters were computed by the well known technique of extrapolating against the function $1/2\ (\cos^2\theta/\theta + \cos^2\theta/\sin\theta)$, obtaining a normal precision of about one part in 30,000.

The primary function of X-ray diffraction work is the identification of the phases in their equilibrium state. Unfortunately, because of the high temperatures required for heat treatment, the conventional technique of annealing and quenching powder specimens in evacuated, sealed-off silica capsules could not be employed. The alternative procedure was to heat treat and quench the lump samples, crush, sieve through 400 mesh gauze and X-ray. Although the high order reflections of the primary solid solutions were somewhat broadened on account of residual cold work, the patterns were sufficiently well resolved to identify the various constituent phase structures. Care had to be taken to ensure that all the crushed sample went through the sieve to avoid the effects of differential sieving which could give an erroneous indication of the balance of the phases. This was particularly true in the case of molybdenum-osmium alloys containing σ-phase. The latter is extremely brittle and passes through the sieve, while the more ductile α-Mo or θ-Os constituent is retained. Thus, diffraction patterns of improperly sieved material were invariably biased in favor of σ-phase.

Patterns with broadened doublets are for the most part unsatisfactory for lattice parameter work and the problem was how to overcome this difficulty. This was achieved by making small cylindrical containers approximately 3/8 inch in diameter and 1/2-inch high, wall thickness approximately 1/16 inch, fitted with a loosely-fitting lid about 1/16 inch in thickness, the material being of molybdenum, tungsten or hafnium according to the system for which they were employed. The crushed powders were placed in these containers and heated rapidly in a vacuum of 10^{-5} mm to a temperature at which the specimen recovered from the cold work without appreciable diffusion taking place, held there for a few minutes, then rapidly cooled. The temperatures, found by trial and error, were usually of the order of 2100°C although in some cases higher temperatures were employed. By this means, excellent diffraction patterns could be obtained from which accurate lattice parameters could be determined. In the case of hafnium-rich molybdenum-hafnium alloys, heat treatments of one months' duration were required at 800 and 700°C. These were carried out in the conventional manner, with sealed evacuated silica capsules.

In general, most of the primary solid solution and intermediate phases could be powdered by conventional filing methods or by crushing in a steel percussion mortar. Because of its peculiar work hardening properties mentioned above, the alloy 85 Mo, 15 Os could not be examined in the powder form. Instead, a rod 1/2 mm in diameter and 6 mm long was prepared by centerless grinding under a

liquid coolant to prevent oxidation. This was heated to 2000°C, the equilibrating temperature of the original ingot and radiation quenched. Although considerable grain growth had occurred and the diffraction pattern was correspondingly spotty, the pattern was single phase, in agreement with the microstructure, and a satisfactory lattice parameter could be obtained. Diffusion in this alloy must be extremely rapid, for annealing it at 1200°C for only 5 minutes causes the β phase to precipitate, the phase being clearly visible in both the photomicrographs and the X-ray diffraction patterns.

After heat treatment, powder samples were pickled in an acid solution as a check on the possibility of surface impoverishment. Invariably the diffraction patterns were the same before and after such treatment, showing that the heat treated powders were substantially homogeneous throughout.

APPENDIX II: Crystallographic Data on $Re_{52}Hf_{48}$

An intermediate phase, designated ϕ, of undetermined atomic arrangement has been discovered in the compositional range 47.5 - 50 atomic percent Hf in the rhenium-hafnium system. A powder pattern of a sample of approximate composition $Re_{52}Hf_{48}$ shows it to be tetragonal with a = 8.90, c = 13.97 Å. Crystallographic data are presented in Table V:4. A similar phase has since been discovered by Beck[9] in the Ti-Mn system.

Table V:4

Crystallographic Data on $Re_{52}Hf_{48}$

Heat Treatment:

18 hours at 2000°C, and quenched.
Chromium Kα radiation, Philips 114.6 mm Debye Scherrer Camera.
Unit cell: Tetragonal with a = 8.90, c = 13.97 Å.

h k l	Intensity	Observed Uncorrected $Sin^2\theta$	Calculated $Sin^2\theta$
101	VVW	.0237	.0233
---	VVW	.0282	
---	VVW	.0355	
---	VVW	.0523	
201	VVW	.0713	.0729
222	VVW	.1619	.1593
005	VVW	.1696	.1691
302	VW	.1778	.1759
105	W	.1858	.1857
223 303	W	.1979	.1931 .2097
320	S	.2140	.2149
Hf	VW	.2180	Hf
313	S	.2266	.2262
---	VVW	.2301	
205	S	.2377	.2353
304	S	.2572	.2570
106	S	.2612	.2601

Table V:4 (Continued)

h k l	Intensity	Observed Uncorrected $Sin^2\theta$	Calculated $Sin^2\theta$
116	M	.2767	.2766
410	VW	.2811	.2810
411	VW	.2851	.2878
402	W	.2925	.2916
331	W	.3048	.3043
412	M	.3084	.3081
332	M	.3241	.3246
107	VVW	.3487	.3481
333	M	.3518	.3585
422	VVW	.3557	.3577
404	W	.3710	.3728
325	M	.3878	.3841
207	VW	.3988	.3977
316	VVW	.4102	.4089
510	VW	.4298	.4298
227	VVW	.4620	.46[illegible]
503	VVW	.4765	.4742
513	VW	.4937	.4907
522	VW	.5061	.5065
406	VVW	.5120	.5081
523	MS	.5408	.5403
228	VVW	.5648	.5652
426	VW	.5751	.5742
443	VVW	.5892	.5899
515	VVW	.5995	.5990
209	W	.6147	.6142
533	W	.6234	.6230
612	S	.6388	.6387
525	S	.6506	.6486

Table V:4 (Continued)

h k l	Intensity	Observed Uncorrected $Sin^2\theta$	Calculated $Sin^2\theta$
427	S	.6661	.6622
541	M	.6853	.6845
604	M	.7016	.7034
11.10	M	.7093	.7097
319	M	.7118	.7134
614	S	.7173	.7199
526	M	.7251	.7230
535	VVW	.7328	.7312
20.10	W	.7406	.7427
631	WM	.7527	.7507
605	M	.7632	.7643
615	M	.7798	.7808
700α α_1	S	.8098	.8100
α_2		.8134	
710α α_1	W	.8263	.8266
419α α_2		.8290	.8291
634α α_1	S	.8503	.8522
11.11α			.8517
712α α_2		.8538	.8536
α_1	W	.8583	
640α			.8596
447α α_2		.8615	.8605
20.11α α_1	M	.8854	.8848
713α			.8874
642α α_2		.8883	.8867

Table V:4 (Continued)

h k l		Intensity	Observed Uncorrected $Sin^2\theta$	Calculated $Sin^2\theta$
	α_1		.8962	
537α		S		.8936
21.11α	α_2		.8998	.9013
	α_1		.9040	
722α		VW		.9032
626α	α_2		.9078	.9048
	α_1		.9166	
704α		S		.9183
643α	α_2		.9203	.9205
546α	α_1	VVW	.9237	.9213
607α				.9267
	α_1		.9321	
714α		VW		.9348
	α_2		.9364	
40.10	α_1	VVW	.9408	.9411
	α_1		.9443	
617α		S		.9432
	α_2		.9476	
22.11α	α_1	WM	.9521	.9509
41.10α				.9576
	α_2		.9555	
	α_1		.9639	
731α		W		.9656
644α	α_2		.9676	.9679

Table V:4 (Continued)

h k l		Intensity	Observed Uncorrected $Sin^2\theta$	Calculated $Sin^2\theta$
	α_1		.9719	
33.10α		W		.9742
00.12α	α_2		.9755	.9743
705α	α_1	VVW	.9791	.9792
31.11α	α_1		.9834	.9840
732α		W		.9858
724α	α_2		.9868	.9844

APPENDIX III: METALLOGRAPHIC PROCEDURES FOR MOLYBDENUM-OSMIUM AND MOLYBDENUM-HAFNIUM-RHENIUM ALLOYS

Specimens for these studies were furnished in the form of small pieces cut from buttons of the alloy. Since these specimens were used for further heat treating experiments following metallography, they were mounted in a cast lucite (KOLDMOUNT) composition. With this mounting method they could be removed from the mounts without the introduction of mechanical strain simply by immersing in glycerin at 175°C until the mount softened and the specimen fell out.

Grinding operations on all specimens were performed on Automet polishing equipment. The grinding steps were the same in all cases consisting of grinding on silicon carbide papers. The grit sequence was 120, 240, 400, 600. Water was used as a lubricant-coolant. Fine grinding was with 6μ diamond on white duck cloth with kerosene as a lubricant and also in the Automet equipment.

Final polishing had to be varied to meet the requirements of the individual alloy. In nearly all cases, however, it also was done on the Automet equipment. All of the refractory metals are difficult to polish. Polishing artifacts are common and care must be exercised that these artifacts are not considered as the true microstructure. Most of the specimens are more rapidly finished and with less trouble from artifacts if an attack-polishing technique is used. The reagents used for the purpose cannot be employed safely with hand polishing techniques. In the entire molybdenum-osmium series and in the molybdenum-hafnium-rhenium series with the exception of those alloys high in hafnium the best results were obtained with an attacking etchant consisting of 5% chromic acid and 30% gamma alumina (Linde B) in water. Hafnium and high hafnium alloys were finished with the following etchant as the attacking agent again combined with Linde B and diluted with water.

30% peroxide	50 ml
Nitric acid	50 ml
Hydrofluoric acid	5 ml

This solution undiluted also can be used as a chemical polish for single-phase, high-hafnium, alloys.

Rhenium and the high rhenium alloys are extremely susceptible to cold working and the formation of mechanical twins. Unlike the remainder of the platinum metals, rhenium is attacked readily by nitric acid.

Pure molybdenum and single phase molybdenum alloys are best finished by electropolishing. One of the best electrolytes for the purpose consists of the following.

Methanol	150 ml
Hydrochloric acid	50 ml
Sulfuric acid	20 ml

This is used at about 25-30 volts and preferably at near $0^{o}C$. The time for a properly ground specimen is 10-20 seconds or only until the residual scratches and cold work are effectively removed.

Etching procedures must be varied to suit the material. Molybdenum and high molybdenum alloys are etched nicely in the following solution.

Water	100 ml
Potassium ferricyanide	5 gm
Potassium hydroxide	2 gm

This etchant also will etch the entire molybdenum-rhenium series up to 95% Re. The molybdenum-hafnium series from 80 Mo - 20 Hf to 50 Mo - 50 Hf is etched satisfactorily in the following solution.

Lactic acid	40 ml
Nitric acid	40 ml
Hydrofluoric acid	2 drops

Hafnium and high hafnium alloys are optically anisotropic and best examined in polarized light. The chemical polishing solution previously given for hafnium will produce an etched structure if diluted slightly with water.

Osmium is not attacked by any mineral acid or combination of mineral acids. It also is anisotropic and is best examined by means of polarized light. Where etching is necessary this can be done electrolytically in 10% alcoholic hydrochloric acid at 10 volts and 30 secs. Second phases are rapidly attacked by this procedure.

Pure rhenium is etched nicely by 5% Nital. This etchant, however, will not attack rhenium containing any appreciable alloying addition. In these cases it is sometimes difficult to find an etchant that will reveal the microstructure without developing severe pitting of the rhenium rich phases.

Etching in this class of materials has not, in all cases, proven to be a reliable or reproducible procedure and adjustments to compensate for the individual characteristics of certain specimens have been necessary. These things may be due to the complex phase picture and an uncertain knowledge of it on the part of the metallographer.

REFERENCES

1. Taylor, A., Kagle, B. J., and Doyle, N. J., J. Less Common Metals, 3, 333 (1961); WADD Technical Report 60-132, Wright Air Development Division.

2. Dickinson, J. M., and Richardson, L. S., Trans. ASM, 51, 1055, (1959).

3. Knapton, A. G., Trans. ASM, 51, 1067, (1959); J. Inst. Metals (London) 87, 62, (1958-59).

4. Taylor, A., Doyle, N. J., and Kagle, B. J., J. Less Common Metals, 3, 265 (1961); WADD Technical Report 60-132, Wright Air Development Division.

5. Langeron, J. P., and Lehr, L., Mem. Sci. Rev. Met., 56, 307, (1959).

6. Newkirk, J. B., and Geisler, A. H., Acta Met., 2, 117, 1954.

7. Taylor, A., Doyle, N. J., and Kagle, B. J., WADD Technical Report 60-132, Oct. 1960, Wright Air Development Division.

8. Compton, V. B., and Matthias, B. T., Acta Cryst.,12, 651 (1959).

9. Beck, P., Private communication.

10. McHargue, C. J. and Maynor, H. W., Trans. AIME, J. of Metals, 197, 1382, (1953).

11. Sims, C. T., Trans. ASM, 51, 1068 (1959).

12. Savitskii, E. M., Tylkina, M. A., and Povarova, K. B., Russian Journal of Inorganic Chemistry (Translation of Zhurnal Neorganicheskoi Khimii) 4, 190, (1959).

13. Blaugher, R. D., and Hulm, J. K., J. Phys. Chem. Solids, 19, 134, 1961.

14. Blaugher, R. D., Hulm, J. K., and Taylor, A., I.B.M. Journal (To be published).

15. Baird, J. D., Geach, G. A., and Knapton, A. G., 1958 Plansee Proceedings, High Melting Metals, p. 371, (Published by Metallwerk Plansee A.G., Reutte/Tyrol, 1959).

16. Raub, E., Zeits Metallk., 45, 23, 1954.

17. Elliott, R. P., Technical Report No. 1. OSR-TN-247 (Armour Research Foundation, August, 1954).

VI. CONSTITUTION DIAGRAMS Ta-Rh, Ta-Ir (Work done at Massachusetts Institute of Technology by B. Giessen)

A. General

The Ta-Rh and Ta-Ir phase diagrams have not been treated in the literature; however, intermetallic phases occurring in them have been described[1-4]. This study attempts to work out the diagrams covering the details of phase boundaries as well as the crystallography of the intermediate phases.

B. Material

Starting Materials were Ta powder of 99.8 percent purity, supplied by National Research Corporation. Rh and Ir of 99.9 percent purity were supplied by Bishop Company, Malvern, Pennsylvania. The purities were as given in Table VI:1. In addition to the spectroscopic analysis, an oxygen analysis has been made of all elements used.

Table VI:1

Analyses of Metals Used

Element	Ta, ppm	Rh, ppm	Ir, ppm
C	40		
O	574		
H	55		
N	35		
Fe	64	60	50
Cr	26		
Ni	55		
Si	180	80	30
Nb	75		
Al	<50	5	3
Cu	<50	5	3
Ti	<10		
Mo	78		
Na	40		
Pb		20	
Mg		1	10
Mn		1	
Ag		10	1
Sn		30	
Pt		20	50
Pd		30	1
Ir		300	major
Rh		major	200
Ru		200	

C. Alloy Preparation

After various trials, the standard procedure employed in making the ingots was as follows: the powders were mixed manually, compacted under 16,000 psi and arc melted at max. 500A, standard melting grade argon. The buttons were reversed or, if possible, crushed and remelted three times. Due to the price of Rh and Ir, button size varied between 5 - 10 g. Melting presented no difficulties except for Ta-rich alloys, which showed considerable splashing as a result of purification taking place during melting. The average weight loss of 2 atomic percent rose to 5 percent in such cases. However, subsequent remelting resulted in weight losses of a maximum of 0.1 atomic percent. Thus, it can be assumed that the losses incurred result mainly from splashing and would therefore be of a composition similar to the initial one for a well-mixed compact.

Some alloys were melted from premelted stock. In agreement with previous findings, the homogeneity is somewhat impaired in high melting samples; therefore, the absence of any weight loss did not constitute a sufficient advantage and almost all alloys were melted from powder compacts. The buttons obtained often showed inhomogeneities. This is not due to insufficient blending of the elements but to crystallization taking place from the bottom. Further remelting is no remedy and an estimate of the diffusion coefficients shows that the times necessary for macro-homogenization are prohibitive. Cross-section slices of most buttons were made, especially in the Ta-rich section of the diagram, and the distribution of the phases was checked. Small buttons show smaller concentration gradients and are preferable. Sometimes only the center portions of the buttons were used.

Objections to the procedures utilized might include the following: (a) Presintering could reduce the splashing losses. It was felt, however, that the uncertainty of concentration resulting from inhomogeneities outweighs that incurred by the weight loss. (b) The argon used in melting might be sent through a purification train. But since a test reported previously[5] had not shown an oxygen pickup of >10 ppm in Hf, the gas employed was regarded as sufficiently clean. This weight check also excluded tungsten pickup from the electrode in this case.

D. Concentration Determination

On the basis of the above melting results, it was felt that the weight balance method was sufficient as sole composition check. Estimates were made assuming extreme concentrations of the lost material, then a reasonable mean value was adopted. Since in crucial parts of the diagram a spacing of 1.5 atomic percent is used, an additional check was made. Only one alloy at 50 percent had picked up oxygen through impure preparation and was discarded. In this case a gray and a white oxide were found to occur. The alloys used are given in Table VI:2 (a) and (b).

E. Temperature Measurements

Temperature measurements were carried out with the Leeds and Northrup optical pyrometer used previously. In the middle and toward the termination of the work, a calibration using the melting points of Au, Pt, Rh and Nb was carried out. This calibration showed a higher deviation from the specimen temperature

Table VI:2(a)

Compositions of Ta-Rh Alloys

(atomic percent)

2 ± .5	40.0 ± 0	69.7 ± .3
4 ± 1	44.5 ± .5	72.3 ± .5
6.5 ± 1	45 ± .2	74.5 ± .5
9.5 ± 1	49.7 ± .2	78.0 ± .5
12 ± .5	52 ± .5	79.3 ± .7
15 ± .5	53 ± .5	81.0 ± 1.0
16.5 ± 1	54.7 ± .3	84.5 ± .5
19 ± 1	56.0 ± .5	85.5 ± .9
22 ± 1	57.3 ± .7	86.5 ± .5
24 ± 1	59.5 ± .5	89.5 ± .5
25 ± 1	60.5 ± .5	91.3 ± .7
26.5 ± 1	62 ± .5	94.4 ± .6
29.5 ± .5	64.5 ± .5	97.5 ± .5
34.5 ± .5	66.5 ± .5	
37.5 ± .5	68 ± .5	

Table VI:2(b)

Compositions of Ta-Ir Alloys

(atomic percent)

2.4 ± .2	39.5 ± .5	67.0 ± .5
4.6 ± .5	40.8 ± 1	70.0 ± .2
6.0 ± .5	42.7 ± 1	74.5 ± .2
8.0 ± .1	44.5 ± .5	77.0 ± .5
9.7 ± .5	49.2 ± 1	79.0 ± 1
12.2 ± .5	51.7 ± 1	80.8 ± 1
14.6 ± .5	53.9 ± 1	84.5 ± .5
17.2 ± .5	57.0 ± .5	85.5 ± 1
19.6 ± .5	58.5 ± 0	87.5 ± .5
21.7 ± .5	59.0 ± 0	89.2 ± 1
23.6 ± .5	59.5 ± .5	90.8 ± 1
24.9 ± .1	59.7 ± 0	92.8 ± 1
29.9 ± .2	61.0 ± 0	94.2 ± 1
34.5 ± .5	61.6 ± 1	96.9 ± 1
37.2 ± .5	64.0 ± 1	

than would be expected by using the known corrections for the Pyrex window. The reason was found to be an interference of the magnetic field caused by the AC power leads of the furnace with the pyrometer filament. However, with these corrections applied, the accuracies of the temperature are: $\pm$ 15°C at 1800°C, $\pm$ 25°C at 2500°C. For thermal analysis, Pt-Pt 10 percent Rh thermocouples and a "Speedomax" recorder were used. The thermocouple was calibrated by direct measurement of the melting points of Au and Ni, as well as comparison with the optical pyrometer.

F. Heat Treatment

All heat treatments were carried out in a tantalum tube furnace constructed for this program. The heating element is a tube of 12-inch length, 1-inch diameter, surrounded by 10 spiral heat shields. The power input is 2.7 kVA at 1800°C. It is equipped with two sight ports, thermocouples, etc. Quenching is done by melting a suspension wire, and while provisions exist for a tin bath, all quenching was done by dropping the specimens on a cool molybdenum plate.

1. Ta-Rh

Samples annealed in Ta-containers were cooled from 1800°C to 1000°C in 5 seconds; those in crucibles cooled in 15 - 30 seconds. This proved to be sufficient to prevent transformations except for one case to be mentioned. Ta-containers and Al_2O_3 and ThO_2 crucibles were employed. All specimens were homogenized by holding them at 1600°C for 72 hours. The Ta-rich specimens (<15 atomic percent Rh) were held at 1970°C for an additional 36 hours. This treatment eliminated all coring found in as-cast structures. The heat treatments of the samples were carried out according to the schedule given in Table VI:3 (a). These time values are sufficient above 1700°C, where longer times cause no further change of the structure. Below 1700°C, however, longer times might have been useful, but the slope of all phase boundaries is such that no significant changes are expected.

Table VI:3(a)

Schedule of Heat-Treatments for Ta-Rh

1320°C	6 days
1495°C	3 days
1675°C	1 day
1810°C	3 hours
1955°C	1 hour
2045°C	12 hours (Ta-rich specimen)

2. Ta-Ir

Thermal treatments are listed in Table VI·3 (b). The specimens were homogenized for 24 hours at 1784°C or held for a comparable time at a comparable temperature. Ta-rich compositions were treated in Ta buckets. Ir-rich compositions were treated in thoria crucibles. Compositions in the range 40 - 75 atomic percent Ir were treated in Al_2O_3 crucibles below 1800°C; zirconia crucibles 1800 to 2000°C; and in thoria above 2000°C.

Table VI:3(b)

Schedule of Heat-Treatments for Ta-Ir

1525°C	2 days
1628°C	3 days
1784°C	1 day
1940°C	1 day
2044°C	16 hours
2252°C	2 hours
2330°C	1/2-hour

G. Techniques for Phase Boundary Determinations

1. Solidus Points

All solidus points were measured by using the technique described by Rapperport and Smith[6] utilizing a tantalum black-body to which the specimen is fastened using ThO_2 or ZrO_2 insulation. Heating steps were about 20°C. Since the pyrometer calibration was carried out the same way, no significant errors are introduced except through failure to notice incipient melting. Metallographic checks were used. Thus, temperatures of invariant reactions are more accurate than those for solid solutions, which may be too high in some cases.

The 45 atomic percent Rh alloy was measured by thermal analysis. Solidus measurements are given in the diagrams. The eutectic temperature measured in this manner checked well with the value obtained by incipient melting.

2. Metallography

Metallographic examination of the alloys included cutting on abrasive wheels, mounting in bakelite, grinding through No. 600 paper, and polishing on alumina and No. 4, 6, and 8 diamond compound lap. Alloys with less than 25 atomic percent Rh were etched in 50 percent HF for about 2 seconds (etchant I). This etchant stains α-Ta, and does not attack the σ phase. Etchant II consists of electrolytically etching the alloys in concentrated HCl at 5 volts AC for 5

seconds to 5 minutes, depending on the concentration. This etchant stains σ and α_1, consecutively, then shades α_2 and finally marks the grain boundaries between α-$TaRh_3$ and α-Rh, and does not attack α-Ta or α-Rh. This method proved satisfactory for the entire diagram. Identical procedures applied to Ta-Ir samples.

3. X-Ray Analysis

X-ray analysis was carried out using a General Electric XRD5 diffractometer and Norelco 114.6 mm and 57.3 mm Debye Scherrer cameras. The cameras were used for crystal structure and lattice parameter determination; the diffractometer permitted fast surveys and series measurements of back-reflection lines, while the cameras gave better resolution for the line-rich patterns of σ, α_1 and α_2 and the superstructure lines of α-$TaRh_3$.

To prepare specimens, annealed samples were powdered in the concentration ranges 10 - 45 and 57 - 90 atomic percent Rh, in which the powders were brittle. The terminal solid solutions between 0 and 10 and 90 to 100 atomic percent Rh were hammered into flat platelets suitable for diffractometer work. The material between 45 and 57 atomic percent Rh, which is hard and cannot be deformed or powdered easily, was ground into rods of 5-mil diameter and 1/8-inch length for use in the Debye Scherrer camera. Subsequent to specimen preparation all material was annealed for short periods at the original heat treating temperature in Ta-foil baskets or if the temperatures were higher, in ThO_2 crucibles. No sintering occurred. This yielded stress-free powders, and high angle lines could be readily observed. Procedures employed for Ta-Ir were similar.

The detailed Ta-Rh system is given in Figure VI:1 and lattice parameters for both systems are given in Figure VI:2 and VI:3.

The accuracy of the lattice parameter work varies from 0.002 Å to 0.0002 Å for solid solutions α-Ta, α-Rh, α-$TaRh_3$, α-$TaIr_3$ and α-Ir, and is 0.01 Å for σ (Ta-Rh, Ta-Ir), α_1 (Ta-Rh), α_2 (Ta-Rh) and α_2 (Ta-Ir). The structure determinations for α_1 and α_2 (Ta-Rh) will be given in the Appendix. To find the crystal structure of α_3 (Ta-Rh) a 52.5 atomic percent Rh specimen was ground and heated in a Rigaku-Denki high temperature X-ray camera. This camera was not equipped with a good vacuum system, and the specimen oxidized rapidly. Also, the maximum temperature (1350°C) was not sufficient to reach the eutectoid. No useful results were obtained.

4. Reactions and Phase Boundaries

a. Ta-Rh

Except for the eutectoid $\alpha_3 = \sigma + \alpha_1$, all non-variant temperatures were found by solidus measurements; for this reaction, thermal analysis was used. The transformation occurs instantaneously and is quite exothermic, thus the transformation point could be exactly recorded. It was confirmed by micrographic studies of alloys quenched from above and below the transformation temperature.

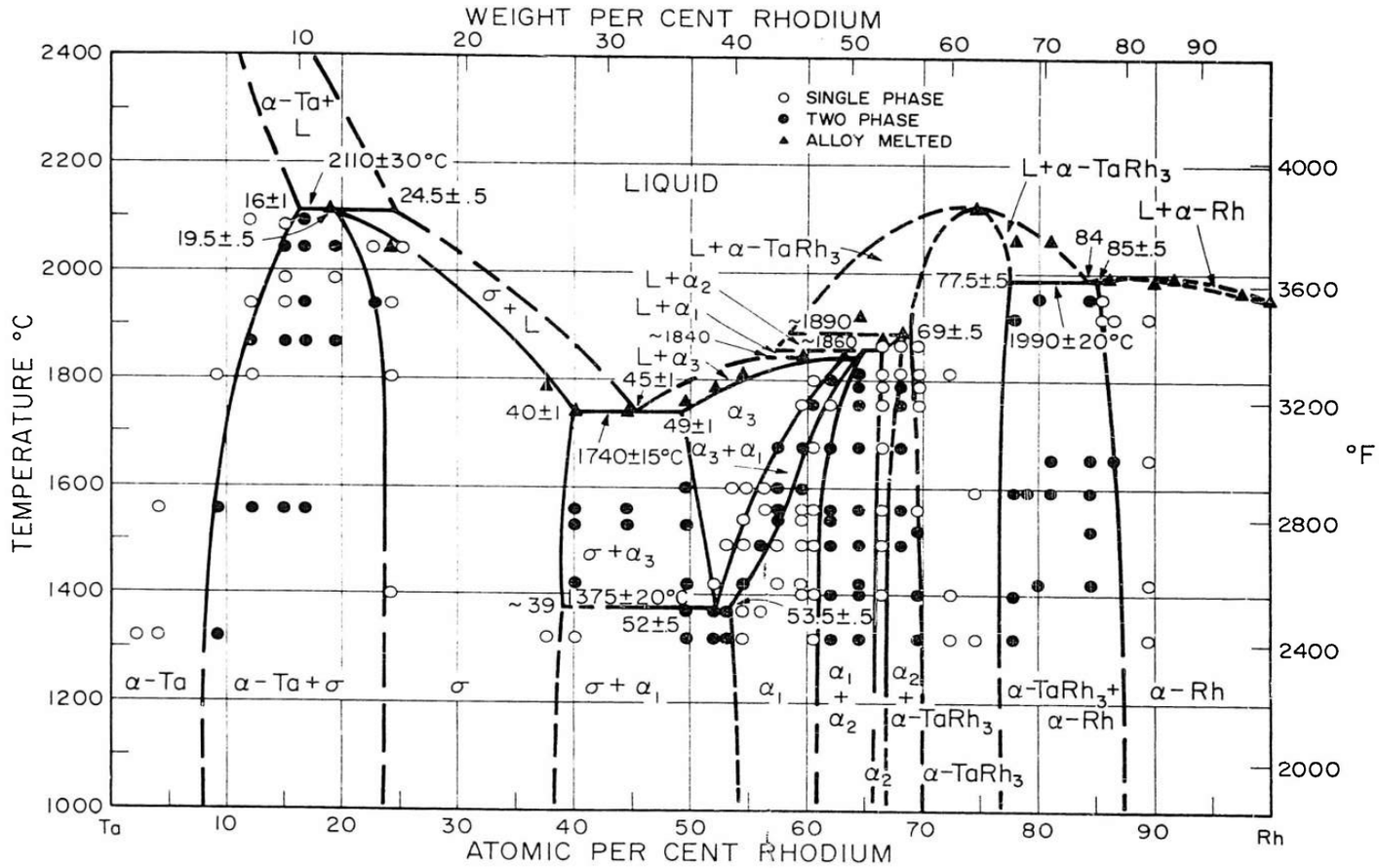

Figure VI:1 - Tantalum-rhodium constitution diagram.

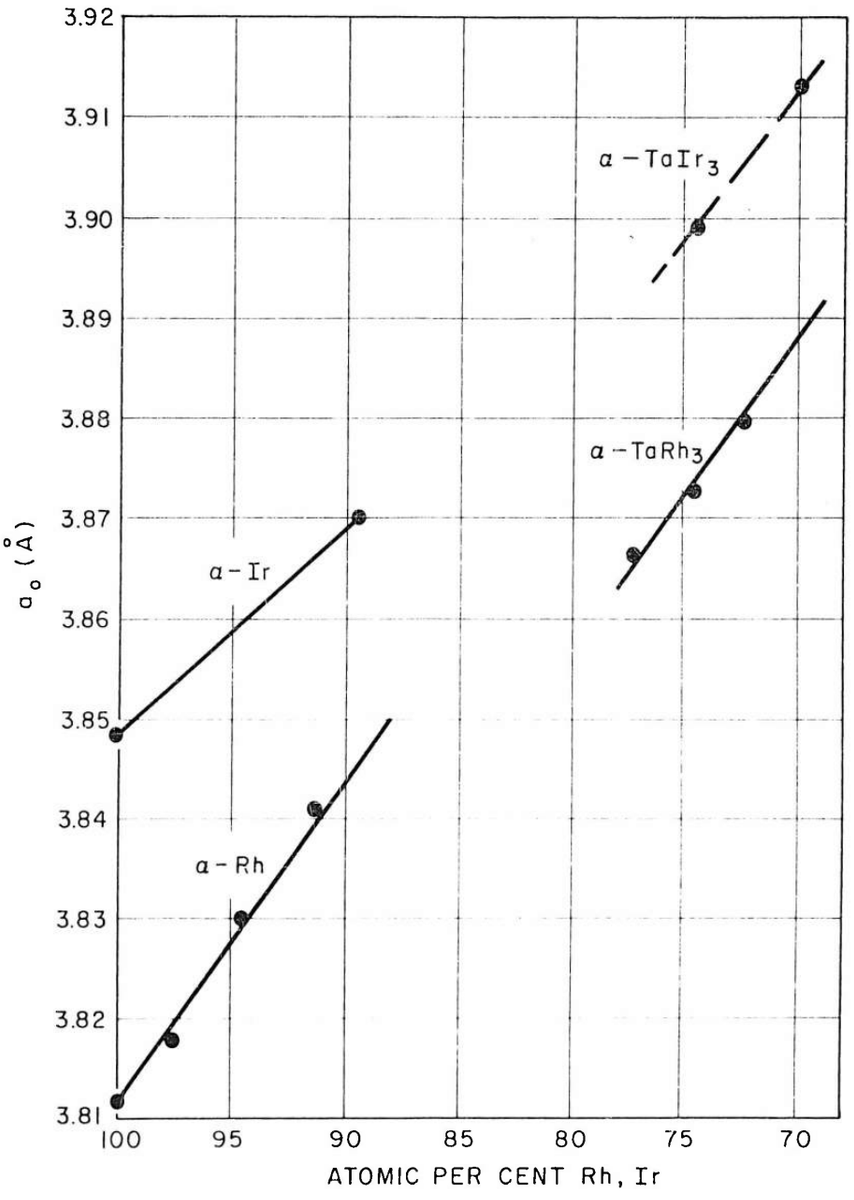

Figure VI:2 - Lattice parameters of α-Rh and α-Ir.

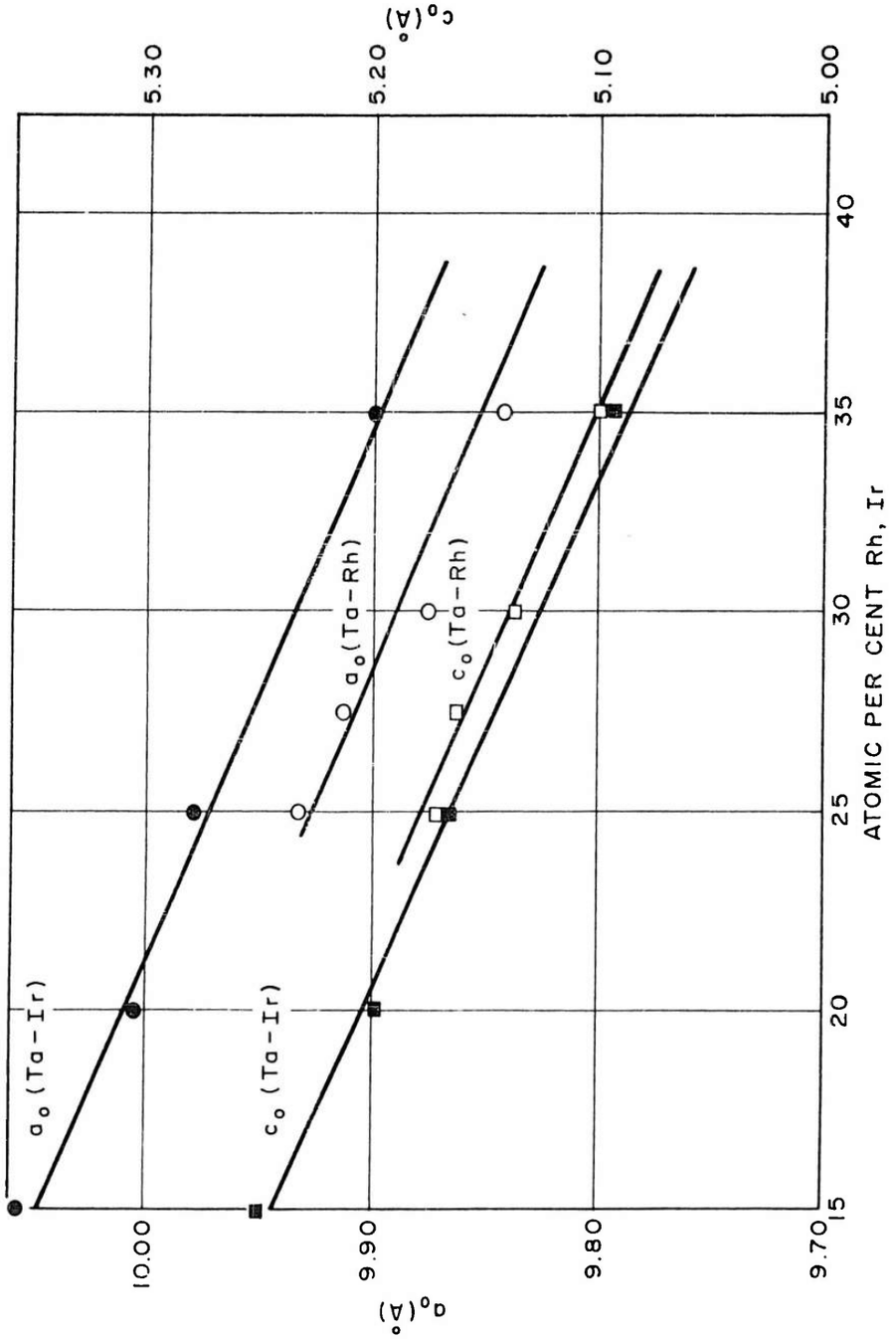

Figure VI:3 - Lattice parameters of σ-(Ta-Rh) and σ-(Ta-Ir).

The concentrations involved were obtained by metallography and extrapolation of phase boundaries. The liquidus composition in α-Ta + L = σ was obtained by examination of as-cast structures for α-Ta cores, for L = σ + α_1 and L = α-$TaRh_3$ + α-Rh. The areas of the eutectic constituent were extrapolated to 100 percent. The accuracy of all points thus determined was better than $\pm$ 1 percent. Only the reactions L + α_1 = α_3, L + α_2 = α_1, and L + α-$TaRh_3$ = α_2 could not be satisfactorily defined and are thus tentative.

Phase boundaries were determined primarily by metallographic examination and extrapolation of the amount of second phase present. The accuracy thus obtained is in most cases equivalent to that of the isoparametric method, $\pm$ 1 percent.

b. Ta-Ir

Solidus measurements were performed as described in the Ta-Rh work on specimens which were microscopically homogeneous. The iridium used in this work was found to have a melting point of 2360°C $\pm$ 25°C, although the most recent published value is 2443°C. The melting points of the Ir-rich compositions are somewhat sensitive to oxygen pick-up, and it is possible that the true melting points for these alloys are higher than observed in this investigation.

The phase boundaries were determined microscopically. It is believed that due to the steep slope of all the boundaries below 2000°C, metallographic determination is accurate to $\pm$ 1 atomic percent.

The eutectic temperature and reaction at 44.5 atomic percent Ir was found by the partial melting and fusing together of an annealing run at this temperature. The eutectic temperature and reaction at 84.5 atomic percent Ir was determined metallographically, and further corroborated by the melting of an annealing run at 2340°C and the incipient fusion of an annealing run at 2330°C.

H. Tantalum-Rhodium Constitution Diagram

The tantalum-rhodium phase diagram is marked by the occurrence of five intermediate phases:

σ	(tetragonal, analogous to σ (FeCr) between 23.5 and 39 atomic percent Rh at 1500°C)
α_1	(orthorhombic, similar to VCo_3 between 53.5 and 61 atomic percent Rh at 1300°C)
α_2	(orthorhombic, probably isomorphous with Co_2Si, at 66.5 atomic percent Rh at 1500°C)
α_3	(high temperature phase of unknown structure between 50 and 58 atomic percent Rh at 1700°C)
α-$TaRh_3$	(superstructure of the $AuCu_3$ type between 70 and 76.5 atomic percent Rh at 1500°C)

σ forms peritectically at 2110°C according to α-Ta + L = σ. σ and α_3 form a eutectic at 1740°C (L = σ + α_3), α_3 forms by a peritectic reaction L + α_1 = α_3

at approximately 1840°C and decomposes according to $\alpha_3 = \sigma + \alpha_1$ at 1375°C. α_1 forms peritectically at approximately 1860°C, ($L + \alpha_2 = \alpha_1$). α_2 also forms by a peritectic reaction $L + \alpha\text{-}TaRh_3 = \alpha_2$ at approximately 1890°C, although there is some doubt about this reaction. An alternative possibility will be discussed below. Finally, $\alpha\text{-}TaRh_3$ forms a eutectic with α-Rh at 1990°C, $L = \alpha\text{-}TaRh_3 + \alpha\text{-}Rh$.

Some details are illustrated through the following micrographs.

Figure VI:4 (9.5 atomic percent Rh, six days at 1320°C) shows the equilibrium two-phase structure consisting of brown stained Ta and a network of white σ-phase. Figure VI:5 is an as-cast structure of a 24 atomic percent Rh alloy with dark Ta-dendrites in a matrix of σ. This illustrates the determination of the peritectic liquidus point. Figures VI:6 and VI:7 demonstrate the decomposition of α_3. On cooling, α_3 decomposes into a network of needles of α_1 and σ at T = 1375°C; these needles are shown in Figures VI:8 - VI:10. In Figure VI:6, a 50 percent Rh alloy is given which was first homogenized at 1600°C forming large α_3 grains with a coarse grain boundary segregate of brown σ phase. α_3 was transformed into lamellar $\sigma + \alpha_1$ on cooling and later σ was spheroidized through heat treatment at 1320°C for six days. This structure must not be confused with that of the eutectic at 45 atomic percent Rh, which is destroyed by homogenization and can be seen only in as-cast specimens. The alloy at 52 percent Rh given in Figure VI:7 was quenched from the α_3 one phase region and then spheroidized at 1320°C for six days, showing dark σ in a white matrix of α_1. In Figure VI:8 (57.3 percent Rh, three days at 1557°C) isothermal α_1 (white) and fine eutectoid ($\sigma + \alpha_1$) can be seen. The appearance of isothermal α_1 in plates as well as spheres was noticed. Figure VI:9 of a 59.5 atomic percent Rh alloy annealed for 16 hours at 1754°C in the α_3 field shows only the decomposition structure, dark σ needles in α_1. In Figure VI:10 (60.5 atomic percent Rh, 16 hours at 1754°C) a substantial amount of isothermal α_1 is present, bracketing the phase boundary. Figure VI:11 (64.5 atomic percent Rh at 1754°C) shows the two phase region α_1 - α_2. Light α_1 grains are mixed with gray grains of α_2 which show strong twinning typical of α_2. Dark lines are cracks. Figure VI:12 (66.5 atomic percent Rh, 6-1/2 days at 1392°C) shows one phase α_2. Figure VI:13 (68 atomic percent Rh, 6-1/2 days at 1392°C) is taken from the two phase field of $\alpha_2 + \alpha\text{-}TaRh_3$. Twinned α_2 (gray) is in equilibrium with $\alpha\text{-}TaRh_3$ (white). At this temperature, incipient precipitation of α_2 in the $\alpha\text{-}TaRh_3$ matrix can be seen. Figure VI:14 shows a 69.7 atomic percent Rh alloy which was one phase after homogenization at 1600°C. After six days at 1320°C, it had segregated into α_2 and $\alpha\text{-}TaRh_3$. The structure in Figure VI:15 (79.3 atomic percent Rh, 2 hours at 1930°C) consists of white dendritic primary $\alpha\text{-}TaRh_3$ and a eutectic between $\alpha\text{-}TaRh_3$ (white spheres) and α-Rh. This eutectic is better illustrated by Figure VI:16 of 84.5 atomic percent Rh alloy annealed at 1961°C for 1/2 hour. This eutectic could first be resolved only by electron-microscopy (Formvar-Replica, Siemens EM, X6000); later, annealing slightly below the melting point coarsened the structure sufficiently for light microscopy (see below).

The diagram is well established except for the following points:

(1) The crystal structure of α_3, which remains unknown.

(2) The melting temperatures of α_3, α_1 and α_2 should be determined more accurately, and the postulated relations should be checked. α_2 shows very strong

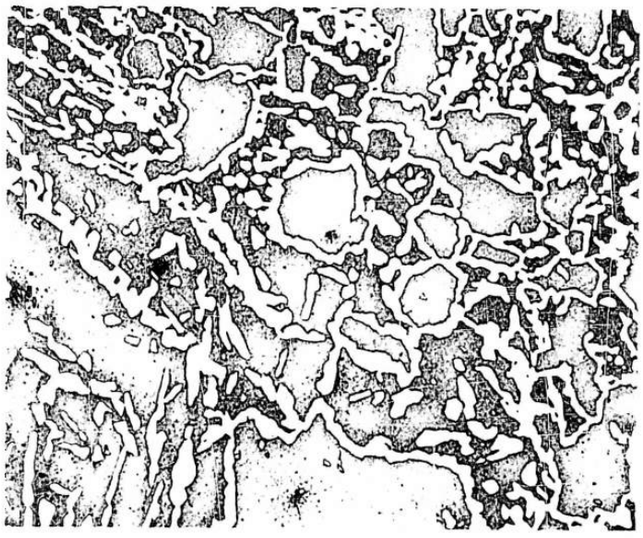

500X

Figure VI:4 - 9.5 ± 1% Rh, 6 days, 1320° ± 20°C, etchant I. α-Ta (gray) + σ (white).

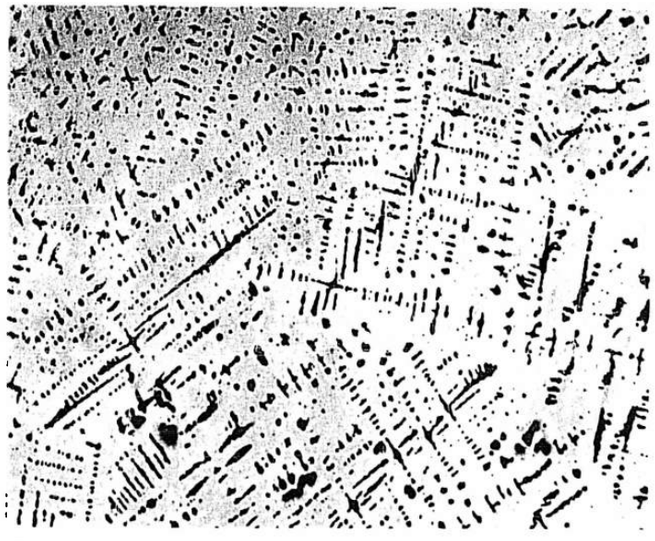

200X

Figure VI:5 - 24 ± 1% Rh, as cast, etchant I. α-Ta (gray) + σ (white).

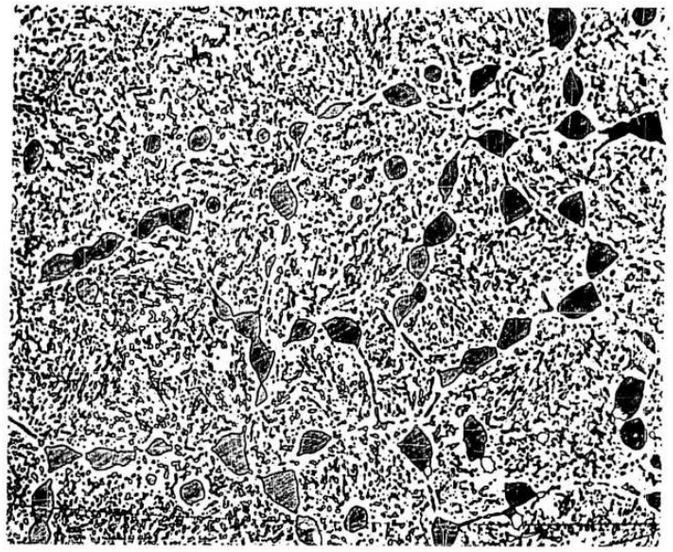

200X

Figure VI:6 - 49.7 ± 0.2% Rh, 6 days, 1320° ± 20°C, etchant II. σ (dark) + α_1 (white).

200X

Figure VI:7 - 52 ± 0.5% Rh, 6 days, 1320° ± 20°C, etchant II. σ (dark) + α_1 (white).

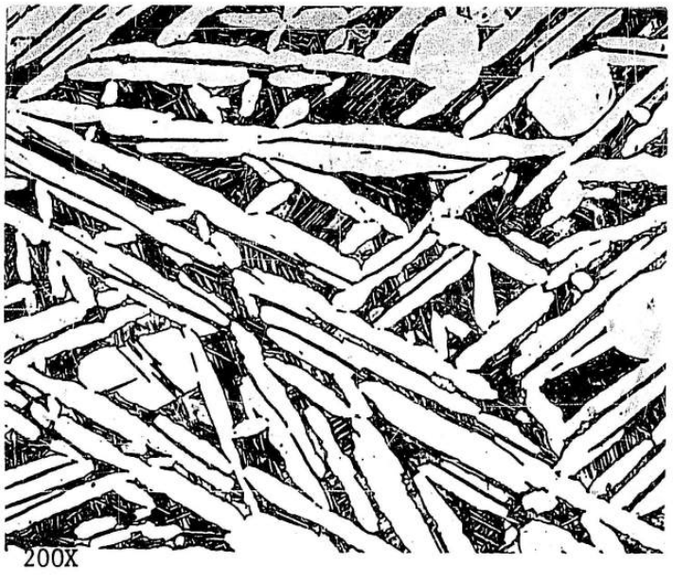

Figure VI:8 - 57.3 ± 0.7% Rh, 3 days 1557° ± 15°C, etchant II. α_1 (white) + eutectoid α_1 - σ (dark).

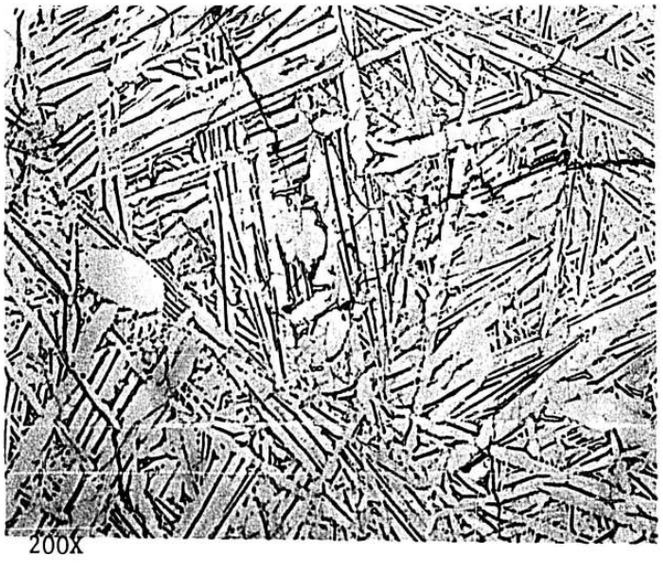

Figure VI:9 - 59.5 ± 0.5% Rh, 16 hours 1754° ± 20°C, etchant II. α_1 (white) + σ (dark).

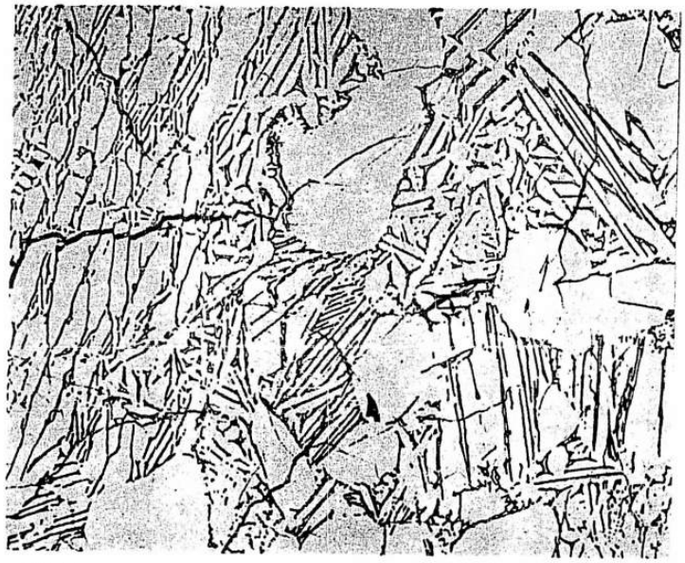

200X

Figure VI:10 - 60.5 ± 0.5% Rh, 16 hours 1754° ± 20°C, etchant II. α_1 (white) + σ (dark).

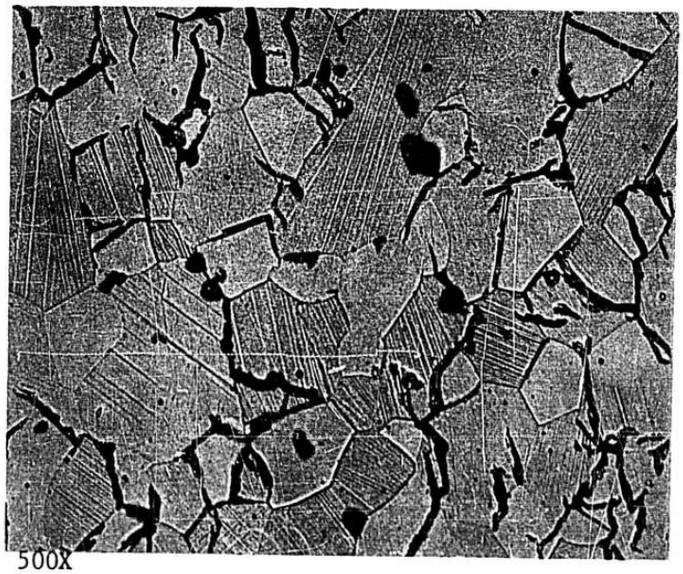

500X

Figure VI:11 - 64.5 ± 0.5% Rh, 16 hours 1754° ± 20°C, α_1 (light) + α_2 (dark, twinned).

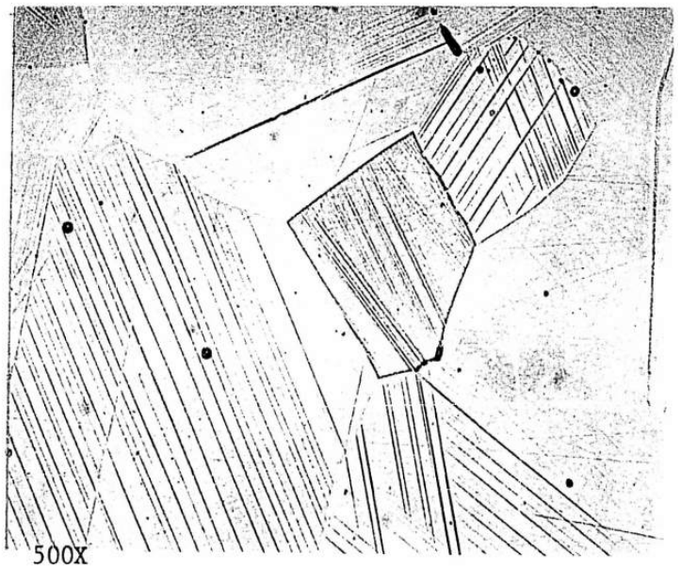

Figure VI:12 - 66.5 ± 0.5% Rh, 6-1/2 days 1392° ± 15°C, etchant II. α_2 (one phase).

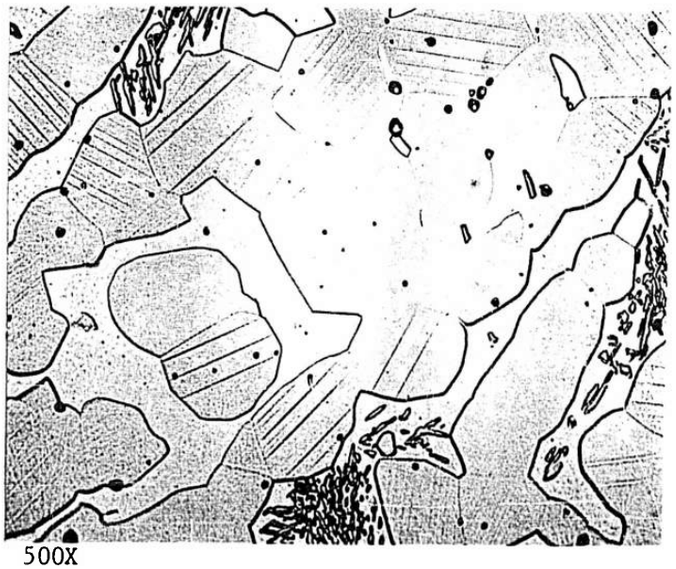

Figure VI:13 - 68 ± 0.5% Rh, 6-1/2 days 1392° ± 15°C, etchant II. α_2 (gray, twinned) + α-$TaRh_3$ (light).

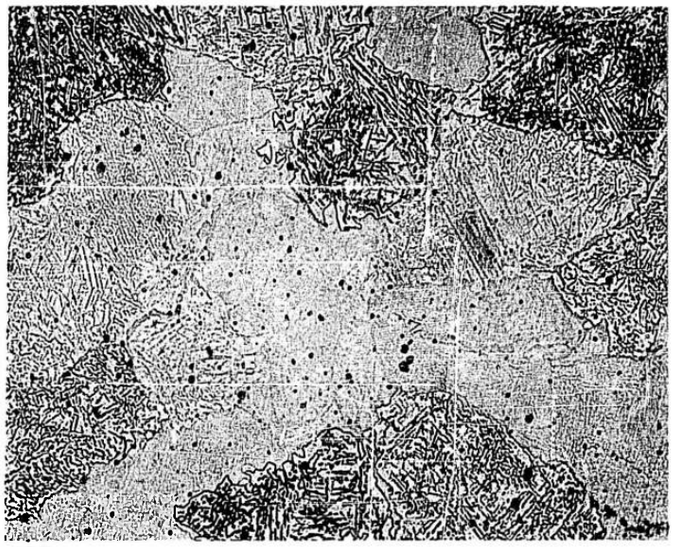

200X

Figure VI:14 - 69.7 ± 0.3% Rh, 6 days 1320° ± 20°C, etchant II. α_2 (dark segregate) in matrix of α-$TaRh_3$ (white).

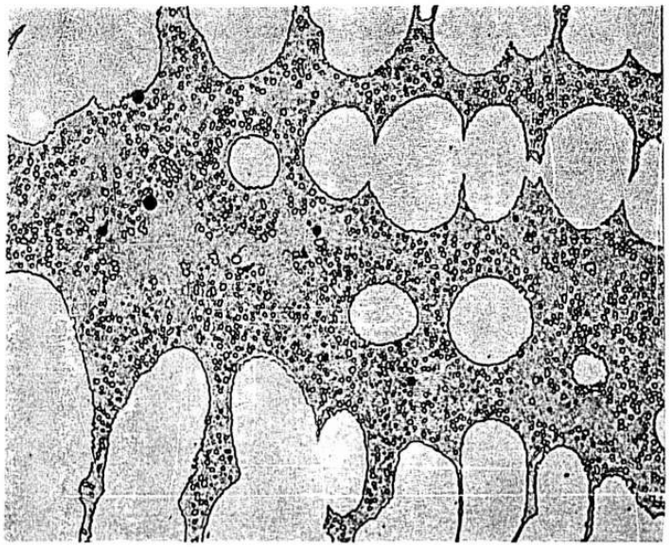

500X

Figure VI:15 - 79.3 ± 0.7% Rh, 2 hours 1930° ± 25°C, etchant II. Primary α-$TaRh_3$ (white) + eutectic α-$TaRh_3$ (white) + α-Rh (gray).

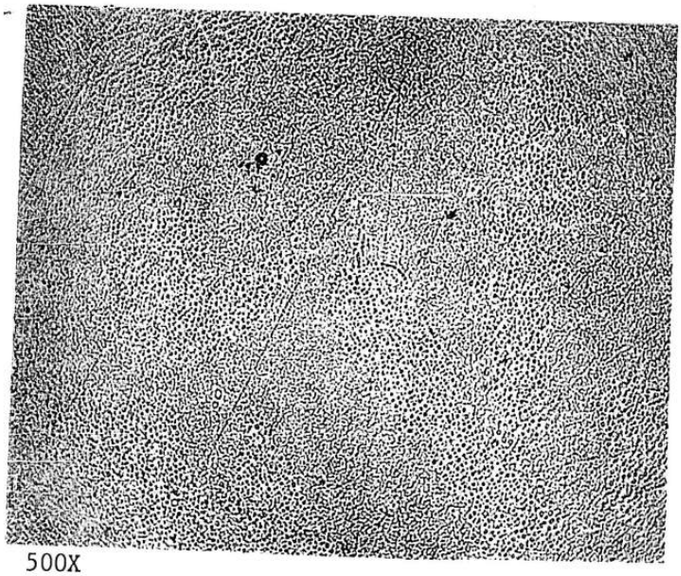

500X

Figure VI:16 - 84.5 ± 0.5% Rh, 1/2 hour 1961° ± 25°C, etchant II. eutectic α-$TaRh_3$ + α-Rh.

twinning at high temperatures and the fact that a 68 atomic percent Rh alloy becomes one phase twinned α_2 at about 1840°C indicates a possibly more complicated diagram in this region. Perhaps there is a high temperature phase at the composition of α_2, responsible for the strong twinning.

(3) The eutectic between α-Rh and α-$TaRh_3$ seems established, but the change of its appearance between 78 and 85 atomic percent Rh and the absence of primary α-Rh is only tentatively explained as degeneration of the eutectic. The maximum in the solidus at about 92 atomic percent Rh may be due to further ordering at that composition; however, no additional superlattice lines indicating a superstructure lower in Ta were found.

It may be noted that emphasis was laid on the proof that no compound Ta_3Rh (β-W type) exists. A series of four alloys in the pseudo-binary Nb_3Rh-Ta_3Rh were prepared and heat-treated at 1300°C for one week; β-W was found only in Nb_3Rh, not in any of the ternary alloys.

I. Tantalum-Iridium Constitution Diagram

The tantalum iridium phase diagram is presented in Figure VI:17. It is marked by the occurrence of the following four intermediate phases:

σ (tetragonal, identical to σ in Ta-Rh) between 11.4 atomic percent Ir at 2475°C to 41 atomic percent Ir at 1950°C.

α_1 (orthorhombic, identical to α_1 in Ta-Rh) between 50.4 atomic percent Ir at 1950°C to 56.0 atomic percent Ir at 1800°C.

α_2 (tetragonal, AuCu-structure) between 58 and 59 atomic percent Ir at 1800°C.

α-$TaIr_3$ (cubic, $AuCu_3$-structure), between 70.0 and 75.5 atomic percent Ir at 1800°C.

α-Ta has a maximum solid solubility of 7.2 atomic percent Ir at 2475°C. σ forms peritectically at 2475°C (α-Ta + L = σ), and forms a eutectic with α_1 (L = σ + α_1) at 1948°C. α_1 forms according to α_2 + L = α_1 at 2056°C. α_2 forms by a peritectic reaction α-$TaIr_3$ + L = α_2 at approximately 2120°C.

A eutectic (L = α-$TaIr_3$ + α-Ir) exists at 2355°C. α-Ir has a maximum solid solubility for Ta of 14.5 atomic percent Ta.

The phase diagram is illustrated by the microsections described below. Figure VI:18, (8 atomic percent Ir, 2252°C, two hours) shows brown α-Ta solid solution with approximately 5 percent white σ phase. Figure VI:19, (39.5 atomic percent Ir) is a melting point determination sample, showing primary unmelted σ phase with re-solidified eutectic σ + α_1. Figure VI:20 is 49.2 atomic percent Ir, annealed at 1914°C for 13 hours and quenched, showing α_1 (white) + σ (dark). Figure VI:21 shows the 59.5 atomic percent Ir alloy, annealed for 17 hours at 1992°C, and then quenched. The characteristic twinning which has been identified with the α_2 structure is present. The untwinned material is α-$TaIr_3$. Figure VI:22

is the most striking photomicrograph of the series. The very strong twinning, characteristic of α_2 at high temperatures, is clearly defined. This alloy is 64.0 atomic percent Ir, and was annealed at 2096°C for 14 hours and furnace quenched. The twinned, single phase structure proves the existence extended range of stability of α_2 at high temperatures, as assumed in the diagram.

Figure VI:23 is a melting point sample of 64.0 atomic percent Ir, which was quenched at 2180°C. It shows rounded grains of α-$TaIr_3$ with a thin border zone of α_2, a matrix of α_1 (white) + σ (small black particles).

Figure VI:24 is the 70.0 atomic percent Ir alloy, composed of primary α-$TaIr_3$ and the twinned α_2 phase. Coring is present in the α-$TaIr_3$ phase, although the alloy was annealed at 1992°C for 17 hours, after a 20 hour homogenizing heat treatment at 1733°C. The α-$TaIr_3$ solid solution exhibits a melting point higher than the melting point of the iridium used in this investigation.

Figure VI:25 is the eutectic alloy 84.5 atomic percent Ir, annealed at 2330°C for 30 minutes. The eutectic is α-$TaIr_3$ solid solution and α-Ir solid solution.

Figure VI:26 is hypoeutectic 85.5 atomic percent Ir, of the same annealing run as alloy 84.5. The white phase is α-Ir and the eutectic structure probably is α-Ir and α-$TaIr_3$. The investigation of this region is being continued, since the appearance of these alloys is not fully understood.

The high temperature region of α_2 is marked by very strong twinning as it is observed on the occurrence of the ordered AuCu-structure and the orthorhombic high temperature transformation of AuCu and CoPt[7,8]. More exact X-ray determinations are being conducted. The change of a two phase specimen annealed at 1992°C into the twinned single phase structure is explained as an extension of the α_2 field, with a peritectic reaction α-$TaIr_3$ + L = α_2 occurring. However, other configurations in this region are possible, e.g., a eutectic L = α_2 + α-$TaIr_3$ (as indicated by the incipient melting points).

The strength and toughness of the alloys in the 53.9 - 57.0 Ir compositions were noted in the attempts to produce powders for X-ray analysis. In addition, it was found necessary to cut specimens on an abrasive wheel for metallographic mounting. Alloys between 52 and 59 atomic percent Rh exhibit the same property.

J. Discussion of Prior Work

1. Ta-Rh

Greenfield and Beck[1] investigated eight alloys annealed at 1000°C. They found only the σ phase, α-Ta and α-Rh. Since seven of their alloys were at the concentrations of α-Ta, σ and α-Rh, their failure to find the other intermediate phases is understandable. Only one alloy (at 52.0 atomic percent Rh) might have exhibited σ + α_1, but it was annealed at too low a temperature to reach an equilibrium structure, and the Debye-Scherrer diagram of α_1 was probably read as α-Rh.

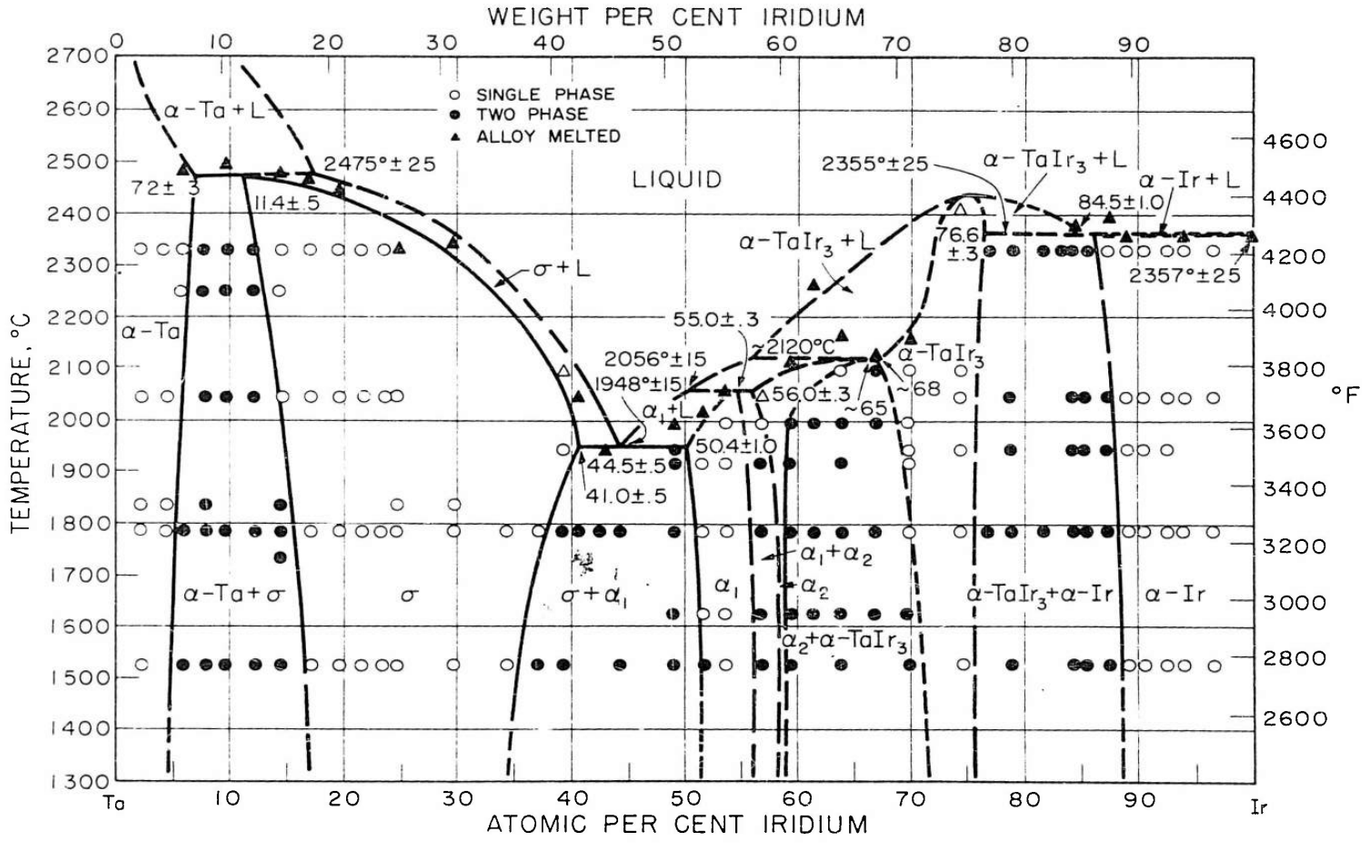

Figure VI:17 - Tantalum-iridium constitution diagram.

200X

Figure VI:18 - 8.0 ± 0.1 atomic percent Ir, 2 hours, 2252 ± 20°C, etchant I. α-Ta (gray) + σ (white).

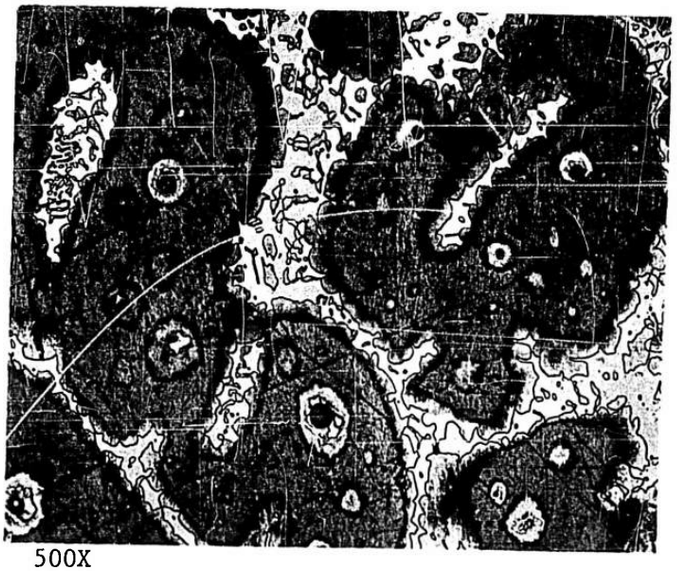

500X

Figure VI:19 - 39.5 ± 0.5 atomic percent Ir, melting point, 2045 ± 20°C, etchant II. σ (gray) + α_1 (white).

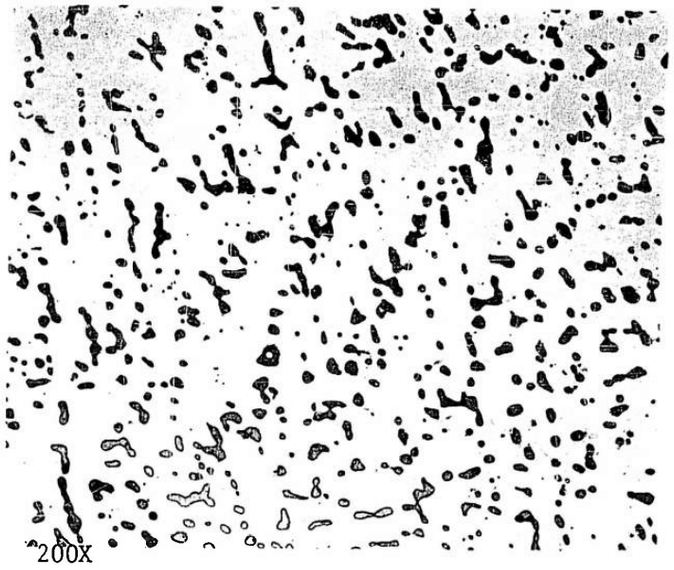

Figure VI:20 - 49.2 ± 1.0 atomic percent Ir, 13 hours, 1914° ± 15°C, etchant II. σ (gray) + α_1 (white).

Figure VI:21 - 59.5 ± 0.5 atomic percent Ir, 17 hours, 1992° ± 15°C, etchant II. α_2 (twinned, gray) + α-$TaIr_3$ (white).

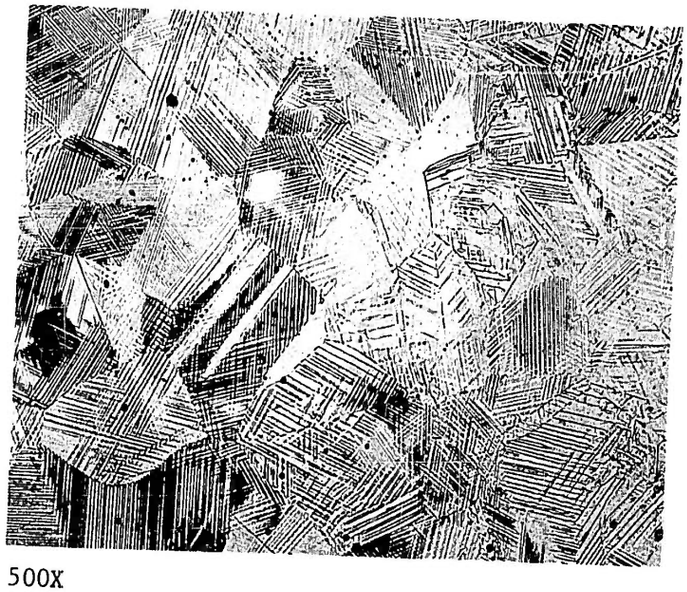

500X

Figure VI:22 - 64.0 ± 1.0 atomic percent Ir, 14 hours, 2096° ± 20°C, etchant II. One phase α_2.

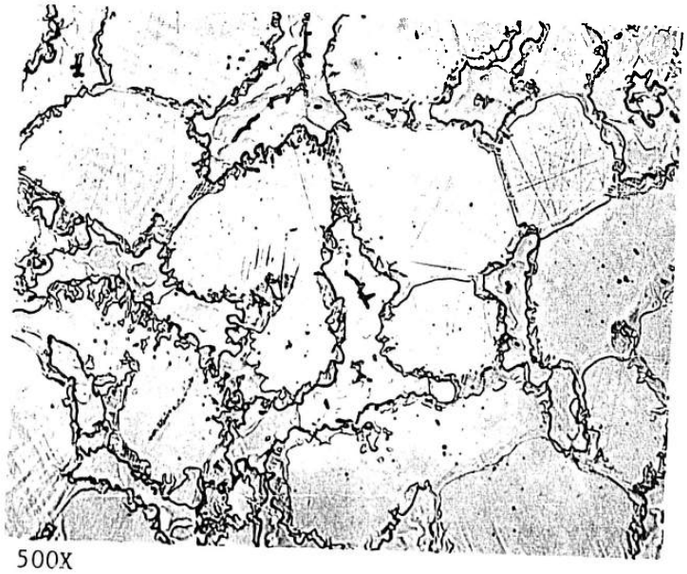

500X

Figure VI:23 - 64.0 ± 1.0 atomic percent Ir, melting point, 2180° ± 20°C, etchant II. α-$TaIr_3$ (white), seams of α_2 (gray), matrix of α_1 (gray) + σ (black).

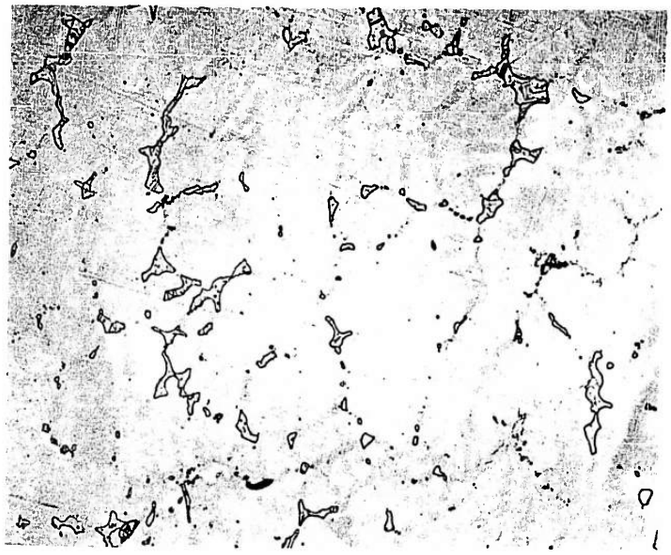

500X

Figure VI:24 - 70.0 ± 0.2 atomic percent Ir, 17 hours, 1992° ± 15°C, etchant II. α-$TaIr_3$ (white) + α_2 (gray).

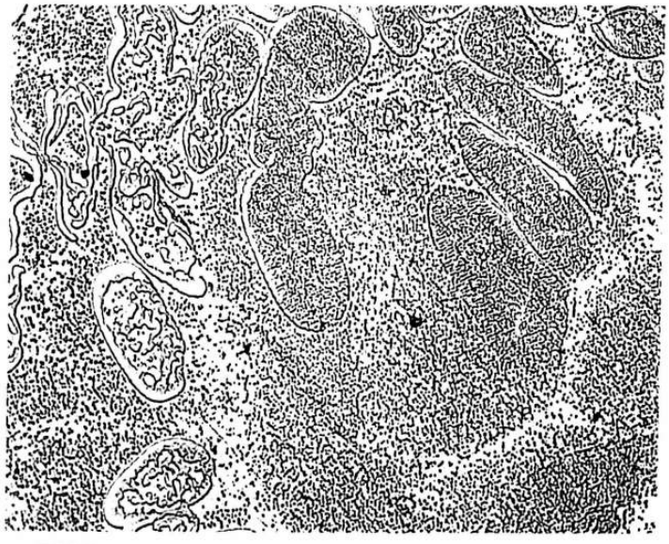

500X

Figure VI:25 - 84.5 ± 0.5 atomic percent Ir, 1/2 hour, 2330° ± 25°C, etchant II. α-$TaIr_3$ (dark) + α-Ir (white).

500X

Figure VI:26 - 85.5 $\pm$ 1.0 atomic percent Ir, 1/2 hour 2330° $\pm$ 25°C, etchant II. α-$TaIr_3$ (dark) + α-Ir (white).

Dwight and Beck[2] list the ordered structure $TaRh_3$ (a_o = 3.86 Å). Knapton[4] mentions the Ta-Rh phase diagram, and indicates the existence of σ and $TaRh_3$. These findings were confirmed here.

2. Ta-Ir

Dwight and Beck[2] list the ordered structure $TaIr_3$ (a_o = 3.889 Å). Nevitt and Downey[3] have found σ to exist between 15 - 25 atomic percent Ir; they list lattice parameters of a_o = 9.938 Å and c_o = 5.172 Å at 25 atomic percent Ir.

Knapton[4] lists both σ (melting peritectically) and $TaIr_3$. These previous findings were confirmed.

APPENDIX I: CRYSTALLOGRAPHIC WORK

The crystallographic work in the system Ta-Rh centered around the structure determinations for α_1 and α_2. Both structures could be annealed into fairly large grains; the alloys were crushed and small single crystals of irregular shape and an average length of 2/10 mm were selected and mounted on glass sticks. A 57.3 mm rotating crystal camera was used, orienting was done by trial and error. The recurrent occurrence of fundamental lines in α_1, α_2 and α-$TaRh_3$ was useful.

A. Determination of α_1 (Ta-Rh)

Disregarding a small orthorhombic deformation, the lines of α_1 could be indexed on the basis of a hexagonal unit cell with a_o = 5.52 Å; c = 13.61 Å; c/a = 2.46. This cell is of a type reported by Saito[9] for VCo_3, (space group P $\bar{6}$m2) which consists of six close-packed layers of the composition AB_3 in a stacking sequence abcacb. All lines can be indexed on that basis, which was indicated by the rotation crystal pictures taken around the a and c axes. The first lines show a slight doubling due to an orthorhombic deformation. This changes the unit cell dimension into a = 5.62 Å; b = 9.48 Å; c = 13.61 Å. Since the composition of the alloy is between 53.5 and 61 atomic percent Rh, it can be expected to deviate from the hexagonal symmetry of VCo_3. Additional work on the change of the parameters with the concentration and the exact distribution of the atoms is required.

B. Determination of α_2 (Ta-Rh)

It was more difficult to obtain a good single crystal of α_2, since α_2 twins strongly and the crystals had to be remounted frequently. Two rotation photographs around the a and c axes were obtained and on their basis the parameters could be measured. They were found to be a_o = 5.45 Å; b_o = 8.15 Å; c_o = 4.01 Å. All lines can be accounted for. The orthorhombic structure is probably of the space group Pnam, and similar to that of Co_2Si described by Geller[10]. It contains 4 molecules/unit cell and is centered sharply around $TaRh_2$. Also in this case, additional work to elucidate the positions of the atoms is needed.

C. α_1 (Ta-Ir)

The lattice constants of this phase were not determined, but they are very close to those of α_1 (Ta-Rh).

D. α_2 (Ta-Ir)

α_2 has the tetragonal AuCu structure, with a_o = 3.991 Å and c = 3.856 Å ($\pm$ .001 Å); c/a = .966.

APPENDIX II: QUENCHING TECHNIQUES

Although the existence of α_3 and its phase boundaries were well established by metallography, an attempt was made to quench samples to room temperature without the decomposition occurring at 1375°C. The methods employed in the rest of the diagram failed to indicate retained α_3; therefore, the following methods were employed.

(1) Since a rough calculation indicated that quenching in a helium-jet is faster than in any liquid bath, ground specimens of 5-mil diameter and 1/8-inch length of a well-annealed 50 atomic percent Rh alloy were suspended in the tube furnace, heated above 1375°C and dropped into a copper cup, into which helium was blown before the quench. Next, to decrease the time taken by the specimen for a free fall, an ejector gun was built. It consisted of a copper tube cooled by a water flow. The specimen was suspended from a plug in the tube and was ejected by a helium jet for the quench, thus reducing the time of the fall to 1/10 that of free fall. This design yielded cooling rates estimated at >10,000°C per second.

Another procedure utilized direct electric heating of the specimen held by thin Pt leads in a jet of helium. On quenching the current was switched off while the helium jet continued, bringing about an even larger cooling rate. Neither method was successful; quenched specimens showed only the lines of α_1. These results are in keeping with the rather high exothermic effect of the transformation.

REFERENCES

1. Greenfield, P., and Beck, P. A., Trans. AIME, 206, (1956), p. 265.
2. Dwight, A. E., and Beck, P. A., Trans. AIME, 215, (1959), p. 976.
3. Nevitt, M. and Downey, J., J. of Metals, 9, (1957), p. 1072.
4. Knapton, A. G., J. Less Common Metals, 2, (1960), p. 113.
5. WADD Technical Report 60-132, p. 116.
6. Ibid, p. 16.
7. Bowles, J. S. and Malin, A. S., J. Austr. Inst. Met., 5, (1960) p. 131.
8. Newkirk, J. B. Smoluchowski, R., Geisler, A. H., Martin, D. L., J. Appl. Phys., 22, (1951), p. 290.
9. Saito, S., Acta Cryst., 12, (1959), p. 500.
10. Geller, S., Acta Cryst., 8, (1955), p. 83.

VII. HARDNESS SURVEY (Work done at Nuclear Metals by A. Geary and E. Rapperport)

A. Introduction

The hot-hardness measurements described in this section were performed in order to obtain a preliminary estimate of the high temperature strength properties of the alloys generated by the phase diagrams reported in Part 1 of this series. Those systems are: Mo-Hf, W-Hf, W-Os, W-Ru, Nb-Re, Ta-Os, Ta-Re, Ta-Ru, Re-Hf and W-Ta-Re[1]. Since the properties of these alloys had not been investigated, a cursory examination of their high temperature strength capabilities was of interest. Although hot-hardness does not correlate directly with the long-time properties measured in creep tests, it does give an indication of the short-time strength properties. For example, Maykuth and Jaffee[2] report that the ultimate and yield strengths of niobium base alloys at temperatures up to 815°C could be roughly approximated from hot-hardness data through the use of the relationships: UTS (psi) = 400 DPH and YS (psi) = 333 (DPH-10). Wilson and McKinsey[3] also report a linear correlation between hot-hardness and ultimate tensile strength of niobium, tantalum, tungsten and several of their alloys. In the temperature range of 2000 to 2900°F, the higher hardnesses were associated with the higher tensile strengths and both decreased in a similar manner with temperature. This correlation was obtained even though the hardness specimens were arc cast buttons and the tensile specimens were of wrought and recrystallized stock.

B. Experimental Procedures

1. Materials

The hardness samples furnished by the investigators of each system, and their compositions, are given in Table VII: 1A. The compositions were selected as far as possible to represent the major areas of interest in the diagrams: refractory metal-rich solid solution fields, intermediate single-phase fields and extensive two-phase fields. With the exception of the W-Hf and Nb-Re alloy samples, the samples had been heat treated in the diagram determinations to establish equilibrium conditions. The W-Hf and Nb-Re alloys were in the form of arc cast buttons which had not been homogenized or equilibrated. Mo-Hf and Ta-Re alloy samples were also received but were too small for the hot hardness measurements. Replacement alloys for these systems were prepared at NMI by the non-consumable arc-melting technique. The compositions of the replacement alloys are given in Table VII: 1B. In addition, unalloyed Mo, W, Nb and Ta arc-cast buttons were prepared to serve as reference materials in the hardness measurements.

2. Specimen Preparation

All specimens were prepared for testing in the "as-received" or as-cast condition, no attempt being made to homogenize or equilibrate the structures at the testing temperature of 800°C. They were first mounted in a castable plastic to facilitate handling and were ground on opposite sides to produce parallel faces. One of the parallel faces was then hand-polished through 4/0 metallographic abrasive paper and, finally, electropolished to remove the cold worked surface layer. All measurements were made on the electropolished faces and the specimens were repolished between the room temperature and elevated temperature measurements.

TABLE VII:1

Compositions of Alloys Included in the Hot Hardness Study

System	Source	Number of Alloys	Compositions a/o
A. Alloys fabricated in phase diagram determinations			
Mo-Hf	Westinghouse	3	10, 35, 75 a/o Hf
W-Hf	MIT	5	1, 8, 33.3, 93, 98.3 a/o Hf
W-Os	Westinghouse	5	2.5, 10, 25, 60, 80 a/o Os
W-Ru	NMI	3	10, 40, 60 a/o Ru
Nb-Re	MIT	5	10, 20, 37, 44, 70 a/o Re
Ta-Os	NMI	4	10, 30, 50, 80 a/o Os
Ta-Re	MIT	9	5, 15, 26, 32, 41, 61, 70, 79, 98 a/o Re
Ta-Ru	NMI	5	10, 30, 55, 70, 90 a/o Ru
Re-Hf	Westinghouse	1	32.5 a/o Hf
B. Replacement Alloys Fabricated at NMI			
Mo-Hf		4	
Ta-Re		3	

3. Room Temperature Measurements

Room temperature hardnesses were measured on a standard Vickers hardness tester, using a 1 kilogram load. Five impressions were made on each specimen and the hardness values averaged for the table entry.

4. Elevated Temperature Measurements

A vacuum hot-hardness apparatus designed to operate at temperatures up to about 1600°C was used for measuring the elevated temperature hardnesses of the alloys. This apparatus functions in a manner similar to that of a standard Vickers hardness tester in that the impressions are made with a standard Vickers pyramid indenter under constant load for a predetermined period of time. The unit is contained within a cylindrical vacuum chamber and the specimen is heated by a molybdenum-wound resistance element. The normal operating pressure is less than 0.05 micron Hg. The stage on which the specimen holder rests can be rotated through 360 degrees in increments as small as 5°. Since the axis of the stage is displaced about 1/2-inch from the axis of the indenter, a large number of impressions can be made without dismantling the apparatus.

For the measurements, four to six specimens were mounted in the specimen holder and fixed in position by means of molybdenum wedges. The holder was placed on the rotating stage and the chamber evacuated to less than 0.02 microns Hg. The specimens were then heated to the test temperature and held there for 1/2-hour before making the hardness impressions.

Four hardness runs were made at 1200°C on specimens from the Ta-Ru, W-Os and W-Ru systems using a synthetic sapphire indenter. Although softer than diamond, sapphire is preferred for measurements at temperatures above 1000°C because of its greater chemical stability. Furthermore, the sapphire usually does not deform because its hardness is so much greater than the hardnesses of metallic specimens at the same temperature. However, in these runs at 1200°C, the sapphire indenter fractured. Although it was first thought that fracture was the result of tangential forces or shock loading, modifications to the loading mechanism of the unit failed to eliminate the problem. It was then concluded that the high hardnesses of the test specimens caused fracture. This conclusion was later substantiated by the successful use of a sapphire indenter in other programs at NMI to test materials at 1200°C exhibiting DPH hardnesses as high as 300 kg/mm^{-2}. Since it was desired to test all of the alloys at the same elevated temperature, a diamond pyramid indenter was substituted for the sapphire indenter and the impressions made at 800°C using a 1-kilogram load applied for 20 seconds. A minimum of three impressions was made on each specimen. The diamond indenter performed satisfactorily at this temperature; examination after each run failed to reveal any evidence of deterioration.

The hot-hardness impressions were measured at room temperature with a Tukon optical unit, no correction being made for thermal contraction.

C. Results

Table VII:2 gives the average hardness values for the alloys tested at room temperature and 800°C, together with the fraction of room temperature strength which was retained at 800°C. The condition of the alloys and equilibrium phases at 800°C are included in the table for reference only, since positive identification

Table VII:2

Hardness Results for Alloys Tested at Room Temperature and 800°C

Composition a/o	Condition	Equilibrium[1] Phases at 800°C	DPH[2] - 1 Kg/mm²		Fraction RT retained hardness at 800°C
			RT	800°C	
Mo	Arc-cast	αMo	188	76	0.40
Mo-2Hf	"	"	306	142	0.46
Mo-5Hf	"	"	428	193	0.45
Mo-10Hf	"	"	495	383	0.77
Mo-70Hf	"	η+αHf	854	494	0.58
W	Arc-cast	αW	417	73	0.18
W-1Hf	"	"	424	163	0.38
W-8Hf	"	αW+W_2Hf	613	302	0.49
W-33Hf	"	W_2Hf	1415	737	0.52
W-93Hf	"	W_2Hf+αHf	600	265	0.44
W-98.3Hf	"	W_2Hf+αHf	498	118	0.24
W-2.5 Os	As Rec'd.	αW	534	238	0.45
W-10 Os	"	αW+σ	873	547	0.63
W-80 Os	Arc-cast	θ Os	1159	485	0.42
W-10Ru	As Rec'd.	αW+βRu	1578	675	0.43
W-40Ru	"	αW+βRu	831	1282[4]	1.54
W-60Ru	"	αW+βRu	716	414	0.58
Nb	Arc-cast	αNb	94	46	0.49
Nb-10Re	"	"	403	309	0.76
Nb-20Re	"	"	678	485	0.72
Nb-70Re	"	χ	(1680)[3]	1120	(0.67)
Ta	Arc-cast	αTa	138	85	0.62
Ta-10 Os	As-Rec'd.	αTa	608	322	0.53
Ta-5Re	Arc-cast	αTa	283	194	0.70
Ta-10Re	"	"	430	301	0.70
Ta-15Re	"	"	538	390	0.72

Table VII:2 (Continued)

Composition a/o	Condition	Equilibrium Phases at 800°C	DPH(2) - 1 Kg/mm² RT	DPH(2) - 1 Kg/mm² 800°C	Fraction RT retained hardness at 800°C
Ta-20Re	Arc-cast	αTa	650	388	0.60
Ta-10Ru	As Rec'd.	"	564	304	0.54
Ta-55Ru	"		1272	668	0.52
Ta-70Ru	"	γ+βRu	1400	1008	0.72
Ta-90Ru	"	βRu	561	591	1.05

1. Extrapolated from phase diagrams presented in WADD-TR 60-132.
2. One Kg load applied for 20 seconds. Impression measured at room temperature.
3. Doubtful value; specimen fractured around impression
4. Anomaly: possible specimen contamination.

of the phases present on each alloy was not attempted. For most of the alloys investigated, the five room temperature hardness values were within ±5% of the average and the three 800°C values within ±10% of the average.

Results are given in Table VII:3 for the alloy specimens which were not tested at 800°C either because of their small size or because of difficulties in preparing their surfaces. These results are included for completeness and will not be discussed.

As expected, solid solution alloying significantly improved the hardnesses of the refractory metals, both at room temperature and at 800°C. The greatest improvement was observed in the Nb-20 a/o Re alloy whose hardness at 800°C was about 10 times that of unalloyed niobium. In general, however, alloying increased the hardness by a factor of two to five. Within the solid solution ranges which were investigated, the hardness appeared to increase with increasing alloy content.

Solid solution alloying additions were also found to improve resistance to softening. In solid solution alloys, only the Ta-10 a/o Os, Ta-10 a/o Ru and Ta-20 a/o Re alloys softened as rapidly as the unalloyed base metal. All other alloys softened far less rapidly than the base metal. For example, the tungsten base alloys at 800°C retained about 40% of their room temperature hardnesses compared with only 18% for unalloyed tungsten.

Peak hardness in most of the systems was found in the more highly alloyed samples. Outstanding among these alloys were the Nb-70 a/o Re and Ta-70 a/o Ru compositions; both had DPH values above 1000 kg/mm^{-2} at 800°C and above 1400 kg/mm^2 at room temperature. The Nb-70 a/o Re alloy was brittle at room temperature, and fracture cracks around the impressions prevented accurate hardness measurements.

Both of the alloys appeared to soften slowly with increasing temperature, the 800°C hardnesses were about 70% of the room temperature values, and possibly would continue to exhibit outstanding hardnesses at still higher temperatures.

D. Discussion of Results

The survey revealed three alloy compositions with DPH hardnesses at 800°C greater than 1000 kg/mm^2 and five additional ones with hardnesses greater than 500 kg/mm^2. If the correlation between hardness and strength which was reported by Maykuth and Jaffee may be extrapolated to these hardness values, these alloys would be expected to have ultimate tensile strengths at 800°C of about 200,000 to 400,000 psi. Furthermore, these alloys soften relatively slowly with increasing temperature and may continue to be hard and strong at temperatures well above 800°C.

It appears that large alloying additions are required to achieve peak hot hardness values. Among the six hardest alloys, only two, the W-10 a/o Os and W-10 a/o Ru, contain only relatively small additions. Presumably precipitation hardening contributes to the hardnesses observed for these alloys. The remaining alloys contain rhenium and ruthenium in excess of 50 a/o. It is interesting that of the two hardest alloys, one, the Nb-70 a/o Re, corresponds to an intermediate phase composition whereas the other, the Ta-70 a/o Ru, corresponds to a composition capable of undergoing eutectoid decomposition.

Table VII:3

Hardness Results for Alloy Specimens Tested

Composition a/o	Condition	Room Temp[1] DPH - kg/mm^2
A. Alloy specimens which were too small for hot hardness measurements		
Mo-10Hf	As Rec'd.	467
Mo-35Hf	"	908
Mo-75Hf	"	492
Re-32.5Hf	As Rec'd.	(1041)[2]
Ta-5Re	As Rec'd.	454
Ta-15Re	"	686
Ta-26Re	"	673
Ta-32Re	"	655
Ta-41Re	"	643
Ta-61Re	"	(1634)[2]
Ta-98Re	"	320
B. Friable alloy specimens which could not be prepared with satisfactory surfaces		
W-25 Os	As Rec'd.	---
W-60 Os	"	---
Nb-37Re	"	---
Nb-44Re	"	---
Ta-30 Os	"	---
Ta-50 Os	"	---
Ta-80 Os	"	---
Ta-30 Ru	"	---

1. One Kg load applied for 20 seconds.

2. Doubtful values. Specimens fractured around impressions.

REFERENCES

1. Refractory Metal Constitution Diagrams, WADD TR 60-132, June 1960

2. D. J. Maykuth and R. I. Jaffee, "The Fabrication and Mechanical Properties of Some Columbium Alloys for Use in Pressurized Water Reactors", Columbium Metallurgy, edited by D. L. Douglass and F. W. Kunz, Interscience Publishers, 1961

3. J. L. Wilson and C. R. McKinsey, "Tungsten-Columbium-Tantalum Alloys, Their High Temperature Properties", Journal of Metals, July 1961, p 477

Aeronautical Systems Division, Dir/Materials and Processes, Metals and Ceramics Lab, Wright-Patterson AFB, Ohio.
Rpt Nr WADD-TR-60-132, Part II. REFRACTORY METAL CONSTITUTION DIAGRAMS. Final report, 185p. incl illus., tables, 43 refs. Sept.62.
Unclassified Report

Data on six binary constitution diagrams and two ternary constitution diagrams of some of the refractory metals are presented. The binary diagrams include Mo-Os, Ta-Ir, Ta-Rh, Ta-Zr, W-Ir, and W-Rh; the ternaries are Mo-Hf-Re and Ta-W-Zr.

Care was taken to obtain reliable diagrams. In particular the purity of the constituents

(over)

(99.9 percent plus) was protected at all times, and the temperatures were measured to an accuracy of ± .0°C.

1. Refractory metals
2. Metallurgy
I. AFSC Project 7351, Task 735101
II. Contract AF 33 (616)-7157
III. Nuclear Metals, Inc. Concord, Mass.
IV. E. J. Rapperport, et al.
V. Secondary Report No. 9237
VI. Aval fr OTS
VII. In ASTIA collection

Aeronautical Systems Division, Dir/Materials and Processes, Metals and Ceramics Lab, Wright-Patterson AFB, Ohio.
Rpt Nr WADD-TR-60-132, Part II. REFRACTORY METAL CONSTITUTION DIAGRAMS. Final report, 185p. incl illus., tables, 43 refs. Sept.62.
Unclassified Report

Data on six binary constitution diagrams and two ternary constitution diagrams of some of the refractory metals are presented. The binary diagrams include Mo-Os, Ta-Ir, Ta-Rh, Ta-Zr, W-Ir, and W-Rh; the ternaries are Mo-Hf-Re and Ta-W-Zr.

Care was taken to obtain reliable diagrams. In particular the purity of the constituents

(over)

(99.9 percent plus) was protected at all times, and the temperatures were measured to an accuracy of ± .0°C.

1. Refractory metals
2. Metallurgy
I. AFSC Project 7351, Task 735101
II. Contract AF 33 (616)-7157
III. Nuclear Metals, Inc. Concord, Mass.
IV. E. J. Rapperport, et al.
V. Secondary Report No. 9237
VI. Aval fr OTS
VII. In ASTIA collection

Aeronautical Systems Division, Dir/Materials and Processes, Metals and Ceramics Lab, Wright-Patterson AFB, Ohio.
Rpt Nr WADD-TR-60-132, Part II. REFRACTORY METAL CONSTITUTION DIAGRAMS. Final report, 185p. incl illus., tables, 43 refs. Sept.62.
Unclassified Report

Data on six binary constitution diagrams and two ternary constitution diagrams of some of the refractory metals are presented. The binary diagrams include Mo-Os, Ta-Ir, Ta-Rh, Ta-Zr, W-Ir, and W-Rh; the ternaries are Mo-Hf-Re and Ta-W-Zr.

Care was taken to obtain reliable diagrams. In particular the purity of the constituents

(over)

(99.9 percent plus) was protected at all times, and the temperatures were measured to an accuracy of ± 20°C.

1. Refractory metals
2. Metallurgy
I. AFSC Project 7351, Task 735101
II. Contract AF 33 (616)-7157
III. Nuclear Metals, Inc, Concord, Mass.
IV. E. J. Rapperport, et al.
V. Secondary Report No. 9237
VI. Aval fr OTS
VII. In ASTIA collection

Aeronautical Systems Division, Dir/Materials and Processes, Metals and Ceramics Lab, Wright-Patterson AFB, Ohio.
Rpt Nr WADD-TR-60-132, Part II. REFRACTORY METAL CONSTITUTION DIAGRAMS. Final report, 185p. incl illus., tables, 43 refs. Sept.62.
Unclassified Report

Data on six binary constitution diagrams and two ternary constitution diagrams of some of the refractory metals are presented. The binary diagrams include Mo-Os, Ta-Ir, Ta-Rh, Ta-Zr, W-Ir, and W-Rh; the ternaries are Mo-Hf-Re and Ta-W-Zr.

Care was taken to obtain reliable diagrams. In particular the purity of the constituents

(over)

(99.9 percent plus) was protected at all times, and the temperatures were measured to an accuracy of ± 20°C.

1. Refractory metals
2. Metallurgy
I. AFSC Project 7351, Task 735101
II. Contract AF 33 (616)-7157
III. Nuclear Metals, Inc, Concord, Mass.
IV. E. J. Rapperport, et al.
V. Secondary Report No. 9237
VI. Aval fr OTS
VII. In ASTIA collection